CONTEMPORARY GENETIC TOOLS FOR IN VIVO INVESTIGATIONS OF H3K27 DEMETHYLASES IN ZEBRAFISH CARDIOGENESIS

by

ALEXANDER ANDREW AKERBERG

A DISSERTATION

Presented to the Department of Biology
and the Graduate School of the University of Oregon
in partial fulfillment of the requirements
for the degree of
Doctor of Philosophy

September 2016

DISSERTATION APPROVAL PAGE

Student: Alexander Andrew Akerberg

Title: Contemporary Genetic Tools for In Vivo Investigations of H3K27 Demethylases in Zebrafish Cardiogenesis

This dissertation has been accepted and approved in partial fulfillment of the requirements for the Doctor of Philosophy degree in the Department of Biology by:

Dr. Eric Selker	Chairperson
Dr. Kryn Stankunas	Advisor
Dr. Judith Eisen	Core Member
Dr. Monte Westerfield	Core Member
Dr. Ken Prehoda	Institutional Representative

and

Scott L. Pratt	Dean of the Graduate School

Original approval signatures are on file with the University of Oregon Graduate School.

Degree awarded September 2016

DISSERTATION ABSTRACT

Alexander Andrew Akerberg

Doctor of Philosophy

Department of Biology

September 2016

Title: Contemporary Genetic Tools for In Vivo Investigations of H3K27 Demethylases in Zebrafish Cardiogenesis

Dynamic histone modification has emerged as a robust and versatile regulator of gene expression in eukaryotic cells. One such modification, the trimethylation of lysine 27 on histone H3 (H3K27me3) is facilitated by the Polycomb repressive complex 2 (PRC2) and contributes to the localized repression of transcription. Subsequently, lysine specific demethylase *Kdm6b* (*Jmjd3*) can relieve the repressive H3K27me3 mark, allowing for transcriptional activation. *In vitro* studies have suggested a role for *Kdm6b* during mesodermal and cardiovascular differentiation in mammalian embryonic stem cells; however, this relationship has yet to be characterized *in vivo*. I utilized the advantages of the zebrafish model to investigate the *in vivo* roles of Kdm6b-family demethylases during development using a reverse genetic approach.

I carried out two independent loss-of-function studies to analyze the role of Kdm6b-family demethylases during embryonic development in zebrafish. By comparing genetic loss-of-function and morpholino-mediated knockdown approaches, I found that morpholino–mediated knockdown of *kdm6bb* transcript produces off-target effects and does not portray an accurate representation of *in vivo* function. I then show that, while not required for early cardiogenesis, histone demethylases *kdm6ba* and *kdm6bb* function

redundantly to promote late stage proliferation during heart ventricle trabeculation. These data reveal a previously unknown functional relationship and support the hypothesis that Kdm6b-family demethylases function primarily during later stages of development. Additionally, my description of morpholino-induced off-target effects supports the need to use extreme caution when interpreting morphant phenotypes.

Due to the embryonic lethality exhibited by *kdm6b*-deficient embryos and the limited tools available for spatiotemporal transgene control in zebrafish, I was unable to investigate demethylase function within adult animals. I attempted to circumvent these limitations by creating an inducible gene expression system that uses tissue-specific transgenes that express the Gal4 transcription factor fused to the estrogen-binding domain of the human estrogen receptor. I showed that these Gal4-ERT driver lines confer rapid, tissue-specific induction of UAS-controlled transgenes following tamoxifen exposure in both embryos and adult fish. I then demonstrated how this technology could be used to define developmental windows of gene function by spatiotemporally controlling expression of constitutively active Notch1 in embryos.

This dissertation includes previously published co-authored material.

CURRICULUM VITAE

NAME OF AUTHOR: Alexander Andrew Akerberg

GRADUATE AND UNDERGRADUATE SCHOOLS ATTENDED:

University of Oregon, Eugene
Saint Louis University, Saint Louis
University of Colorado, Boulder

DEGREES AWARDED:

Doctor of Philosophy, 2016, University of Oregon
Master of Science, Biology, 2009, Saint Louis University
Bachelor of the Arts, Molecular Cellular and Developmental Biology (MCDB), University of Colorado at Boulder

AREAS OF SPECIAL INTEREST:

Molecular Cell Biology
Chromatin Dynamics
Genetics
Cardiovascular Biology

PROFESSIONAL EXPERIENCE:

Senior research technician, Washington University School of Medicine, 2009-2010
Microbiologist technician, Coors Brewing Co, 2007-2008

GRANTS, AWARDS, AND HONORS:

Best Poster Award, *Histone demethylases kdm6ba and kdm6bb function redundantly during zebrafish development*, Institute of Molecular Biology, 2015
Developmental Biology Training Grant, National Institutes of Health (NIH), 2013
Developmental Biology Training Grant, National Institutes of Health (NIH), 2012
Developmental Biology Training Grant, National Institutes of Health (NIH), 2011

PUBLICATIONS:

Akerberg, A. A., Stewart, S. & Stankunas, K. Spatial and temporal control of transgene expression in zebrafish. *PLoS ONE* **9,** e92217 (2014)

Akerberg, A. A., Stewart, S. & Stankunas, K. Histone demethylases *kdm6ba* and *kdm6bb* redundantly promote late stage proliferation during heart ventricle maturation in zebrafish. In preparation.

ACKNOWLEDGMENTS

I would like to thank my advisor, Dr. Kryn Stankunas, for being an excellent mentor and providing me with much needed guidance throughout my time here at the University of Oregon. Despite his many other responsibilities, Kryn's door was perpetually open and he was always willing to have impromptu discussions whenever I had a new idea, problems with an experiment, or if I simply wanted to brainstorm. He pushed me to excel and I am undoubtedly a better researcher because of it. I would also like to thank Dr. Scott Stewart for being an invaluable presence in the lab and for serving as my unofficial mentor. Scott is a superb experimentalist who provided me with key technical and theoretical guidance throughout my research. I would like to thank the entire Stankunas lab for their critical feedback and support. I also greatly appreciate the guidance and feedback provided by my dissertation committee members: Eric Selker, Judith Eisen, Monte Westerfield, and Ken Prehoda. They were all integral to my success as a graduate student. I would also like to thank my wife and partner in crime (in the proverbial sense, this is not an admission of actual crime), Brynn Akerberg. Her ability to make me smile is what made all the late nights and early mornings worthwhile. Lastly I would like to thank my parents, Jan and Nora Akerberg and my brother Nick Akerberg for all their support throughout the years. All of my accomplishments, both past and future, I owe to them.

Dedicated to my cousin Daniel Dutch Cassill (1979-2014) and my sister in law Emily Ihrke Akerberg (1981-2012) who both continue to inspire

TABLE OF CONTENTS

Chapter Page

LIST OF FIGURES

CHAPTER I

INTRODUCTION

"We had described competence as a state of disequilibrium in a complex system of reactants, and had suggested that the reactants are ultimately genes or gene products"

-C.H. Waddington, 1940

In a manuscript that predates our understanding of nucleic acid structure and function, Conrad Waddington (quoted above) detailed his theories of developmental "competence" that are strikingly amenable to our modern understanding of cellular specification and differentiation. It was here that Waddington coined the term "epigenetic landscape" to describe an unknown mechanism of development that existed "on top" of heritable genetics and that could, in effect, either mask or reveal underlying genetic traits. This idea has been expounded upon by researchers over the last half-century and has given rise to the field of modern epigenetics in which Waddington's theories of development are being applied to the microcosm of molecular genetics. As a corollary, the concept of an "epigenetic landscape" has been transformed to fit within our current body of knowledge. Contemporary definitions of epigenetic landscape, though still the subject of debate, describe any *non-genetic* mechanism that contributes to the transcriptional programing of a cell. To date, researchers have identified several such modes of epigenetic gene regulation including covalent histone modification, DNA methylation, and chromatin remodeling, which have all been shown to dynamically contribute to a cell's expression program. Despite these advancements, we are only just

beginning to discover how these mechanisms contribute to vertebrate development and homeostasis.

Post-translational histone modification has emerged as a particularly active area of research due, in part, to the complexity arising from the multitude of different modifications and target residues. One such example is the trimethylation of lysine 27 on histone H3 (H3K27me3). The trimethylation of H3K27 is facilitated by Enhancer of zest (Ezh2), a component of the Polycomb repressive complex (PRC2), and contributes to the localized repression of transcription (Cao et al., 2002; Margueron and Reinberg, 2011; Müller et al., 2002). This repressive mark can subsequently be relieved by lysine specific demethylases such as Kdm6a (UTX) and Kdm6b (Jmjd3), thus promoting transcriptional activation (Cloos et al., 2008; Klose and Zhang, 2007; Mosammaparast and Shi, 2010). Together these processes constitute a dynamic and potentially versatile layer of transcriptional regulation; however, the biological significance of this particular modification is currently a topic of debate. Numerous genome-wide descriptions of H3K27me3 localization suggest chromatin modifiers like EZH2 and Kdm6b have key contributions during development, adult tissue homeostasis, and even tissue dedifferentiation and regeneration.

In vitro studies of H3K27 demethylases have described roles for Kdm6b within development of all three germ layers, which suggest that localized demethylation may be a fundamental mechanism of gene regulation. In mouse and human embryonic stem (ES) cells, researchers have implicated Kdm6b in relieving the repressive H3K27me3 marks

decorating promoter regions, thereby contributing to the activation of important endodermal-commitment markers such as *Eomes* (Kartikasari et al., 2013; Kim et al., 2011), *WNT3* (Jiang et al., 2013), and *Nodal* (Kim et al., 2011). Kdm6b-deficient mice have also been shown to exhibit defects in endodermal derivatives such as the lung (Burgold et al., 2012; Li et al., 2014b); however, the Kdm6b target genes revealed by these studies did not coincide with *in vitro* data. Instead, these mouse models implicated Kdm6b in the activation of lung specific genes such as AQP-5 and SB-P (Cao et al., 2002; Li et al., 2014b; Margueron and Reinberg, 2011; Müller et al., 2002) that represent stages of development much later than endodermal commitment.

Further reports have demonstrated that Kdm6b is required for ectoderm induction in embryonic stem (ES) cells (Cloos et al., 2008; Klose and Zhang, 2007; Morales Torres et al., 2013; Mosammaparast and Shi, 2010) via regulation of *Msi1*, *Sox1*, *Otx2* and *Pax6*. Interestingly, a separate study that eliminated both Kdm6b and Kdm6a found no change in ectodermal induction (Shpargel et al., 2014), however it is unclear if they probed for the presence of the same proteins. *In vivo,* Kdm6b has also been shown to contribute to endochondral bone formation by promoting proliferation and hypertrophy via association with Runx2 (Kartikasari et al., 2013; Kim et al., 2011; Zhang et al., 2015). Importantly, the Kdm6b-deficient mice generated for this study exhibited perinatal lethality due to inability to breathe, which does not reflect the expected phenotype if early ectoderm specification were disrupted.

Similar to *in vitro* reports of Kdm6b function within both endodermal and ectodermal lineages, investigations using mouse ES cells have implicated Kdm6b as a contributor to mesodermal specification (Jiang et al., 2013; Morales Torres et al., 2013; Ohtani et al., 2013; Shpargel et al., 2014), T-cell differentiation (Kim et al., 2011; Manna et al., 2015), and the differentiation of several different lineages within the cardiovascular system (Burgold et al., 2012; Li et al., 2014b; Ohtani et al., 2013). An *in vivo* assessment of Kdm6b function within cardiovascular development was precluded by the early lethality (embryonic day 6.5) of $Kdm6b^{KO}$ mice generated by Ohtani et al. (2013). Importantly, the early lethality observed in these mice is consistent with the hypothesis that Kdm6b has a role during early development; however, this stands in contrast to the perinatal lethality reported by others (Li et al., 2014b; Shpargel et al., 2014; Zhang et al., 2015). Comprehensively, these data provide insights into potential functions of Kdm6b during development; however, inconsistencies between *in vitro* and *in vivo* data sets cast uncertainty over Kdm6b's role during early development and highlight the need for further investigation.

While there are many well-known benefits of using the mouse as a model for development, there are limitations to their utility when studying early developmental events. Mice are viviparous and as such, embryos proceed through much of development obscured from view within the uterus. Small litter sizes can also render large-scale screens intractable. One of the reasons for the ongoing success of zebrafish as a model organism is that they are oviparous, allowing direct observation of embryogenesis in its entirety. Furthermore, zebrafish remain optically transparent through much of

adolescence during which observations can be made regarding tissue maintenance and homeostasis. Zebrafish can therefore circumvent several experimental limitations imposed by the mouse model.

Generation of genetic mutations in zebrafish have traditionally depended on random mutagenesis screens (Mullins et al., 1994), thus confining researchers to a forward genetic approach. Until recently, reverse genetic approaches were largely performed using morpholino-mediated knockdown, which are less consistent than genetic knockdowns and are speculated to be prone to off-target effects (Lawson, 2016). With the recent development of techniques such as clustered regularly interspaced short palindromic repeats (CRISPR) /Cas9 and transcription activator-like effector nucleases (TALENs), the generation of targeted mutations for proper reverse genetic experimentation can now be achieved in zebrafish. In applying these techniques, researchers have overcome a substantial limitation and drastically increased the utility of the model.

The material presented in Chapter II utilizes the advantages of the zebrafish model by capitalizing on contemporary techniques such as CRISPR/Cas9 targeted mutagenesis. Using this technology, we describe a novel model for *kdm6b*-demethylase function during development in zebrafish. We show that while not required for early cardiogenesis, ohnologous histone demethylases *kdm6ba* and *kdm6bb* function redundantly to regulate proliferation during late stage cardiac morphogenesis and trabeculation. These data reveal a previously unknown functional relationship between

kdm6b ohnologs and support the hypothesis that *kdm6b* demethylases function primarily during later stages of organogenesis. Additionally, our description of morpholino-induced off-target effects supports the need to use extreme caution when interpreting morphant phenotypes.

CHAPTER II

HISTONE DEMETHYLASES *KDM6BA* AND *KDM6BB* REDUNDANTLY PROMOTE LATE STAGE PROLIFERATION DURING HEART VENTRICLE MATURATION IN ZEBRAFISH

JOURNAL STYLE INFORMATION

AUTHOR CONTRIBUTIONS

I performed the experiments and collected the data presented in this manuscript. Dr. Kryn Stankunas aided in experimental design as well as manuscript preparation and composition. Dr. Scott Stewart contributed to experimental design.

INTRODUCTION

Covalent histone modifications establish chromatin landscapes that influence gene expression programs by promoting active or silenced transcriptional states. Localized trimethylation of lysine 27 on histone 3 (H3K27me3) is deposited by Enhancer of zeste homolog 1 and 2 (Ezh1 and 2), the catalytic subunits of the Polycomb repressive complex 2 (PRC2), and is associated with gene silencing (Cao et al., 2002; Margueron and Reinberg, 2011; Müller et al., 2002). H3K27me3 marks can be relieved by the lysine-specific demethylases Kdm6a (Utx) and Kdm6b (Jmjd3) (Cloos et al., 2008; Klose and Zhang, 2007; Mosammaparast and Shi, 2010). Therefore, H3K27me3 modifications provide an epigenetically inherited but reversible layer of transcriptional control. In

vertebrates, H3K27me3 dynamics are implicated in cell fate specification (Alder et al., 2010; Dahl et al., 2010; Rugg-Gunn et al., 2010) activation of gene expression programs in response to cell signaling or transcription factors (Jiang et al., 2013; Kartikasari et al., 2013; Ramadoss et al., 2012), and cell reprogramming associated with acquired pluripotency (Azuara et al., 2006; Bernstein et al., 2006; Mikkelsen et al., 2007) as well as de-differentiation during organ regeneration (Stewart et al., 2009).

In vitro studies using embryonic stem cells (ES cells) suggest Kdm6b enables early cell specification of all three germ layers (Burgold et al., 2008; Kartikasari et al., 2013; Ohtani et al., 2013; Ohtani et al., 2011). These results predict that Kdm6b is responsible for relieving H3K27me3 at fate specifying genes as pluripotent cells adopt distinct cell lineage identities (Bernstein et al., 2006; Mikkelsen et al., 2007). However, in vivo tests of this model using mouse *Kdm6b* reverse genetics have yielded conflicting results. Mice homozygous for a *Kdm6b* allele that deletes exons encoding N-terminal regions of the protein are peri-implantation lethal at embryonic day 6.5 (E6.5) (Ohtani 2013). In contrast, mice homozygous for several independently generated *Kdm6b* mutant alleles that delete the catalytic JmjC domain survive embryogenesis before dying perinatally with lung development defects (Li et al., 2014b; Satoh et al., 2010; Shpargel et al., 2014; Zhang et al., 2015). The discrepancy in phenotypes between the N-terminal and JmjC-deletion *Kdm6b* alleles is unresolved, but may reflect demethylase-independent functions of Kdm6b (Miller et al., 2010) retained in truncated protein produced by the JmjC-domain targeted alleles.

Kdm6b-deficient embryos are smaller and edematous (Li et al., 2014b), suggesting that Kdm6b contributes to cardiovascular development. In further support, H3K27me3 marks are conspicuously lost from key cardiogenic genes during in vitro cardiac differentiation of ES cells (Paige et al., 2012; Wamstad et al., 2012)) and PRC2 is required to maintain cardiomyocyte identity (Delgado-Olguín et al., 2012; He et al., 2012). Additionally, *Kdm6b*$^{-/-}$ ESCs induced to undergo cardiomyocyte differentiation misexpress many genes implicated in early heart development, including decreased levels of the cardiac progenitor factors *Mesp1*, *Pdgfra*, and *Mef2c* (Ohtani et al., 2011). Correspondingly, *Kdm6b*-deficient ES cells exhibit reduced ability to form differentiated cardiomyocytes and contractile embryoid bodies (EBs). While in vivo mouse and zebrafish studies demonstrate Kdm6a contributes to the activation of core cardiac transcription factors (Lee et al., 2012; Van Laarhoven et al., 2015; Welstead et al., 2012), the in vivo contributions of Kdm6b to cardiovascular development have not been examined.

We pursued in vivo loss-of-function studies in zebrafish to define *Kdm6b*'s evolutionarily conserved contributions to vertebrate development. Due to teleost whole genome duplication, the zebrafish genome contains two *Kdm6b* orthologs, *kdm6ba* and *kdm6bb*. In such instances of duplicated genes, the "ohnologs" commonly acquire unique expression patterns and therefore functions or one "ohnolog" becomes non-functional due to relaxed selective pressures (Brunet et al., 2006; Force et al., 1999; Jaillon et al., 2004; Lynch and Force, 2000; Woods et al., 2005). While there is no literature describing *kdm6ba* function, *kdm6bb* is speculated to support the re-activation of embryonic

developmental gene programs during fin regeneration (Stewart et al., 2009) and therefore was the focus of our initial studies.

Exemplified by CRISPR/Cas9 methodologies, genome editing recently has enabled genuine reverse genetics studies in zebrafish (Foley et al., 2009; Hruscha et al., 2013; Hwang et al., 2013; Shin et al., 2014). The resulting rapid emergence of targeted alleles has uncovered multiple cases of discrepancy between genetic mutant and morpholino-induced phenotypes, raising substantial concern about the reliability of even well-controlled zebrafish morpholino studies (Kok et al., 2014; Lawson, 2016). Conversely, the historic contributions of morpholino-mediated knockdowns along with their versatility and ease of use are cited as justifying their continued use (Blum et al., 2015). The phenomenon of genetic compensation in zebrafish further supports this argument exemplified by a case in which morpholino-mediated knockdown portrays a more complete representation of gene function than the corresponding genetic mutant (Rossi et al., 2015).

We generated *kdm6bb* loss-of-function alleles using CRISPR/Cas9 mutagenesis and novel *kdm6bb* "morphants" given the reported advantages of each loss-of-function approach. We found that specific cardiovascular defects produced by morpholino-mediated knockdown of *kdm6bb* are not recapitulated in *kdm6bb*$^{-/-}$ embryos and instead originate from spurious off-target effects. Through further genetic loss-of-function studies, we show that *kdm6bb* functions redundantly with *kdm6ba*, consistent with their largely overlapping expression patterns. *Kdm6ba*$^{-/-}$;*kdm6bb*$^{-/-}$ zebrafish larvae have

pleiotropic yet specific organogenesis defects, including a small heart ventricle. This phenotype originates from insufficient cell proliferation of both endo- and myocardial cells associated with the initiation of cardiac trabeculation at larval hatching. Our data provides an example of straightforward non-compensatory redundancy between duplicated genes in zebrafish that, together with off-target morpholino effects, can explain "mutant" vs. "morphant" phenotype discrepancies. Further, we show that Kdm6b's unique functions (those not shared with Kdm6a) are largely restricted to later stages of organ growth and morphogenesis rather than early cell fate specification or progenitor cell activity.

RESULTS

Cardiovascular defects in *kdm6bb* morphant zebrafish are not recapitulated with a CRISPR/Cas9-generated *kdm6bb* null allele

To investigate the role of H3K27me3 histone demethylase *kdm6bb* during zebrafish development, we performed loss-of-function experiments targeting the essential catalytic JmjC domain (Hong et al., 2007; Xiang et al., 2007) using two parallel approaches. First, we generated a mutant allele of *kdm6bb* using CRISPR/Cas9 targeted mutagenesis. Second, we employed antisense morpholinos to target *kdm6bb* transcript splicing.

CRISPR/Cas9 mutagenesis was used to induce insertion-deletion (indel) mutations near the 5' end of the JmjC-coding domain of *kdm6bb*. We isolated a germline-transmitted allele (*kdm6bb*^{b1307}, abbreviated *kdm6bb*$^{-}$ from here forth) with a 40 bp deletion spanning the first 14 bp of exon 15 (Fig. 1A). The resulting frameshift and early stop codon is

predicted to result in a truncated Kdm6bb protein lacking the entire JmjC domain. Further, *kdm6bb* transcript levels were decreased nearly nine fold in homozygous *kdm6bb*$^{-/-}$ animals at 30 hpf due to nonsense mediated decay, as shown by qRT-PCR and *in situ* hybridization (Fig. 1B-D). Surprisingly, *kdm6bb*$^{-/-}$ fish did not exhibit any overt developmental defects and were viable through adulthood (Fig. 1E-H). A recent report proposes that unknown genetic compensation mechanisms specifically can obscure gene function in genetic mutants (Rossi et al., 2015). Therefore, to determine if the absence of developmental phenotypes in *kdm6bb*$^{-/-}$ animals accurately reflects Kdm6bb's biological roles, we pursued parallel loss-of-function experiments using a traditional morpholino-mediated knockdown approach.

Figure 1. Comparative loss-of-function studies of *kdm6bb* yield conflicting phenotypes.
(A) Schematic showing binding sites for anti-*kdm6bb* morpholinos (red bars) and the deleted sequence in the *kdm6bb* mutant allele recovered from CRISPR/Cas9 targeted mutagenesis (red bases). (B-C) In situ hybridization on *WT* and mutant animals at 24 hpf. (D) qRT-PCR using cDNA from 3 separate pools (n = 10) of *kdm6bb*$^{-/-}$ and WT embryos, normalized to *rpl18*. P-value determined by Student's two-tailed *t*-test. (E-H) DIC images of *kdm6bb*$^{-/-}$ and clutch mate control animals. (I-L) Whole mount DIC images of *kdm6bb* morphants. (M-N) Whole mount immunostaining with DIC overlay of morphant embryos. Arrows indicate ventricular position. (O-P) Fluorescent imaging of aortic arch arteries in 72 hpf *kdm6bb* morphants. (Q-R) Whole mount immunostaining with DIC overlay of *kdm6bb*$^{-/-}$ embryos. (S-T) Fluorescent imaging of aortic arch arteries in 72 hpf *kdm6bb*$^{-/-}$ Tg(flk:EGFP) animals. *Abbreviations used:* h, heart; ora, opercular artery; 3, first branchial arch artery; 4, second branchial arch artery; 5, third branchial arch artery; 6, fourth branchial arch artery. Asterisk denotes malformed aortic arches.

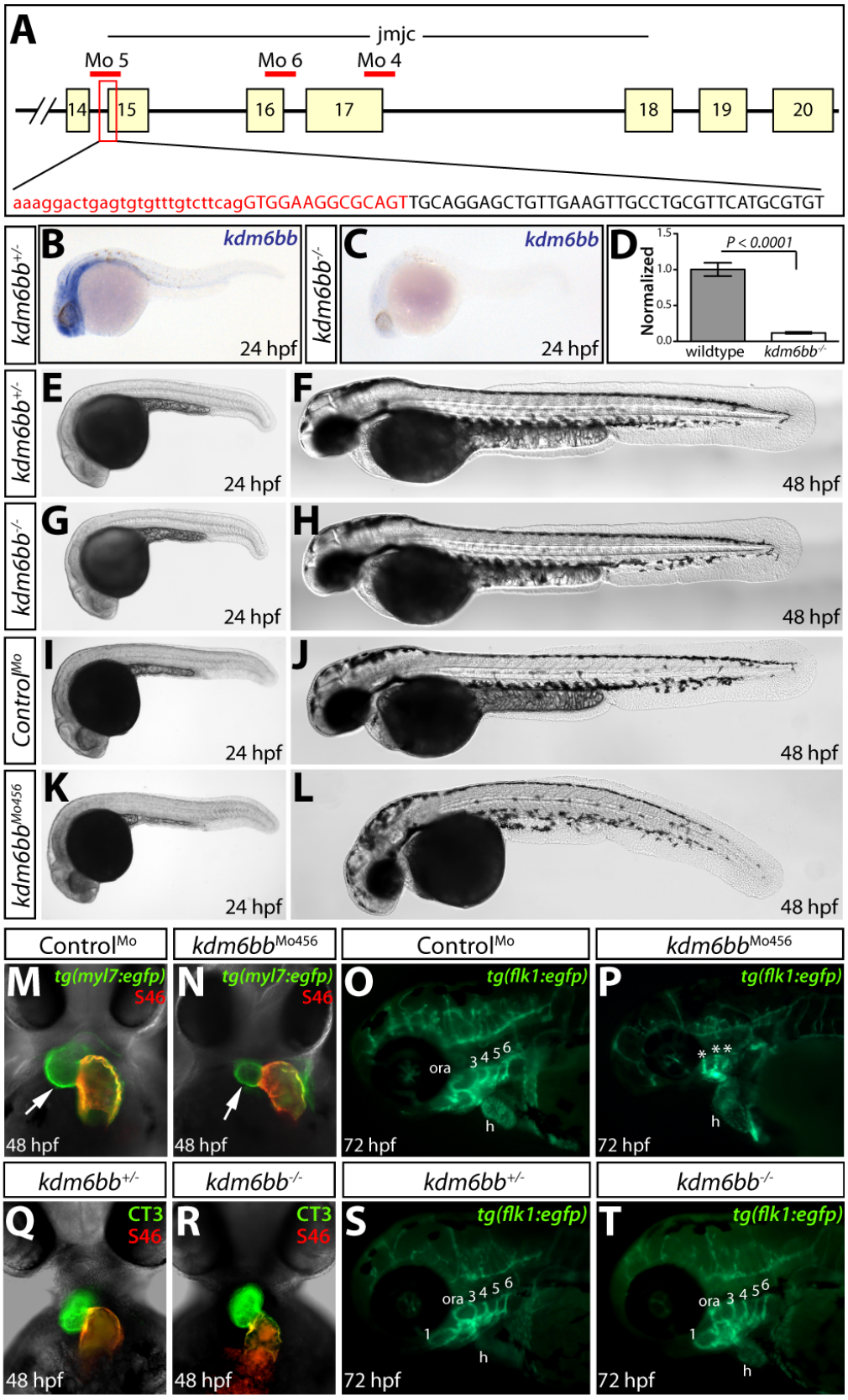
A
jmjc
Mo 5
Mo 6
Mo 4
14
15
16
17
18
19
20
aaaggactgagtgtgtttgtcttcagGTGGAAGGCGCAGTTGCAGGAGCTGTTGAAGTTGCCTGCGTTCATGCGTGT
kdm6bb+/-
B
kdm6bb
24 hpf
kdm6bb-/-
C
kdm6bb
24 hpf
D
P < 0.0001
Normalized
1.5
1.0
0.5
0.0
wildtype
kdm6bb-/-
kdm6bb+/-
E
24 hpf
F
48 hpf
kdm6bb-/-
G
24 hpf
H
48 hpf
ControlMo
I
24 hpf
J
48 hpf
kdm6bbMo456
K
24 hpf
L
48 hpf
ControlMo
kdm6bbMo456
ControlMo
kdm6bbMo456
M
tg(myl7:egfp)
S46
48 hpf
N
tg(myl7:egfp)
S46
48 hpf
O
tg(flk1:egfp)
ora
3 4 5 6
h
72 hpf
P
tg(flk1:egfp)
* **
h
72 hpf
kdm6bb+/-
kdm6bb-/-
kdm6bb+/-
kdm6bb-/-
Q
CT3
S46
48 hpf
R
CT3
S46
48 hpf
S
tg(flk1:egfp)
ora 3 4 5 6
1
h
72 hpf
T
tg(flk1:egfp)
ora 3 4 5 6
1
h
72 hpf

Following guidelines for best practice morpholino use in zebrafish (Eisen and Smith, 2008), we developed an antisense morpholino "cocktail" approach to target *kdm6bb* transcripts. We targeted the splice junctions of the first three exons within the JmjC domain with a previously published morpholino (Mo4) (Stewart et al., 2009) and two novel oligos (Mo5 & Mo6) that each prevented the splicing of an adjacent intron (Fig. 1A and Fig. S1B). To minimize toxicity or off-target effects, we used a morpholino cocktail containing each anti-*kdm6bb* morpholino at a concentration of 133 μM, which was below that where each individual morpholino produced developmental defects (Fig. S1C). *Kdm6bb*^{Mo456} embryos had no overt phenotypes at 24 hours post fertilization (hpf) (Fig. 1I & 1K), suggesting that the morpholino cocktail did not promote general toxicity or aberrant p53 activation (Nasevicius and Ekker, 2000; Robu et al., 2007). By 48 hpf, *kdm6bb*^{Mo456} embryos exhibited abnormal dorsal curvature and yolk sac extension (Fig. 1J and 1L), often accompanied by cardiac edema and poor blood flow (Movie S1).

To investigate potential cardiovascular defects in *kdm6bb*^{Mo456} embryos, we performed whole-mount anti-GFP immunostaining on morpholino-injected animals carrying the *Tg(myl7:EGFP)* transgene. While 48 hpf *kdm6bb*^{Mo456} embryos had a normal atrium and atrioventricular canal, they exhibited a notably smaller ventricle (Fig. 1M-N). We next injected morpholinos into embryos carrying the *Tg(kdrl:EGFP)* transgenic reporter (Jin et al., 2005), which fluorescently labels endothelial cells, to assess vascular network development. 72 hpf *Kdm6bb*^{Mo456}; *Tg(kdrl:EGFP)* larvae had malformed aortic arch arteries, with several arches failing to develop entirely (Fig. 1O-P). Together, the defects

observed in *kdm6bb*^{Mo456} zebrafish embryos suggest Kdm6bb has multiple specific roles during cardiovascular development.

Contrary to *kdm6bb*^{Mo456} morphants, *kdm6bb*$^{-/-}$ larvae did not exhibit an overtly diminished ventricle at 48 hpf (Fig 1Q-R) nor malformed aortic arch arteries at 72 hpf (Fig 1S-T). The discrepancies between *kdm6bb* mutant and morpholino-mediated phenotypes is reminiscent of inconsistencies observed by other groups that have challenged the reliability of morpholino studies (Kok et al., 2014; Law and Sargent, 2014). Conversely, other reports highlight the potential benefits of antisense morpholinos in avoiding maternal contributions, genetic compensation, and sometimes unpredictable protein products that can undermine genetic mutant studies (Blum et al., 2015; Rossi et al., 2015). Given the widespread ramifications of the morpholino vs. mutant debate, we pursued *kdm6bb* as a model locus to compare the two loss-of-function approaches while continuing to characterize *kdm6bb*'s developmental roles.

Off-target morpholino effects, rather than maternal contributions or genetic compensation, explain the phenotypic discrepancy between *kdm6bb*^{Mo456} and *kdm6bb*$^{-/-}$ zebrafish

Antisense morpholinos inhibit transcript splicing as well as ribosome binding and can therefore affect the translation of both maternally deposited and zygotically produced transcripts. As such, maternal contributions can potentially explain why more severe phenotypes are observed in morphants vs. homozygous null mutants of the corresponding gene (Blum et al., 2015). Therefore, we compared cardiovascular phenotypes between

kdm6bb morphants and maternal zygotic (MZ) *kdm6bb*-deficient (*kdm6bb*^{MZ}) embryos derived from *kdm6bb*$^{-/-}$ females. Using the *Tg(cmlc:DsRed-nuc)* reporter to quantify cardiomyocytes at 72 hpf (Takeuchi et al., 2011), we found that *kdm6bb*^{Mo456} embryos displayed a reduced number of ventricular but not atrial cardiomyocytes (Fig. 2A-C). In contrast, the number of ventricular cardiomyocytes was unchanged in *kdm6bb*^{MZ} embryos (Fig. 2D-F). The depletion of ventricular but not atrial cardiomyocytes in *kdm6bb*^{Mo456} embryos suggested a deficiency in second heart field (SHF) cardiac progenitor cells that contribute to the ventricle and outflow tract (OFT) (Guner-Ataman et al., 2013; Hami et al., 2011; Jahangiri et al., 2016; Zhou et al., 2011). Consistent with this notion, immunostaining for Elastin-B (Eln2), an OFT-enriched extracellular matrix protein (Miao et al., 2007), revealed that the OFT was completely absent in *kdm6bb* morphants at 72 hpf (Fig. 2G-H). Conversely, the OFT of 72 hpf *kdm6bb*^{MZ} animals was qualitatively normal (Fig. 2I-J). Further, *kdm6bb*^{MZ} adult fish were viable and fertile. Therefore, we conclude that the distinct *kdm6bb* morphant cardiovascular phenotypes impacting SHF-derived structures are not caused by inhibition of maternally-deposited *kdm6bb* mRNA.

Figure 2. *Kdm6bb* morphant phenotypes originate from off-target effects
(A-B) Fluorescent cardiomyocyte nuclei at 72 hpf in control and morphant *Tg(cmlc2:DsRed-nuc)* ; *Tg(myl7:EGFP-Hras)* embryos. (C) Quantification of cardiomyocytes in 72 hpf control and morphant embryos. (D-E) Fluorescent cardiomyocyte nuclei at 72 hpf in control and maternal zygotic *kdm6bb*$^{-/-MZ}$ *Tg(cmlc2:DsRed-nuc)* animals counterstained with CT3. (F) Quantification of cardiomyocytes in 72 hpf *kdm6bb*$^{-/-MZ}$ *Tg(cmlc2:DsRed-nuc)* embryos. (G-J) CT3 and ELN2 stained whole mounts show outflow tract (yellow arrows) in morphant and *kdm6bb*$^{-/-MZ}$ embryos. White arrows represent an absent OFT. (K) qRT-PCR using cDNA generated from 3 separate samples of pooled (n = 10) *WT* and *kdm6bb*^{MZ} embryos at 30 hpf. P-value determined via the student's two-tailed *t*-test. (L-Q) Single morpholino injections into both *kdm6bb*$^{-/-}$ shown by whole mount DIC (L&O), *Tg(flk:EGFP)* reporter (M&P) and OFT immunostaining (N&Q). Yellow arrows denote normal OFT and white arrows highlight an absent OFT.

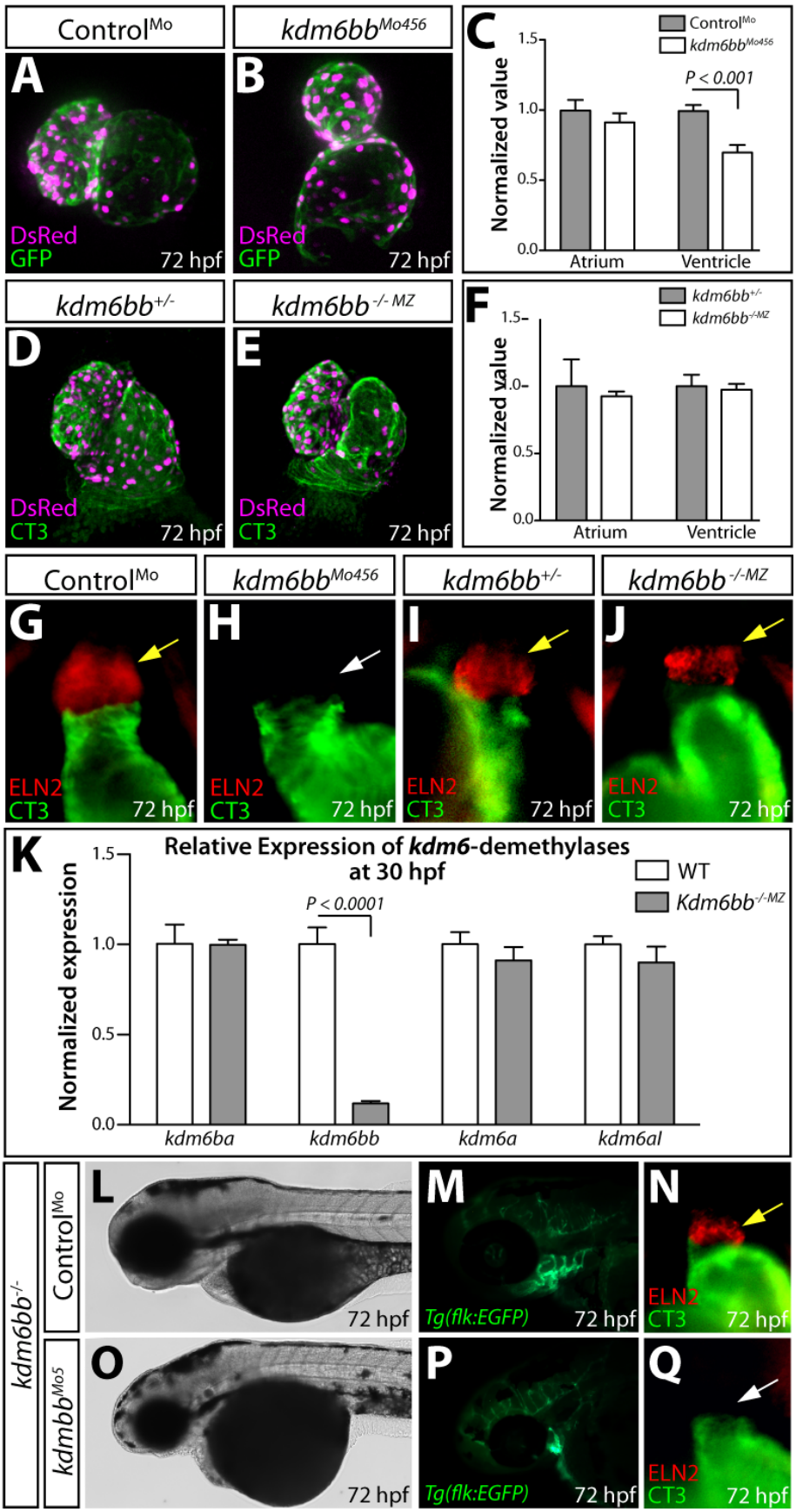
Control^Mo
kdm6bb^Mo456
A
B
DsRed
GFP
72 hpf
C
Control^Mo
kdm6bb^Mo456
P < 0.001
Normalized value
1.5
1.0
0.5
0.0
Atrium
Ventricle
kdm6bb^+/-
kdm6bb^-/- MZ
D
E
DsRed
CT3
72 hpf
F
kdm6bb^+/-
kdm6bb^-/-MZ
Normalized value
1.5
1.0
0.5
0.0
Atrium
Ventricle
Control^Mo
kdm6bb^Mo456
kdm6bb^+/-
kdm6bb^-/-MZ
G
H
I
J
ELN2
CT3
72 hpf
K
Relative Expression of kdm6-demethylases at 30 hpf
WT
Kdm6bb^-/-MZ
P < 0.0001
Normalized expression
1.5
1.0
0.5
0.0
kdm6ba
kdm6bb
kdm6a
kdm6al
kdm6bb^-/-
Control^Mo
kdmbb^Mo5
L
M
N
O
P
Q
72 hpf
Tg(flk:EGFP)
ELN2
CT3

We sought to determine if the phenotypic discrepancy between *kdm6bb*^{MZ} and *kdm6bb*^{Mo456} animals could be attributed to "compensation" by the programmed transcriptional activation of functionally related genes (Rossi et al., 2015). Only four zebrafish genes have predicted H3K27 demethylase activity (*kdm6ba*, *kdm6bb*, *kdm6a*, and *kdm6al)*, enabling us to assay for genetic compensation without performing a whole transcriptome analysis. Neither *kdm6ba* nor the *Utx* orthologs, *kdm6a* and *kdm6al*, were transcriptionally up-regulated in 30 hpf *kdm6bb*^{MZ} embryos as shown by qRT-PCR (Fig. 2K). Therefore, genetic compensation is unlikely to be occurring in *kdm6bb*-deficient animals, and, as such, cannot explain the phenotypic discrepancy between *kdm6bb* mutant and morphant embryos.

Morpholinos can unpredictably affect off-target transcripts even when producing specific phenotypes (Coffman et al., 2004; Ekker and Larson, 2001; Kok et al., 2014; Lawson, 2016). We injected the *kdm6bb* morpholino cocktail into *kdm6bb*$^{-/-}$ embryos and observed indistinguishable aortic arch artery and OFT defects in control and *kdm6bb*-deficient embryos (Fig. S2). Most revealingly, these cardiovascular defects persisted despite the deletion of Mo5's target sequence from the genome of *kdm6bb*$^{-/-}$ animals. Similarly, a higher dose of Mo5 alone produced similar aortic arch artery and outflow tract defects to *kdm6bb*^{Mo456} morphants even in the *kdm6bb*$^{-/-}$ genetic background (Fig. 2L-Q, S3). These data conclusively demonstrate that the observed *kdm6bb* morphant phenotypes are enhanced or even solely caused by morpholino effects on additional unknown transcripts.

Histone demethylases *kdm6ba* and *kdm6bb* have non-compensatory redundant functions during zebrafish development

Sea urchin studies show that morpholinos can affect the translation of off-target transcripts with partially-overlapping target sequences (Coffman et al., 2004). Our morpholinos were designed with broad differences between each target sequence, which excludes synergistic activity with respect to common off-target transcripts. However, other genes within the *kdm6*-family possess short stretches matching each of the three morpholino target sequences due to the highly conserved JmjC-coding regions. Most notably, *kdm6ba,* the ohnolog of *kdm6bb*, contains between 9 and 13 contiguous bases matching each morpholino target sequence. While the key Mo5 did not appear to disrupt splicing of *kdm6ba* (or *kdm6a* and *kdm6al*) transcripts (Fig. S4), we did not have a Kdm6ba antibody to assess Mo5's effects on *kdm6ba* translation. Therefore, while unlikely, we do not exclude the possibility that cardiovascular defects observed in *kdm6bb*^{Mo456} embryos result from the partial loss-of-function of *kdm6ba* in addition to *kdm6bb.* Further, redundant functions of *kdm6ba* and *kdm6bb* may obscure developmental phenotypes in *kdm6bb*$^{-/-}$ fish.

By RNA in situ hybridization studies, we found that *kdm6ba* and *kdm6bb* exhibited largely overlapping expression patterns during early development, supporting their potential redundancy (Fig. 3A-J). While *kdm6ba* transcripts showed a higher maternal contribution (Fig. 3F), both *kdm6ba* and *kdm6bb* transcripts were robustly expressed in the developing brain (Fig. 3B-C and G-H), otic vesicles (Fig. 3C and H), and the heart (Fig. 3D-E and I-J). To test for redundancy, we first generated a *kdm6ba* mutant allele by

CRISPR/Cas9 targeted mutagenesis of the coding region for the JmjC domain. We isolated an allele (*kdm6ba*^{b1308} henceforth denoted *kdm6ba*$^{-}$) containing a single base deletion within exon 14 of *kdm6ba* (Fig. 3K). This frameshift mutation was predicted to result in an early stop codon yielding a truncated Kdm6ba protein lacking the entire JmjC domain. *Kdm6ba*$^{-/-}$ 30 hpf embryos lacking the notable maternal contribution (*kdm6ba*^{MZ}) were homozygous viable, fertile, and showed no overt embryonic defects (Fig. 3L-O). *Kdm6ba*^{MZ} animals expressed three times less *kdm6ba* mRNA than wildtype animals (Fig. 3P), reflecting nonsense mediated decay and further suggesting *kdm6ba* loss of function. As with *kdm6bb*^{MZ} animals, qRT-PCR showed that *kdm6ba*-deficiency did not elicit compensatory expression of *kdm6bb*, *kdm6a*, or *kdm6al* transcripts at 30 hpf (Fig. 3P). These results argue against genetic compensation from an H3K27 demethylase but are consistent with the hypothesis that *kdm6ba* and *kdm6bb* are functionally redundant.

Figure 3. Overlapping transcript expression of *kdm6b*-family genes and generation of a *kdm6ba* mutant allele

(A-J) Whole mount in-situ hybridization for *kdm6bb* (A-E) and *kdm6ba* (F-J). Arrowheads denote cardiac expression. *Abbreviations used:* a, atrium; v, ventricle. (K) Schematic showing the *kdm6ba* mutant allele recovered from CRISPR/Cas9 targeted mutagenesis. Deleted base shown in red. (L-O) DIC images of *kdm6ba*^{MZ} embryos at 24 hpf (L and N) and 48 hpf (M and O). (P) qRT-PCR using cDNA generated from 3 separate samples of pooled (n = 10) *WT* and *kdm6bb*^{MZ} embryos at 30 hpf. P-value determined using a Student's two-tailed *t*-test.

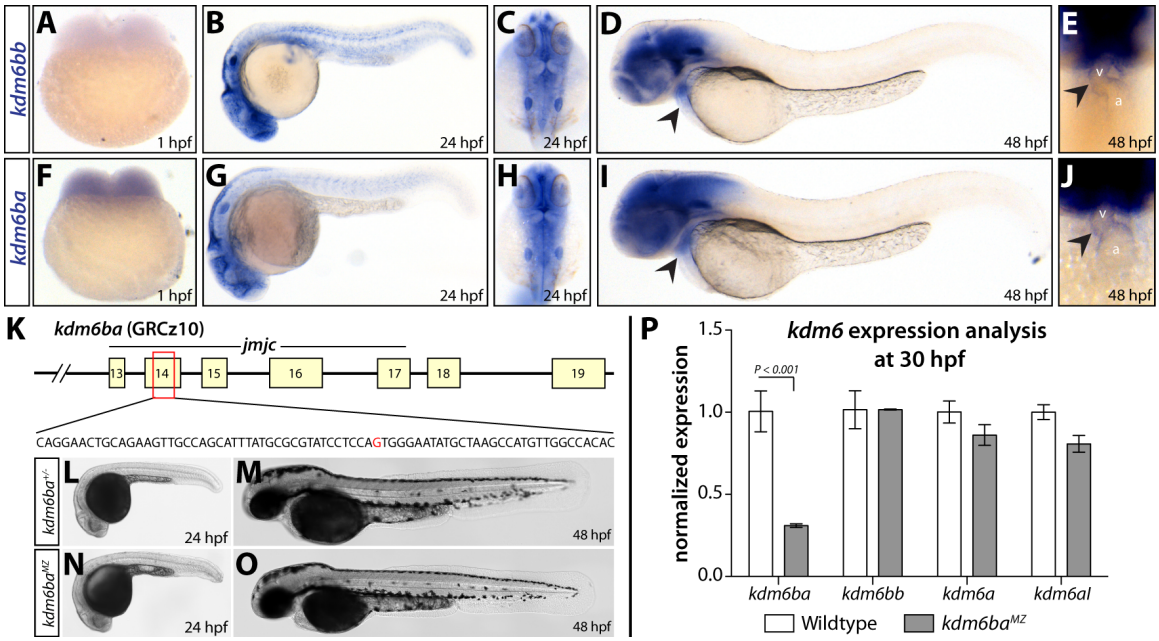

To determine if the H3K27me3 demethylases *kdm6ba* and *kdm6bb* have redundant functions, we next generated *kdm6ba*$^{-/-}$;*kdm6bb*$^{-/-}$ double mutant (or *kdm6b*-deficient) animals. While *kdm6ba*$^{-/-}$;*kdm6bb*$^{-/-}$ fish developed normally over the first three days of development (Fig. S5), they failed to inflate their swim bladder upon hatching and were not viable past 10-12 dpf (Fig. 4A-E). K*dm6b*-deficient larvae also consistently exhibited cardiac edema (Fig. 4D-D') and a craniofacial "slack jaw" abnormality in which the jaw was unable to close (Fig. 4D-D'). *Kdm6ba*$^{-/-}$;*kdm6bb*$^{+/-}$ animals also failed to develop a swim bladder and did not survive to adulthood (Fig. 4C & E). Conversely, *kdm6ba*$^{+/-}$;*kdm6bb*$^{-/-}$ animals were completely viable with no obvious embryonic defects (Fig. 4B & E). Consistent with *kdm6ba* being expressed at three-fold higher levels than *kdm6bb* at 30 hpf (Fig. 4F), this combined dose-dependency suggests that *kdm6ba* has relatively stronger but shared developmental roles with its ohnolog *kdm6bb*.

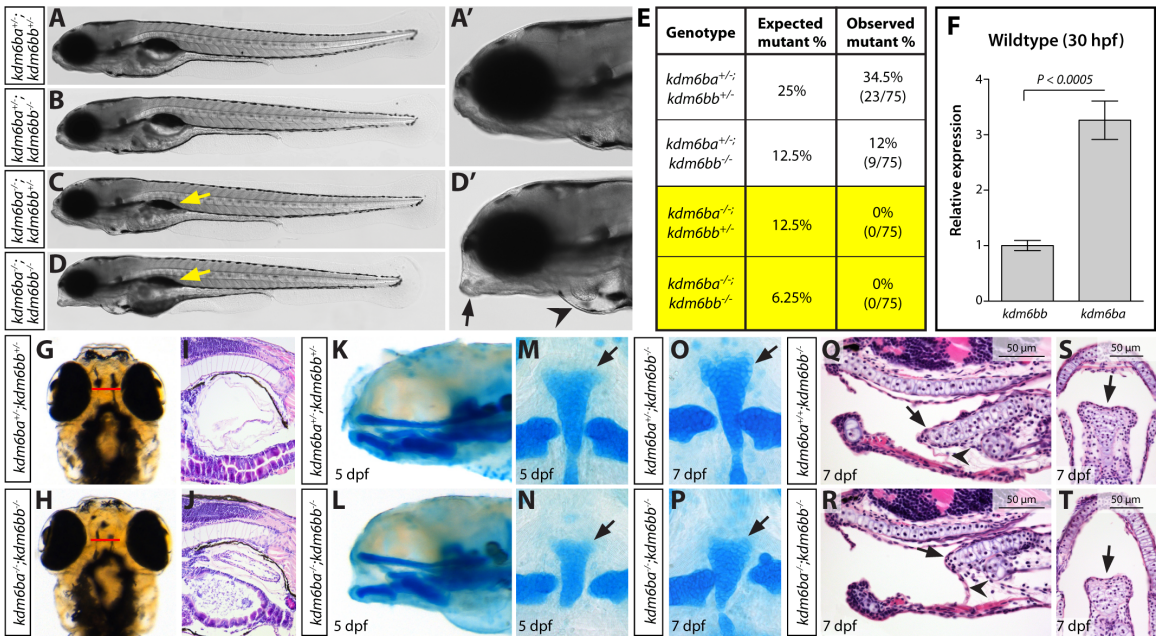

Figure 4. Combined genetic deficiency of *kdm6ba* and *kdm6bb* causes pleiotropic larval development defects

(A-D) Whole mount stitched DIC images of clutch mates. (A' & D') Zoomed image of A and D respectively. (E) Viability table showing the genotype frequencies observed in adult animals derived from a *kdm6ba*$^{+/-}$;*kdm6bb*$^{+/-}$ double heterozygous in cross. (F) qRT-PCR of relative levels of *kdm6ba* and *kdm6bb* transcript in WT fish at 30 hpf. Normalized to *rpl18*. P-value determined with students two-tailed *t-test.* (G&H) Dorsal view of whole-mount embryos. (I&J) H&E sagittal sections showing swim bladder. (K&L) Sagittal whole-mount view of alcian blue staining. (M-P) Flat mount of alcian blue stains showing basihyal cartilage. (Q-T) H&Es showing basihyal cartilage in sagittal (Q&R) and coronal (S&T) sections.

A further analysis of 5 dpf *kdm6ba*$^{-/-}$;*kdm6bb*$^{-/-}$ larvae revealed pleiotropic defects. *Kdm6b*-deficient animals exhibited cranial swelling arising between 4 and 5 dpf (Fig. 4G-H). Hematoxylin and eosin (H&E) staining of paraffin sections confirmed an intact but un-inflated swim bladder in *kdm6ba*$^{-/-}$;*kdm6bb*$^{-/-}$ larvae (Fig. 4I-J). As Kdm6b promotes endochondral bone formation in mice (Zhang et al., 2015), we performed Alcian Blue staining to determine if *kdm6b*-deficient larvae exhibited abnormal cartilaginous bone. While the majority of craniofacial skeletal development was unaffected, *kdm6ba*$^{-/-}$;*kdm6bb*$^{-/-}$ larvae displayed a truncated basihyal cartilage at 5 dpf and 7 dpf that likely accounts for the "slack-jaw" phenotype (Fig. 4K-P). By H&E staining of 7 dpf larvae, we found that that the reduced basihyal in *kdm6b*-deficient larvae contained subjectively

fewer but otherwise normally differentiated chondrocytes and retained associated ligaments (Fig. 4Q-T). These phenotypes and the larval stage lethality of *kdm6ba*$^{-/-}$*;kdm6bb*$^{-/-}$ fish is more consistent with those mouse studies suggesting *Kdm6b* largely functions during later stages of organogenesis rather than during early cell lineage specification (Burgold et al., 2012; Li et al., 2014b; Satoh et al., 2010; Shpargel et al., 2014; Zhang et al., 2015).

Kdm6b proteins promote larval stage cell proliferation associated with heart ventricle trabeculation

We continued our analysis of the cardiovascular system of *kdm6ba*$^{-/-}$*;kdm6bb*$^{-/-}$ fish to determine if they phenocopied *kdm6bb*^{Mo456} animals in any respect. *Kdm6b*-deficient 72 hpf larvae did not display the characteristic aortic arch artery, outflow tract, or ventricular cardiomyocyte defects seen in *kdm6bb*^{Mo456} animals (Fig. 5A-E). Additionally, severe craniofacial defects in morphants at 5 dpf prevented analysis of basihyal cartilage development and reflect the capacity of morpholino-induced off-target effects to mask the presence of specific loss-of-function phenotypes (Fig. S6A-C). Given the disparate collection of *kdm6bb* morphant vs. *kdm6ba*$^{-/-}$*;kdm6bb*$^{-/-}$ phenotypes, we conclude that the *kdm6bb*^{Mo456} fails to accurately portray *kdm6bb* function due to spurious morpholino effects acting alone or in combination with *kdm6bb* transcript knockdown.

Figure 5. *Kdm6ba* and *kdm6bb* redundantly promote cardiac trabeculation
(A&C) Fluorescent imaging of aortic arch arteries in 72 hpf *kdm6b*-deficient and control *Tg(flk:EGFP)* animals. (B&D) Fluorescent cardiomyocyte nuclei at 72 hpf in control and maternal zygotic *kdm6bb*-deficient and control *Tg(cmlc2:DsRed-nuc)* animals counterstained with CT3. (E) Quantification of cardiomyocytes at 72 hpf. (F-G) DIC images of the OFT and ventricle of control and *kdm6b*-deficient embryos at 5 dpf. (H-I) Fluorescent cardiomyocyte nuclei at 5 dpf in control and maternal zygotic *kdm6bb*-deficient and control *Tg(cmlc2:DsRed-nuc)* animals counterstained with CT3. (J-M) H&E stained sagittal sections of 5 and 7 dpf embryos with solid black line indicating trabeculae and dashed yellow line indicating AVC valves. (N-O) Quantification of area and trabeculation index. P-value determined by a Student's two-tailed *t-test*.

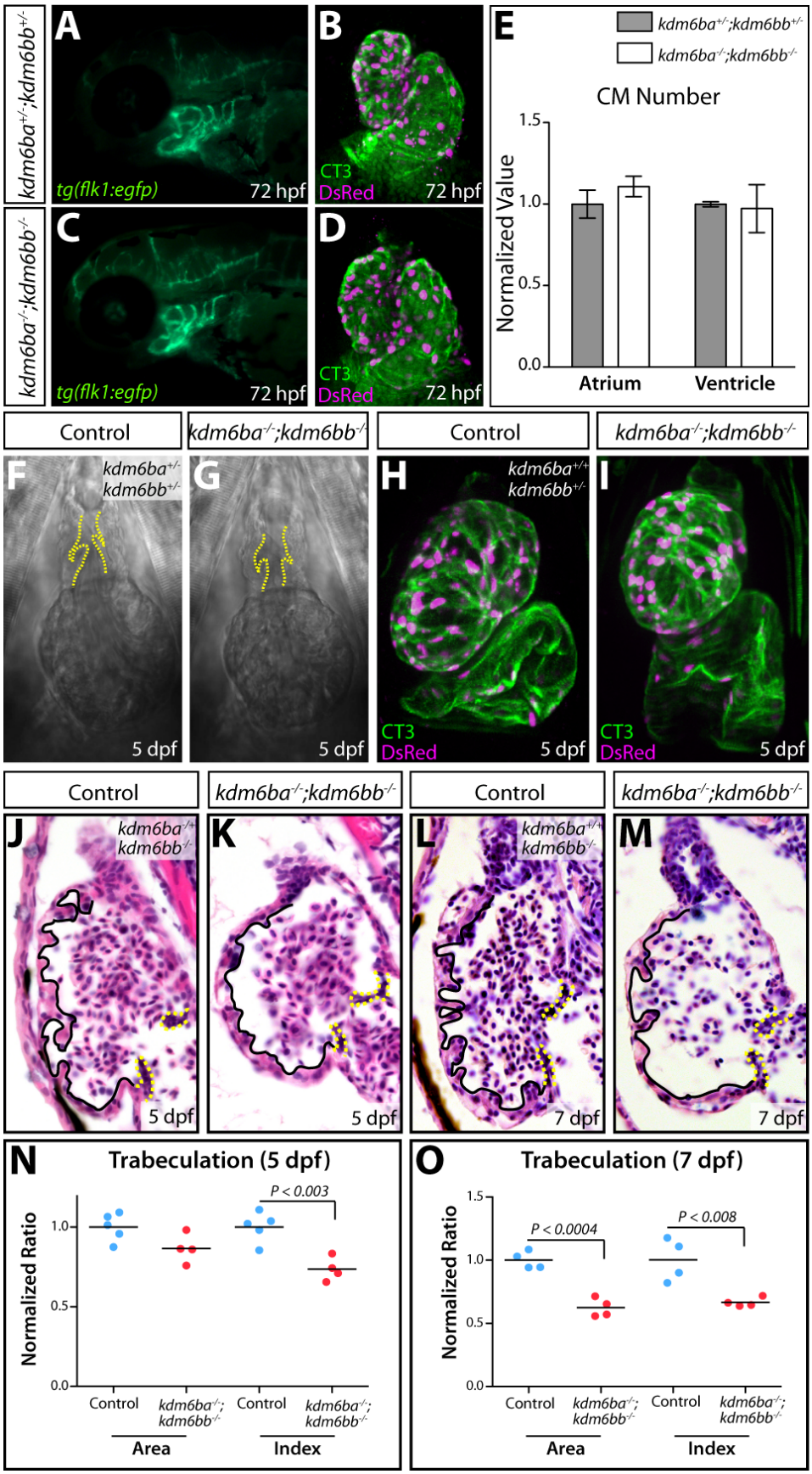
kdm6ba+/-;kdm6bb+/-
kdm6ba-/-;kdm6bb-/-
A
tg(flk1:egfp)
72 hpf
B
CT3
DsRed
72 hpf
C
tg(flk1:egfp)
72 hpf
D
CT3
DsRed
72 hpf
E
kdm6ba+/-;kdm6bb+/-
kdm6ba-/-;kdm6bb-/-
CM Number
Normalized Value
1.5
1.0
0.5
0.0
Atrium
Ventricle
Control
kdm6ba-/-;kdm6bb-/-
Control
kdm6ba-/-;kdm6bb-/-
F
kdm6ba+/-
kdm6bb+/-
5 dpf
G
5 dpf
H
kdm6ba+/+
kdm6bb+/-
CT3
DsRed
5 dpf
I
CT3
DsRed
5 dpf
Control
kdm6ba-/-;kdm6bb-/-
Control
kdm6ba-/-;kdm6bb-/-
J
kdm6ba+/+
kdm6bb-/-
5 dpf
K
5 dpf
L
kdm6ba+/+
kdm6bb-/-
7 dpf
M
7 dpf
N
Trabeculation (5 dpf)
P < 0.003
Normalized Ratio
1.0
0.5
0.0
Control
kdm6ba-/-; kdm6bb-/-
Control
kdm6ba-/-; kdm6bb-/-
Area
Index
O
Trabeculation (7 dpf)
P < 0.0004
P < 0.008
Normalized Ratio
1.5
1.0
0.5
0.0
Control
kdm6ba-/-; kdm6bb-/-
Control
kdm6ba-/-; kdm6bb-/-
Area
Index

The absence of early cardiovascular or other phenotypes in *kdm6ba*$^{-/-}$;*kdm6bb*$^{-/-}$ embryos suggests that *kdm6b* demethylases are not required for early lineage specification events, arguing against models derived from *in vitro* experiments (Burgold et al., 2008; Kartikasari et al., 2013; Ohtani et al., 2011; Ohtani et al., 2013). While the lethality of *kdm6ba*$^{-/-}$;*kdm6bb*$^{-/-}$ animals precluded us from eliminating maternal contributions of both transcripts, only *kdm6ba* transcripts were present prior to zygotic genome activation. To achieve maximum *kdm6b* depletion in the early embryo with respect to both maternal and zygotic contributions, we crossed *kdm6ba*$^{-/-}$;*kdm6bb*$^{+/+}$ females to *kdm6ba*$^{+/-}$;*kdm6bb*$^{-/-}$ males. *Kdm6ba*^{MZ};*kdm6bb*$^{+/-}$ progeny from this cross were phenotypically indistinguishable from *kdm6ba*$^{-/-}$;*kdm6bb*$^{+/-}$ animals, including lacking the severe edema and slack-jaw phenotype of *kdm6ba*$^{-/-}$;*kdm6bb*$^{-/-}$ double mutants (Fig. S6D-F). We conclude that *kdm6b* demethylases do not have unique early embryogenesis roles necessitating maternally contributed transcripts or protein.

Despite the lack of embryonic cardiovascular phenotypes, the presence of cardiac edema in 5 dpf *kdm6ba*$^{-/-}$;*kdm6bb*$^{-/-}$ larvae implied a role for *kdm6b* demethylases in cardiogenesis. Live imaging revealed the hearts of *kdm6b*-deficient 5 dpf larvae produced unidirectional and steady blood flow, consistent with their normal-appearing OFT and OFT valve (Movie S2, Fig. 5F-G). However, *kdm6ba*$^{-/-}$;*kdm6bb*$^{-/-}$ larvae had a smaller and more spherically-shaped ventricle, which was also apparent by whole mount staining for cardiac troponin (CT3) and DsRed in a *Tg(cmlc:DsRed-nuc)* background (Fig. 5H-I). To further characterize ventricle morphology in *kdm6b*-deficient animals, we analyzed H&E stained sagittal sections of 5 and 7 dpf larvae. 5 dpf *kdm6ba*$^{-/-}$;*kdm6bb*$^{-/-}$ larvae had

a smaller and more rounded ventricle with dramatically reduced number and size of trabecular projections that normally form on the outer curvature of the zebrafish ventricle between 3 and 4 dpf (Liu et al., 2010) (Fig. 5J-K). The OFT, atria, and atrioventricular canal (AVC) valves were notably unaffected. The specific trabeculation defect was further apparent at 7 dpf (Fig. 5L-M). Quantitatively, *kdm6b*-deficient larvae first showed diminished trabeculation at 5 dpf followed by reduced ventricular muscle at 7 dpf (Fig. 5N, O, Fig. S7). We conclude that *kdm6ba* and *kdm6bb* share a specific role in promoting early stages of zebrafish cardiac trabeculation.

By immunostaining sectioned larvae, we found that myosin heavy chain (MHC, recognized using the pan-myocardial MF20 antibody) and S46 (atrial cardiomyocyte-specific) were expressed normally in 5 dpf *kdm6ba*$^{-/-}$;*kdm6bb*$^{-/-}$ larval hearts (Fig. 6A-D'). Therefore, the diminished cardiac trabeculation in *kdm6b*-deficient larvae did not reflect an altered chamber identity. CT3 antibody staining further confirmed that ventricular cardiomyocytes of *kdm6*-deficient larvae were differentiated and formed myofibrils (Fig. 6B-B' and D-D'). Finally, we used the Tg(*flk1:EGFP*) reporter line and anti-GFP staining to determine that the endocardium of *kdm6b*-deficient embryos was present and maintained its epithelial organization (Fig. 6E'-F'). Collectively, we conclude that Kdm6b is not required for the specification or differentiation of endocardial and myocardial cells and therefore that the trabeculation defects in *kdm6b*-deficient larvae represents a direct role of Kdm6b in trabecular growth and/or morphogenesis.

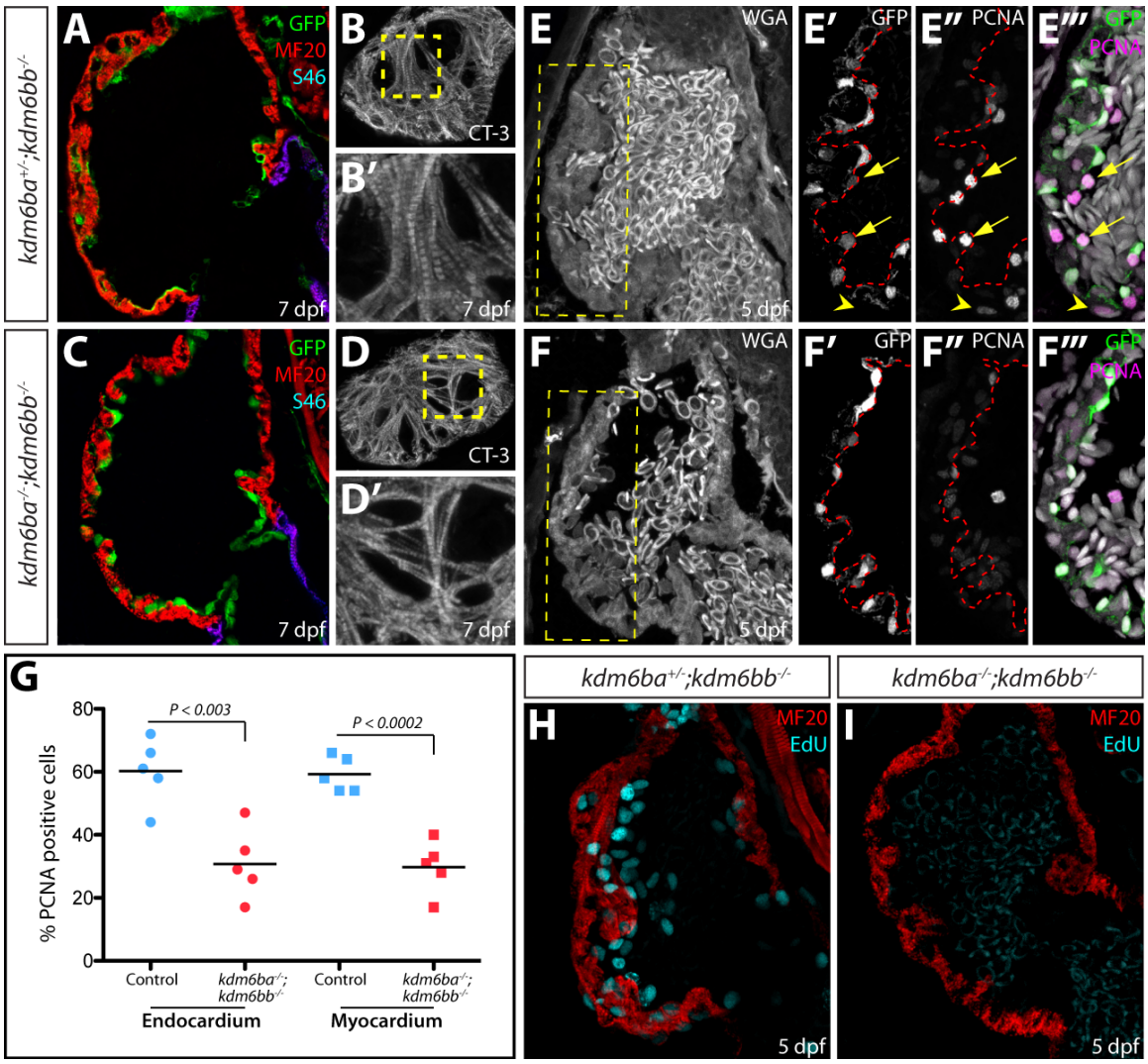

Figure 6. *Kdm6b* proteins enable coordinated endocardial and myocardial proliferation associated with early larval ventricle maturation.
(A-C) Immunofluorescence images of 5 dpf control and *kdm6b*-deficient *Tg(flk:EGFP)* embryos stained with anti-MF20 and anti-GFP antibodies. (B&D) anti-CT3 antibody staining showing superficial sections of the heart at 5 dpf. (E-F') Immunofluorescence images of 5 dpf sections of control and kdm6b-defieient *Tg(flk:EGFP)* embryos stained with wheat germ agglutinin (WGA), anti-GFP, and anti-PCNA antibodies. Yellow boxed indicate zoomed regions in E'&F', arrows indicate PCNA-positive endocardial cells and arrowheads indicate PCNA-positive myocardial cells. (G) Quantification of PCNA positive cells in control and kdm6b-deficient embryos at 5 dpf. P-value determined via students two-tailed *t-test*. (H-I) EdU labeling along with anti-MF20 immunofluorescence in 5 dpf control and *kdm6b*-deficient embryos.

Myocardial proliferation around the time of larval hatching is required for the initiation of trabeculation in zebrafish (Liu et al., 2010). To determine if cardiac proliferation was impaired in *kdm6b*$^{-/-}$;*kdm6bb*$^{-/-}$ larvae, we immunostained sections for proliferating cell

nuclear antigen (PCNA), a marker of cycling cells (Fig. 6E-F'"). *Kdm6b*-deficient animals displayed a near 50% reduction of both PCNA positive endocardial and myocardial cells at 5 dpf (Fig. 6G). This striking decrease in proliferative ventricular cells in *kdm6ba*$^{-/-}$;*kdm6bb*$^{-/-}$ larvae was also apparent using 5-ethynyl-2-deoxyuridine (EdU) incorporation assays to monitor cells that passed through S-phase between 4 and 5 dpf (Fig. 6H-J). In contrast, the normal number of cardiomyocytes in 72 hpf *kdm6ba*$^{-/-}$;*kdm6bb*$^{-/-}$ fish (Fig. 5B and D) showed that embryonic cardiac proliferation was not disrupted in the absence of Kdm6b. We conclude that *kdm6bb* and *kdm6ba* redundantly promote trabecular outgrowth by enabling the coordinated endo- and myocardial proliferation that accompanies the larval stage initiation of trabeculation.

Kdm6b directs global H3K27me3 demethylation in cardiomyocytes coupled with the initiation of myocardial trabeculation

Kdm6b's role in trabecular proliferation presumably involves modifying chromatin landscapes to support gene activation to enable cell cycle entry and/or prevent cellular quiescence. To explore if Kdm6b regulates global changes in H3K27me3 levels during heart ventricle maturation, we immunostained sections of 3 dpf control and *kdm6ba*$^{-/-}$;*kdm6bb*$^{-/-}$ larvae with anti-H3K27me3 antibodies. Strikingly, H3K27me3 levels varied widely between different cell types. Endocardial cells consistently showed very low H3K27me3 levels relative to the myocardium (Fig. 7A-C'). Myocardial cells located on the outer ventricular surface consistently had the highest H3K27me3 signal with more modest levels in myocardial cells undergoing trabeculation adjacent to the ventricular cavity (Fig. 7A-C'). *Kdm6b*-deficient larvae had modestly higher H3K27me3 levels in

many myocardial but not endocardial cells (Fig. 7D-F'). This myocardial-specific role of Kdm6b in moderating cell-wide levels of H3K27me3 was consistent with normal amounts of global H3K27me3 seen by Western blotting 5 dpf whole *kdm6ba*$^{-/-}$;*kdm6bb*$^{-/-}$ larval lysates (Fig. 7G). We conclude that H3K27me3 levels are dynamically regulated in a global in addition to locus- or even nucleosome-specific manner during cardiac development. Further, Kdm6b broadly removes H3K27me3 marks on nucleosomes to temper the overall H3K27me3 load in trabeculating myocardial cells and support their cell cycle entry.

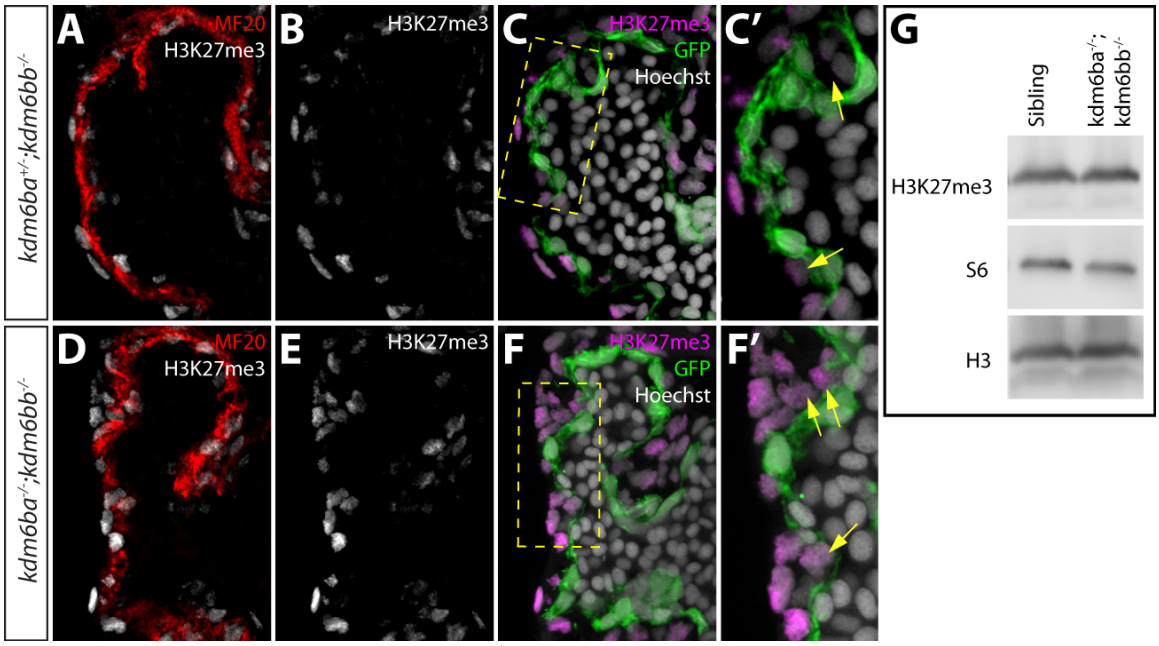

Figure 7. H3K27me3 is retained in *kdm6ba*$^{-/-}$;*kdm6bb*$^{-/-}$ trabeculating cardiomyocytes
(A-C') Immunofluorescence images of 3 dpf control *Tg(flk:EGFP)* embryos stained with anti-MF20, anti-GFP, and anti-H3K27me3 antibodies (D-F') Immunofluorescence images of 3 dpf *kdm6b*-deficient *Tg(flk:EGFP)* stained with anti-MF20, anti-GFP, and anti-H3K27me3 antibodies. (G) Western blot of single animal lysates at 5 dpf.

DISCUSSION

Our investigation of histone demethylases *kdm6ba* and *kdm6bb* during zebrafish development provides two distinct insights. First, we provide a detailed "mutant vs.

morpholino" reverse genetic analysis of a previously unstudied zebrafish gene family that reinforces the need to carefully control morpholino studies to avoid making conclusions based on spurious yet tissue-specific phenotypes. Further, we show how duplicated orthologous genes with retained overlapping expression can obscure loss-of-function phenotypes due to simple non-compensatory genetic redundancy. Second, we show that Kdm6b-family demethylases have pleiotropic roles during larval organ development rather than during embryonic cell specification or the establishment of initial organ "frameworks". Most notably, Kdm6b demethylases specifically contribute to cardiogenesis by supporting augmented cellular proliferation associated with the initiation of ventricular trabeculation during larval metamorphosis. Heightened global H3K27me3 levels in trabeculating cardiomyocytes of *kdm6b*-deficient fish suggests that Kdm6b has a widespread role reversing H3K27me3 repressive marks to support cardiomyocyte cell cycle entry.

***Kdm6b* comparative reverse genetic studies provide an example of off-target morpholino effects and non-compensatory redundancy between duplicated genes**

Recent reports using zebrafish have highlighted cases of phenotypic discrepancy between genetic mutants and antisense mediated morphants (Kok et al., 2014; Law and Sargent, 2014; Rossi et al., 2015). The advent of rapid genome editing methods enabled by CRISPR/Cas9 has led to many more anecdotal examples that are widely discussed and debated informally in the field. Ultimately, we conclude that the distinct embryonic cardiovascular defects we observed in our *kdm6bb* morphants largely result from off-target effects. We systematically eliminated alternative explanations to account for the

lack of similar phenotypes upon *kdm6bb* genetic deficiency including maternal contributions, compensation by increased expression of other H3K27me3 demethylases, or inadvertent morpholino targeting of the ohnologous *kdm6ba* transcript. Most strikingly, *kdm6ba*$^{-/-}$;*kdm6bb*$^{-/-}$ double mutant animals have largely distinct pleiotropic phenotypes from those observed in *kdm6bb*^{Mo456}, animals. Further, a single *kdm6bb* morpholino produces identical development defects in *kdm6bb*$^{-/-}$ zebrafish that lack the target sequence from their genomes.

While our *kdm6bb* morphants had the potential to be highly misleading, we hesitate to conclude the phenotypes entirely misrepresent Kdm6bb function. Clearly, the morpholinos effectively knocked down *kdm6bb* transcripts. Therefore, the phenotypes could represent a synergistic effect between *kdm6bb* loss-of-function and either general or unknown specific off-target effects of the morpholinos. A similar "synthetic" phenotype could explain the incongruous *egfl7* morpholino/mutant phenotypes with or without a programmed compensatory mechanism (Rossi et al., 2015). Further, our *kdm6bb*$^{-}$ and/or *kdm6ba*$^{-}$ alleles could provide some residual protein activity in spite of the considerable nonsense mediated decay and the expected complete loss of JmjC catalytic domains, particularly if hypothetical truncated products unexpectedly retained non-demethylase dependent activity (Miller et al., 2010; Shpargel et al., 2014). Therefore, instances of partial phenocopy may blur the line between off-target and cite-specific phenotypes and demonstrate how cautious morphant studies can empower initial observation and validation experiments.

Nevertheless, our results reinforce the value of using genetic mutants to confirm experimental results obtained through morpholino-mediated knockdown studies. This is especially true when, as in our case, there is limited *a priori* expectation of the "true", if any, loss-of-function phenotype and the inclination becomes to use excess or additional morpholinos until a specific defect is uncovered. Therefore, our work supports existing guidelines that rescue experiments are essential to support claims of morpholino specificity (Eisen and Smith, 2008). Of note, we were unable to rescue the *kdm6bb*^{Mo456} morphants by co-injected *kdm6bb* mRNA (negative data not shown). Unfortunately, however, rescue experiments are not always feasible with highly dose-sensitive transcripts or those with complex expression patterns. Finally, even "successful" rescue experiments can lead to specious conclusions (Law and Sargent, 2014). Given the ease of zebrafish targeted mutagenesis afforded by CRISPR/Cas9, including multiplex targeting and F0 screening (Jao et al., 2013) and efficient homologous recombination (Hoshijima et al., 2016), we suggest inherently more rigorous genome editing approaches should be used whenever possible for zebrafish gene function studies.

Our results also are fully consistent with the proposal that the lack of phenotypes being observed in homozygous mutant zebrafish can be attributed to a high degree of redundancy built into the zebrafish genome (Lawson, 2016). Zebrafish, having undergone a whole genome duplication event, may be more buffered against the effects of a single gene mutation than other vertebrate models. Our combined genetic analysis of *kdm6bb* and *kdm6ba* provides a clear example of how redundant functions between ohnologous genes, without involving any compensatory network, can obscure the effects of single

gene mutation. We suggest this possibility be thoroughly examined for other ohnologous gene pairs, especially when expression patterns largely overlap.

Histone demethylases *kdm6ba* and *kdm6bb* share likely conserved roles in vertebrate organ maturation

Despite *kdm6ba* and *kdm6bb* redundancy and largely similar expression patterns, *kdm6ba* shows increased maternal deposition and 3-fold higher levels of expression at 30 hpf, suggesting it exerts a greater influence over development. In support, *kdm6ba*$^{+/-}$;*kdm6bb*$^{-/-}$ animals are completely viable while *kdm6ba*$^{-/-}$;*kdm6bb*$^{+/-}$ animals do not survive past larval stages. The reduced expression and maternal deposition of *kdm6bb* is likely the result of accumulated loss-of-function mutations within its respective regulatory regions (Bailey et al., 1978; Li, 1980; Takahata and Maruyama, 1979; Watterson, 1983). However, given *kdm6bb* has not have become completely silenced, a competitive advantage, at least outside a laboratory setting, apparently is conferred by retaining both *kdm6ba* and *kdm6bb*.

Independently developed *Kdm6b* presumptive null alleles in mice are either pre-implantation (Ohtani et al., 2013) or perinatal (Burgold et al., 2012; Li et al., 2014b; Satoh et al., 2010; Shpargel et al., 2014; Zhang et al., 2015) lethal. Our studies are consistent with the latter publications and suggest that Kdm6b proteins primarily contribute to organ maturation rather than early cell fate specification, in contrast to some predictions (Kartikasari et al., 2013; Ohtani et al., 2011). These roles are likely evolutionarily conserved as the pleiotropic defects we observe in *kdm6b*-deficient

zebrafish are reminiscent of those reported in mice. For example, *kdm6ba*$^{-/-}$;*kdm6bb*$^{-/-}$ fish display stunted craniofacial bone formation and *Kdm6b*-deficient mice develop skeletal dwarfism during early stages of bone development (Zhang et al., 2015). However, a further characterization is necessary to determine if Kdmb6 proteins have restricted roles in certain bones (e.g. the notably truncated basihyal cartilage in *kdm6b* double mutants) or widely contribute to bone formation, as seen in mice. Similarly, the swim bladder defects we observed in our *kdm6b*-deficient zebrafish may parallel lung structure and respiration defects in *Kdm6b* KO mice (Li et al., 2014b) given the evolutionary homology between the teleost swim bladder and lungs of terrestrial vertebrates (Perry et al., 2001; Winata et al., 2009).

Kdm6b-deficient zebrafish complete the initial stages of cardiac development, forming discrete heart chambers, an outflow tract, and valves. As such, earlier events including the generation and expansion of cardiac progenitors, specification and differentiation of endocardial and myocardial cells, and initial heart tube extension and looping do not require Kdm6b. This conclusion controverts reported roles of *Kdm6b* in mesodermal and cardiovascular differentiation derived from embryonic stem cell studies (Ohtani et al., 2011). Importantly, our zebrafish studies are consistent with the preponderance of *Kdm6b* loss-of-function mouse models that survive to late fetal stages, indicating the overt cardiogenesis is not substantially Kdm6b-dependent.

While our study shows that combined *kdm6ba* and *kdm6bb* are not required for early embryonic development, they may have roles masked by further redundancy with *kdm6a*

(*Utx*) genes. While mouse genetic studies show that *Kdm6a* has essential developmental functions, including in mesoderm lineage differentiation and cardiogenesis (Lee et al., 2012; Shpargel et al., 2012; Wang et al., 2012; Welstead et al., 2012). *Kdm6b* and *Kdm6a* are proposed to function redundantly during thymocyte differentiation (Manna et al., 2015). While both have H3K27-demethylase activity and can associate with conserved components of chromatin organizers such as Brg1 (Miller et al., 2010), the distinct phenotypes observed in *Kdm6a* and *Kdm6b* mouse models along with conflicting reports of shared functional interactions with other chromatin modifiers such as the H3K4 methyltransferase MLL2 (De Santa et al., 2007; Issaeva et al., 2007; Williams et al., 2014), suggest only a partial redundancy that is context dependent. Zebrafish contain two *Kdm6a* orthologs, *kdm6a* and *kdm6al*. While neither gene has been explored genetically, morpholino studies implicate both *kdm6a* and *kdm6al* in *hox*-dependent body plan patterning, craniofacial cartilage development, heart looping, and brain morphology (Lan et al., 2007; Van Laarhoven et al., 2015). However, given concerns about morpholino specificity, reverse genetic studies examining *kdm6a* and *kdm6al* individually, together, and combined with our *kdm6b* alleles are necessary to validate and extend these studies.

Histone demethylases *kdm6ba* and *kdm6bb* promote proliferation coupled with the initiation of cardiac trabeculation

Trabeculation of the zebrafish ventricle initiates around 72 hpf with the specification of a small number of trabeculating cardiomyocytes that separate from the otherwise single cell-thick outer myocardial layer (Gupta and Poss, 2012; Han et al., 2016; Liu et al., 2010; Peshkovsky et al., 2011). These specialized trabeculating cardiomyocytes then

clonally expand during early larval stages to form extensive ridge-like cardiac trabeculae that protrude into the ventricular cavity. The initial phase of trabeculation driven by neuregulin/ErbB2 signaling (Han et al., 2016; Liu et al., 2010; Peshkovsky et al., 2011) does not depend on Kdm6b as we saw that small groups of two cell layer thick myocardium still form in *kdm6b*-deficient fish. Instead, Kdm6b is required for the subsequent boost of proliferation at larval hatching (around 96 hpf) seen in trabeculating myocardial cells (Gupta and Poss, 2012; Han et al., 2016; Liu et al., 2010) as well as adjacent endocardium that concomitantly expands to enshroud the forming trabeculae.

Our H3K27me3 immunostaining studies suggest Kdm6b generally relaxes the repressive epigenetic state of trabeculating cardiomyocytes to enable their transcriptional response to growth-promoting mitogens rather than activating a specific subset of genes that drive cell cycle entry. H3K27me3 are notably lower in both endocardial cells and trabeculating myocardial cells compared to the outer wall cardiomyocytes that forms a thin, incompletely differentiated "primordial" layer retained through juvenile stages of heart development (Gupta and Poss, 2012; Han et al., 2016). In contrast, high H3K27me3 levels are maintained in trabeculating cardiomyocytes lacking Kdm6b. We propose Kdm6b activation, possibly transcriptionally as seen during fin regeneration and immune responses (Manna et al., 2015; Stewart et al., 2009) during specification of trabeculation cardiomyocytes globally removes repressive H3K27me3 marks that otherwise restrain cardiomyocytes from responding to mitogenic signals. As endocardial H3K27me3 levels are very low in both wildtype and *kdm6b*-deficient fish, the endocardial proliferation defect upon *kdm6b* depletion is likely to be a secondary defect reflecting complex

interplay between ventricular endocardium and myocardium that coordinates these neighboring cells' activities during trabeculation (Samsa et al., 2013).

As an alternative to a global H3K27me3 dynamics model, Kdm6b may provide an "epigenetic"-reprogramming component of transcriptional switches acting at a discrete set of specific target genes. Of potential relevance, the Kdm6b-cooperating BAF chromatin remodeling complex (Miller et al., 2010) enables trabeculation in mice by repressing endocardial transcription of the trabeculation-suppressing Adamts1 matrix protease (Stankunas et al., 2008). A further possibility is that Kdm6b acts in both myocardial and endocardial cells to integrate a systemic signal that widely coordinates organ maturation events coupled to larval metamorphosis. Thyroid hormone is one immediate candidate that is upregulated upon hatching (Chang et al., 2012) and is a known cardiomyocyte mitogen in mammals (Chattergoon et al., 2012; Kenessey and Ojamaa, 2006; Li et al., 2014a). Distinguishing between each of these possibilities awaits mosaic studies or cell type-specific targeting of *kdm6b* genes. Regardless, the seemingly isolated cardiac developmental role of Kdm6b in promoting cardiomyocyte proliferation establish these histone demethylases and downstream target genes as candidate genes for congenital heart defects of the ventricle, including hypoplastic left ventricle syndrome.

The recognition that differentiated cardiomyocytes can re-acquire robust proliferative ability during heart regeneration in both zebrafish and mice (Jopling et al., 2010; Porrello et al., 2011; Poss et al., 2002) and that humans retain some proliferative capacity of cardiomyocytes during childhood (Bergmann et al., 2009; Haubner et al., 2016; Ye et al.,

2016) has focused efforts on understanding these mechanisms to recapitulate them for injury repair, notably for congestive heart failure. The role of Kdm6b histone demethylases in developmentally timed cardiomyocyte (but not cardiac progenitor) proliferation suggests the reversal of epigenetic H3K27me3 silencing marks may be essential aspect of innate heart regeneration and a promising path to augment therapeutically delivered cardiomyocytes for heart disease.

MATERIALS AND METHODS

Zebrafish

The University of Oregon Institutional Animal Care and Use Committee (IACUC) approved and monitored all zebrafish procedures following the guidelines and recommendations outlined by the Guide for the Care and Use of Laboratory Animals (National Academic Press). The following established lines were used in this study: *Tg(cmlc2:dsRedExpress-nuc)* (Takeuchi et al., 2011)*, Tg(myl7:EGFP-Hras)s883* (Chi et al., 2008)*, Tg(kdrl:EGFP)* (Jin et al., 2005).

CRISPR-Cas9 generation of mutant alleles

CRISPR-Cas9-mediated mutagenesis was used to generate targeted deletions within the putative Jmjc domains of both *kdm6ba* and *kdm6bb*. Guide RNAs were generated following methods adapted from (Bassett et al., 2013). Guide oligonucleotide sequences were obtained from Integrated DNA Technologies: 5'-AATTAATACGACTCACTATA-NNNNNNNNNNNNNNNNNNN-GTTTTAGAGCTAGAAATAGC-3', with a T7 promoter sequence followed by a series of Ns indicating the targeting sequence. The

guide RNA targeting sequences for *kdm6ba* and *kdm6bb* were 5'-GCTTAGCATATTCCCACTGG-3' and 5'-CAGGTGGAAGGC-GCAGTTGC-3' , respectively. Guide oligonucleotides were annealed to a generic gRNA scaffold (5'-GATCCGCACCGACTCGGTGCCACTTTTTCAAGTTGATAACGGACT-AGCCTTATTTTAACTTGCTATTTCTAGCTCTAAAAC-3') and extended using Phusion polymerase (New England Biolabs) followed by column-based purification.

In vitro transcription of gRNAs was performed using the Megascript T7 Transcription Kit (Thermo Fisher) and purified via RNA Clean & Concentrator column (ZYMO Research). Cas9 mRNA was *in vitro* transcribed from Addgene plasmid 46757:pT3TS-nCas9n (Jao et al., 2013) using the T3 mMessage mMachine kit (Ambion). Cas9 mRNA and gRNA were combined and diluted to a final concentration of 100 ng/µl in Danieau's buffer and phenol red. We injected 1-3 nl of the Cas9/gRNA mix into the developing embryo at the one-cell stage. Fish raised from injected embryos (see below) were screened for mutations by amplicon sequencing (Sequetech). Founders carrying isolated mutant alleles were outcrossed to wildtype fish to isolate stable germline transmitting lines used for subsequent crosses and phenotypic analyses.

Morpholino microinjections

Morpholinos (Gene Tools) were injected into single-cell embryos at the indicated concentrations and in volumes of 2-3 nl.

Mo 4: 5'-CCCCCTATTGTCAGACTTACCATTT-3'

Mo 5: 5'-CCACCTGAAGACAAACACACTCAGT-3'

Mo 6: 5’-TCTGATCTAAAACATACTTTTCACA-3’

Control Mo: 5’-CCTCTTACCTCAGTTACAATTTATA-3’

Genotyping *kdm6ba* and *kdm6bb* mutant alleles

The *kdm6ba* allele was assessed by PCR using primers 5’-TGGCACAAACATTGACCTGT-3’ and 5’-CATCATGGACAGCAAACCAC-3’ followed by restriction digest with NcoI (NEB). The *kdm6bb* mutant allele was assessed by PCR using primers 5’-CTCAAAGCAGAAAGCTGTTGG-3’ and 5’-GTGTGGCCAACATGACTCAG-3’.

In situ hybridization

In situ hybridizations were performed as described by Thisse and Thisse (Thisse and Thisse, 2008b). Stained embryos were dehydrated into 100% methanol and stored at -20°C for overnight. Embryos were then rehydrated and allowed to equilibrate in 100% glycerol at 4°C. Embryos were imaged using Rottermann contrast optics on a Leica M165 FC stereomicroscope. In situ hybridization probes were synthesized from PCRII-based plasmids (Life Technologies) containing a cloned cDNA amplicon. PCR products were obtained from pooled samples of embryonic zebrafish cDNA using the following primers: *kdm6bb 5’-CCACTTGACCAACTGCCTTGCAAAAC-3’*, 5’-CTGAAAACACACTCCGAGAGGTATCGC-3’; *kdm6ba* 5’-TGGCACAAACATTGACCTGT-3’, 5’- GTGTGAGGGAAAGGGATGAG-3’. Plasmids were linearized by digestion with NotI and BamHI respectively. Digoxigenin-11-dUTP (Roche) labeled RNA synthesis was performed using Sp6 (for *kdm6bb* probe)

or T7 (for *kdm6ba* probe). DIG-labeled probes were DNase treated prior to LiCl precipitation and resuspension in RNase/DNase free water.

Whole mount immunofluorescence and imaging

Immunostaining for GFP was performed as previously described (Akerberg et al., 2014). Staining for CT3 (Developmental Studies Hybridoma Bank), Eln2 (generous gift from the Burns lab), dsRed (Clontech) and S46 (Developmental Studies Hybridoma Bank) was performed using a protocol adapted from Zhou et al. (Zhou et al., 2011). Embryonic hearts were arrested in diastole with 0.5M KCl and fixed overnight at 4°C in phosphate-buffered saline (PBS) containing 4% paraformaldehyde. The following day, embryos were washed in PBS and dehydrated through a methanol series. Embryos in 100% methanol were stored at -20°C for at least 24 hours prior to rehydration into PBS containing 0.1% Tween-20 (PBST). Embryos were then blocked with PBS containing 1% BSA, 1% Triton X-100, 0.1% DMSO for four hours. Embryos were incubated with primary antibodies diluted in block solution for 4-5 hours at room temperature with gentle agitation followed by three 20' washes in PBS containing 0.5% Triton X-100 (PB0.5X). Alexa-conjugated secondary antibodies (Invitrogen) were diluted 1:1000 in PB0.5X and incubated with embryos for 2-3 hours at room temperature with gentle agitation. Lastly, embryos were washed and stored in TBST (20 mM Tris pH 7.5, 150 mM NaCl, 0.5% Triton X-100). Primary antibodies CT3, Eln2, dsRed, and S46 were used at dilutions of 1:500, 1:1000, 1:500, and 1:250 respectively. Immunostained embryos, as well as transgenic embryos with native fluorescence, were mounted in low melt agarose and imaged with either a Leica M165 FC stereomicroscope, Nikon Eclipse

Ti inverted fluorescence microscope, or a Leica SD6000 spinning disk confocal. 10x DIC images were taken using a Nikon Eclipse Ti inverted microscope and stitched together using NIS Elements Advanced Research (Ar) software.

Live imaging

Embryos at the desires stage were anesthetized in Tricaine (Western Chemical) and immobilized in 0.75% LMP agarose in embryo media (EM). Embryos were imaged on a glass bottom FluoroDish (World Precision Instruments) using a Nikon Eclipse Ti inverted microscope with Hamamatsu C11440 Orca-Flash2.8 camera.

Quantification

Cell quantification: Cardiomyocyte quantification was performed on Tg(myl7:dsRed-nuc) transgenic embryos that were fixed overnight in PBS and 4% paraformaldehyde. Embryos were then immediately stained for dsRed and CT3 following the above protocol. Embryos were then mounted in low melt agarose and their heads removed to provide an unobstructed view of the heart. Mounted embryos were imaged with a Leica SD6000 spinning disk confocal. Image stacks were processed and analyzed using the ImageJ (NIH) software package.

Tissue quantification: Area measurements of trabeculated muscle located between OFT and the atrioventricular canal (AVC) were made using ImageJ measurement tools. Trabeculation index values were obtained by measuring the perimeter of the interior (trabecular) and exterior of the ventricle (ImageJ) and assigning a normalized value based on their relationship to one another.

Skeletal staining

Alcian Blue staining was performed as previously described (Walker and Kimmel, 2007), and imaged with either the Leica M165 FC stereomicroscope (whole mount) or Leica upright fluorescent microscope (flat mount).

Histological sectioning and immunostaining

Paraffin sections were processed following procedures developed for dissected mouse hearts (Akerberg et al., 2015). Hematoxylin and eosin staining on paraffin sections was performed using conventional reagents and methodology (Ricca Chemical Company). For immunostaining paraffin sections, slides were de-paraffinized using Xylenes and rehydrated into distilled water using a series of graded ethanol washes. Antigens were retrieved by either 1) pressure-cooking for 10' in 1 mM EDTA and 0.1% Tween-20 (CT3, PCNA, MF20, EGFP, and DsRed antibodies) or 2) 10' incubation in 0.25% trypsin solution (H3K27me3 antibody). Slides were blocked for 1 hour in either milk (10% dried milk, 1x PBS, 0.1% Tween-20) or 10% NGS in PBS (for H3k27me3). Primary antibodies were diluted 1:500 (or 1:50 for anti-MF20) in their respective block solution and incubated overnight at 4°C. Slides were then washed 5 x 10' in PBST (1x PBS with 0.1% Tween-20). Slides were then incubated with Alexa-conjugated secondary antibodies diluted 1:1000 in block solution for 1 hr. Slides were then washed 3 x 10' in PBST. To label nuclei, slides were submerged 5' in Hoechst diluted 1:5000 in PBST. Slides were washed in PBST and mounted with Fluorogel (Electron Microscopy Sciences).

Histological slides were imaged with a Leica upright fluorescent microscope or an Olympus Fluoview FV1000 BX61 confocal microscope.

5-ethynl-2-deoxyuridine labeling

Fish were incubated with EdU (Life Tech) at a concentration of 0.1 mg/ml in embryo media for 12-15 hours prior to harvest at 5 dpf. Embryos were then harvested and processed into paraffin sections as described above. EdU Click-It reactions (Life Tech) were performed prior to antibody staining and kept in the dark until imaging.

Quantitative reverse transcription polymerase chain reaction (qRT-PCR)

cDNA was synthesized using SuperScript III (Life Technologies) with Trizol-isolated RNA harvested from pooled embryos (5-10 embryos per pool). qRT-PCR was performed using KAPA SYBR FAST qPCR master mix reagents (Kapa Biosystems). Relative mRNA expression was normalized using *rpl18* to calculate ΔCTs (threshold cycles). Transcript levels were compared using a ΔΔCT approach and two-tailed Student's t-tests to determine significance. qPCR primer sequences: *kdm6bb* 5'-GCATGGCGTGGACTATCTG-3', 5'-CGTGAATCATAGGGACGATTG-3'; *kdm6ba* 5'-GCCCAAACCTCTCCAATGTA-3', 5'-GTGTGAGGGAAAGGGATGAG-3'; *kdm6a* 5'-ACATAAACATTGGCCCTGGA-3', 5'-GCCACCAAGATCCCATTAGA-3'; *kdm6al* 5'-CACAACAACTTCTGCGCTGT-3', 5'-CCTCGTACAGGTCCTCCAGA-3'; *rpl18* 5'- CCGAGACCAAGAAATCCAGA -3', 5'- GAGGCCAGCAGTTTCTCTTG-3'.

BRIDGE TO CHAPTER III

The work in Chapter II demonstrates that Kdm6b demethylases are required for late stage cardiac development in zebrafish. These results provide valuable insights into the general biological significance of H3K27 demethylases and solidify the zebrafish model as a viable platform for further epigenetic investigation. Beyond development, our model provides a tool with which to probe Kdm6b's potential involvement in adult tissue regeneration. Specifically, the requirement of Kdm6b demethylases for cardiac maturation and proliferation lends credence to the hypothesis that they may also be involved in cardiac regeneration. The lethality of *kdm6b*-deficient animals, however, prevents the use of these tools for immediate *in vivo* assessment of Kdm6b function during regeneration. In Chapter III, I describe the creation and utility of novel transgenic tools for spatiotemporal control of transgene expression in both embryonic and adult zebrafish. While the intent was to utilize these tools to achieve RNAi-mediated knockdown of Kdm6b-demethylases in the adult zebrafish, this aspect of the project did not prove fruitful. However, the novel transgenic system I detail in Chapter III provides effective and useful tools that we hope other investigators will take advantage of in their research.

CHAPTER III

SPATIAL AND TEMPORAL CONTROL OF TRANSGENE EXPRESSION IN ZEBRAFISH

JOURNAL STYLE INFORMATION

AUTHOR CONTRIBUTIONS

I performed the experiments and collected the data presented in this manuscript. Dr. Scott Stewart is responsible for transgene design and construction and was co-author of this manuscript. Dr. Kryn Stankunas aided in experimental design as well as manuscript preparation and composition.

BACKGROUND

Research using transgenic zebrafish lines has greatly contributed to our understanding of vertebrate biology. Transgenic zebrafish are used widely for both gain and loss of function experiments as well as a means to track specific cell populations. All such studies require careful consideration regarding the location, timing, and levels of transgene expression. For instance, although constitutive ubiquitous promoters generally produce high levels of transgene expression and generate robust phenotypes, they do not differentiate cell-type specificity or the timing of gene function. To overcome these limitations, tissue specific promoters are used to direct transgene expression to discrete

cell lineages and tissue types. Temporal control of transgene expression further allows the determination of windows during which a gene functions, a feature particularly useful for developmental biology research. Additionally, multiple roles for a gene during development can be distinguished by timing the induction of an appropriate transgene. Temporal control of transgene expression in zebrafish is typically achieved using heat-shock sensitive promoters (Halloran et al., 2000), although small molecule-controlled inducible promoters also can control the timing and tune levels of transgene expression (Knopf et al., 2010).

One elegant method for transgene expression in metazoans uses the Gal4/UAS two component transcriptional activation switch from *Saccharomyces cerevisiae* (Fischer et al., 1988; Sadowski et al., 1988). Gal4 is a transcription factor that functions in yeast galactose metabolism (Laughon and Gesteland, 1984) and binds to a unique DNA sequence found between the GAL1 and GAL10 genes (Giniger et al., 1985). A version of this sequence is now commonly referred to as a UAS (for Upstream Activating Sequence). A discrete DNA-binding domain (DBD) of Gal4 is both necessary and sufficient for high-specificity binding to a UAS (Ma and Ptashne, 1987). Gal4 can activate transcription in heterologous systems by using synthetic promoters consisting of basal transcription initiating elements combined with tandem repeats of the UAS sequence (Fischer et al., 1988; Kakidani and Ptashne, 1988; Lin et al., 1988; Ma et al., 1988; Sadowski et al., 1988). Modified Gal4-based chimeric proteins comprising the Gal4 DBD fused to the strong transcriptional activation domain from the viral VP16 protein are particularly potent and specific transcriptional activators (Louvion et al.,

1993; Wang et al., 1994). The Gal4/UAS system can be readily adaptable for transgenesis studies in diverse biological systems given that any gene of interest can be inserted downstream of a UAS/minimal promoter cassette.

In the Gal4/UAS system, the spatial domain of UAS-controlled transgene expression is determined by the promoter used to express Gal4 (Brand and Perrimon, 1993). Additional refinements of the Gal4/UAS system provide temporal control of transgene expression. Taking advantage of the modular nature of Gal4 (Ma and Ptashne, 1987) and steroid hormone receptors (Webster et al., 1988), chimeric proteins have been produced that fuse the hormone binding domain from either the estrogen (ER) or glucocorticoid receptor (GR) to Gal4 (Webster et al., 1988). The resulting Gal4-ER and Gal4-GR fusion proteins activate UAS-controlled reporter genes only in the presence of the cognate steroid hormone (Louvion et al., 1993; Webster et al., 1988). To overcome effects of endogenous steroid hormones on Gal4-ER chimeras, an ER variant (known as ERT) with reduced affinity for naturally occurring estradiol but very high affinity for the estradiol analogs tamoxifen and 4-hydroxy tamoxifen (4-OHT) has been developed (Danielian et al., 1993; Feil et al., 1997). The collective features of Gal4-ERT-VP16 fusion proteins make them a potent, highly specific, and tightly controllable tool for transgene expression upon administration of either tamoxifen or 4-OHT (Danielian et al., 1993; Feil et al., 1997; Louvion et al., 1993; Wang et al., 1994; Webster et al., 1988).

The Gal4/UAS system has been adapted for use in zebrafish (Halpern et al., 2008; Scheer and Campos-Ortega, 1999; Scott, 2009) and a wide-range of UAS lines are available that

express, for example, wild-type or mutant proteins, fluorescent markers, and Cre recombinase for lineage-tracing studies. However, a search of available zebrafish lines from the Zebrafish International Resource Center (ZIRC) yields only a handful of Gal4 lines that use unique, well-characterized promoters. Further, the majority of available Gal4 lines lack the ability to control the timing of gene expression. This is particularly problematic for larval or adult studies when phenotypes arising from earlier transgene expression obscure or exclude the later studies. Inducible Gal4/UAS switches in zebrafish designed to overcome this problem rely on heat shock promoter control of Gal4 expression (Halloran et al., 2000). This approach produces strong expression but suffers from several major disadvantages, including a lack of cell-type specificity, poor control of expression kinetics, and spurious effects of repeated heat shocks.

To overcome these limitations, we adapted the tamoxifen controlled Gal4-ERT system for use in zebrafish. We describe the generation and characterization of three tissue specific tamoxifen-dependent Gal4-ERT driver lines. These lines achieve rapid, dose-dependent expression of UAS-controlled transgenes by simply adding tamoxifen or 4-OHT to zebrafish water. We also validate this approach for functional analysis by demonstrating that tamoxifen dependent, tissue-specific expression of a constitutively active intracellular Notch domain (NICD) produces dramatic defects in notochord development. This effect requires NICD expression during an early developmental window prior to 10 hpf. The tamoxifen-dependent Gal4-ERT system affords zebrafish researchers the ability to address many biological questions previously limited by reliance upon ubiquitous and/or non-inducible transgene expression.

MATERIALS AND METHODS

Zebrafish

This study was carried out in strict accordance with the recommendations in the Guide for the Care and Use of Laboratory Animals (National Academies Press) and all steps were taken to minimize animal discomfort. Zebrafish were euthanized by overdose with Tricaine. The University of Oregon Institutional Animal Care and Use Committee (IACUC) approved all protocols. PHS assurance number for animal research: A-3009-01. The following established lines were used in this study: wild-type AB, *Tg(5xUAS:EGFP)zf82* (Asakawa et al., 2008), *Tg(14xUAS:LOX2272-LOXP-RFP-LOX2272-CFP-LOXP-YFP)a130* (*UAS:Zebrabow*) (Pan et al., 2013), and *Tg(5xUAS-E1b:6xMYC-notch1a)kca3* (Scheer and Campos-Ortega, 1999).

Transgene construction

The Gateway cloning system (Invitrogen, Carlsbad, CA) and Tol2 kit (Kwan et al., 2007) was used to generate transgenes capable of tamoxifen-dependent expression. First, the coding sequence for the hybrid transcription factor, Gal4-ERT2-VP16 (Feil et al., 1997; Louvion et al., 1993) was inserted into ME-MCS to generate the middle element vector pME-Gal4-ERT-VP16. 5E vectors were constructed as follows: A region of the *krt5* promoter (Wang et al., 2006a) at chr23:10,284,249-10,286,542 (Zv9/danRer7) that drives expression in the epidermis was amplified by PCR from zebrafish genomic DNA and cloned into the Gateway compatible vector p5E-MCS (Kwan et al., 2007) to generate p5E-*krt5*; the p5E-dusp6 plasmid containing the FGF-responsive *dusp6* promoter (Molina

et al., 2007) at chr25: 18,817,373-18,827,789 (Zv9/danRer7) has been described previously (Stewart and Stankunas, 2012); the semi-ubiquitous hybrid promoter, made up of the frog *ef1a* enhancer and the rabbit b-globin intron, from pT2AL200R150G (Urasaki et al., 2006) was inserted into p5E-MCS creating p5E-ef1a. Finally, we used Gateway Clonase LRII enzyme (Invitrogen, Carlsbad, CA) to recombine each of 5E-*krt5*, 5E-*efla*, or 5E-*dusp6* promoter elements with ME-Gal4TVP16, 3E-*polyA* (Kwan et al., 2007), and a modified Tol2 destination vector containing a *myl7*-ECFP cassette as a marker for transgenesis (Stewart and Stankunas, 2012).

Generation of transgenic animals

Plasmid DNA for each construct was co-injected with capped RNA coding for the Tc transposase into one cell stage AB embryos at a concentration of 25 ng/µl as described previously (Stewart and Stankunas, 2012). Animals displaying ECFP expression in the heart at 48 hpf were selected and reared to adulthood. Founders were identified by crossing to *Tg(5xUAS:EGFP)* animals, treating progeny with tamoxifen (3 µM, Sigma) at 8 hpf, and visualizing EGFP expression at 24-48 hpf. Founders with EGFP-positive progeny were then outcrossed to AB fish. The subsequent generation was screened for single transgenic insertions by again crossing to *Tg(5xUAS:EGFP)* fish, treating embryo progeny with tamoxifen, and scoring the clutch for EGFP expression. Stable lines were maintained as heterozygotes by outcrossing to AB fish and picking animals with ECFP expression in the heart. Following this approach, we established the following lines: *Tg(krt5:Gal4-ERT-VP16,myl7:ECFP)b1234*, *Tg(dusp6:Gal4-ERT-VP16,myl7:ECFP)b1235*, *Tg(efla:Gal4-ERT-VP16,myl7:ECFP)b1236*.

Induction of transgenes by tamoxifen

For studies using embryos, 4-hydroxy-tamoxifen (4-OHT, Sigma) was dissolved in ethanol and added directly to the fish water at the times and concentrations indicated in the figure legends. Control animals were treated with the same volume of ethanol. For adult studies, tamoxifen (Sigma) dissolved in DMSO or 4-OHT dissolved in ethanol was added to fish water at a final concentration of 1 μM for 1 hour, after which animals were transferred to fresh fish water. Control animals were treated in the same manner with the same volume of vehicle. Animals were subjected to this regimen 3 consecutive days prior to imaging and tissue harvesting.

Immunostaining and imaging

For immunostaining embryos, animals were manually dechorionated and then fixed overnight at 4°C in phosphate-buffered saline (PBS) containing 4% paraformaldehyde. The next day, embryos were washed extensively in PBS containing 0.1% Tween-20 (PBST) then dehydrated though a methanol series. Embryos in 100% methanol were then transferred to -20°C for at least 24 h prior to rehydration to PBST. Embryos were incubated in blocking buffer (PBST containing 10% normal goat serum) for 1-2 h at room temperature with gentle mixing. Primary antibodies were sourced and diluted as follows in blocking buffer and then incubated overnight at 4°C: anti-GFP (1:1000, Aves Labs), anti-myc epitope (1:1000, Invitrogen). The next day embryos were washed 2 x 30' in PBST followed by 2 h room temperature incubation in Alexa-conjugated secondary antibodies (Invitrogen) diluted 1:1000 in blocking buffer. Embryos were then washed for

30’ in PBST, 30’ in PBS, mounted in low melt agarose, and imaged on a Nikon Eclipse Ti widefield inverted microscope. For Figures 1, 2, 3, and S2A, C, D-G, embryos were fixed as above, washed in PBS, mounted in low melt agarose, and the native fluorescence of marker proteins visualized by epifluorescent microscopy. For scoring phenotypes, animals were manually dechorionated and counted under a stereomicroscope. Adult animals were anesthetized with Tricaine and imaged under a Leica M165 FC stereomicroscope.

For paraffin-embedded eye sections, tamoxifen and control animals were sacrificed and eyes were immediately dissected and fixed overnight at 4°C in PBS containing 4% paraformaldehyde. The next day, samples were extensively washed in PBS, dehydrated, and embedded in paraffin. 7 μM sections were collected. Rehydrated sections were subjected to antigen retrieval by incubating in 0.25% trypsin for 20’ at 37°C, immunostaining with GFP and c-myc antibodies (described above), stained with Hoechst to label nuclei, mounted with Fluorogel (EMS), and imaged on a Leica DM4000B widefield microscope.

Quantification of EGFP expression

High magnification images of ventral EGFP-labeled epidermal cells were captured with a Nikon Eclipse Ti widefield inverted microscope. Unprocessed images from four representative animals for each tamoxifen dose were then analyzed using the ImageJ (NIH) software package to generate pixel intensity values based on the strength of the fluorescent signal. Averaged pixel intensity values for each treatment were then

normalized to that of the lowest tamoxifen dose (0.5 μM) and plotted as "relative fluorescent intensity".

In situ hybridization

In situ hybridizations were performed essentially as described by Thisse and Thisse (Thisse and Thisse, 2008a). Stained embryos were dehydrated in a methanol series and stored overnight at -20°C. Embryos were then rehydrated into PBST and transferred to 100% glycerol. Equilibrated embryos were mounted in glycerol and imaged using Rottermann contrast optics on a Leica M165 FC stereomicroscope.

RESULTS AND DISCUSSION

Novel transgenic lines confer tamoxifen-dependent gene expression

We combined features of the widely used Gal4/UAS and ER-tamoxifen systems and adapted them for use in transgenic zebrafish (Figure 1A). As a first step, we established transgenic zebrafish expressing the tamoxifen-dependent Gal4-ERT transcription factor (Danielian et al., 1993; Feil et al., 1997; Louvion et al., 1993; Wang et al., 1994; Webster et al., 1988) in various tissues and cell types. To generate a broadly expressing Gal4-ERT line for temporal studies, we used a 1.1 kb region from the *Xenopus laevis elongation factor 1 alpha* (*ef1α*) promoter and rabbit b-globin intron sequence (Urasaki et al., 2006). Additionally, we made a Gal4-ERT line driven by a 2.3 kb promoter region from the *keratin 5* (*krt5)* gene that has been reported to express in the epidermis exclusively (Wang et al., 2006b). Finally, we produced a line expressing Gal4 under the control of a 10 kb element from the *dual specificity phosphatase 6* (*dusp6)* gene. *Dusp6* (also known

as *Mkp3*) is an FGF signaling responsive gene that is active in a variety of cells depending on the developmental stage and is induced in regenerating fins (Molina et al., 2007; Stewart and Stankunas, 2012; Tsang et al., 2004).

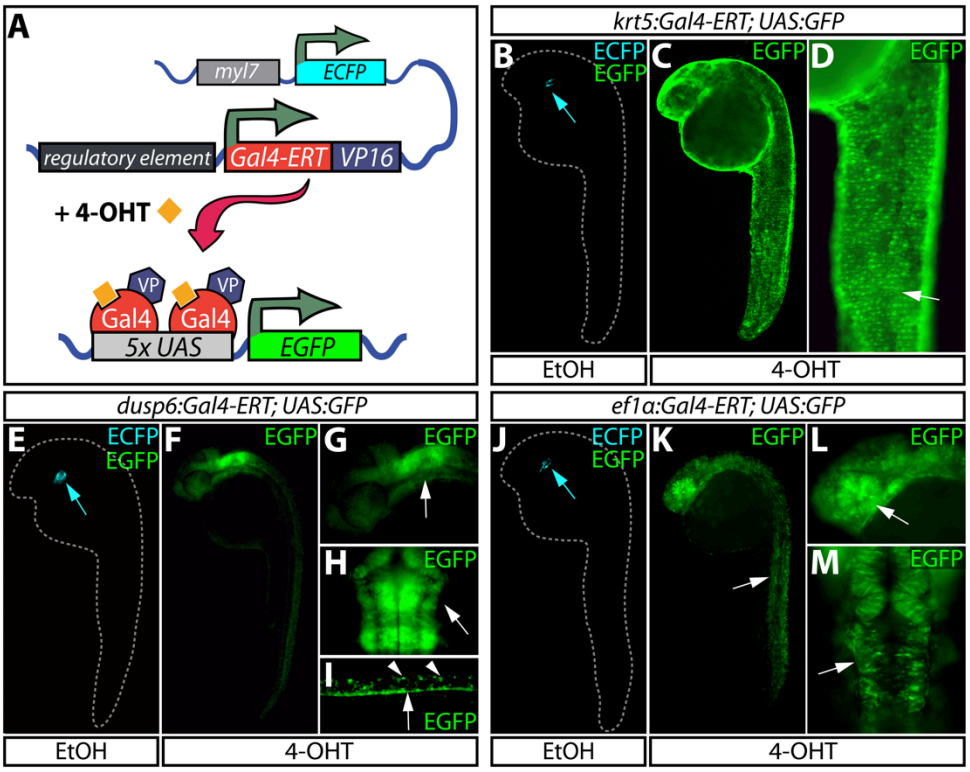

Figure 1. Temporally and spatially controlled transgene expression in zebrafish.
(A) Schematic of transgenic constructs used in the Gal4-ERT system. A tamoxifen-responsive Gal4-ERT-VP16 construct is expressed from a tissue-specific promoter that activates any UAS-linked responder line (shown here as a *5xUAS:EGFP* reporter) upon tamoxifen or 4-OHT exposure (orange squares). The *myl7:ECFP* cassette serves as a transgenesis marker for the Gal4-ERT lines. **(B-D)** Visualization of EGFP expression in *Tg(krt5:Gal4-ERT-VP16; UAS:EGFP)* animals treated with ethanol (B) or 2 µM 4-OHT (C and D) from 4-24 hpf. The white arrow in panel D highlights expression of EGFP in the epidermis. **(E-I)** EGFP expression in *Tg(dusp6:Gal4-ERT-VP16; UAS:EGFP)* animals treated with vehicle (E) or 2 µM 4-OHT (F-I) from 4-24 hpf. In panels G and H, the white arrow indicates EGFP expression in the hindbrain and midbrain-hindbrain boundary. In panel I, arrowheads mark dorsal spinal cord neurons and the arrow points to EGFP expression in the floor plate. **(J-M)** Expression of EGFP in control (J) and 4-OHT treated (2 µM, K-M) *Tg(ef1α:Gal4-ERT-VP16; UAS:EGFP)* animals in a variety of cell types throughout the embryo including skeletal muscle (K, white arrow), the eye (L, white arrow), and the midbrain/ midbrain-hindbrain boundary (M, white arrow). In panels B, E, and J, blue arrows point to myocardial ECFP expression, which represents the marker for transgenesis and serves as an internal control

We crossed each of these driver lines to a *Tg(UAS:EGFP)* reporter line (Asakawa et al., 2008) and treated embryos with 2 µM 4-hydroxytamoxifen (4-OHT) from 4-24 hours post fertilization (hpf). In each case, 4-OHT treatment elicited distinct EGFP expression

patterns in 25% of the fish, as expected from heterozygote intercrosses. *Tg(krt5:Gal4-ERT-VP16; UAS-EGFP)* fish exhibited strong signal solely in the epidermis (Figure 1B-D), mimicking the endogenous *krt5* mRNA expression pattern (Wang et al., 2006b) (Figure S1). The *Tg(krt5:Gal4-ERT-VP16)* line was equally effective at producing a robust response when paired with additional UAS reporter lines (Figure S2A-C). *Tg(dusp6:Gal4-ERT-VP16; UAS-EGFP)* fish expressed EGFP in the expected pattern in the hindbrain, midbrain-hindbrain boundary, pharyngeal endoderm, notochord, and floor plate along with select dorsal motor neurons (Figure 1E-I) (Tsang et al., 2004). Although not ubiquitously expressed, the *Tg*(*ef1α:Gal4-ERT-VP16; UAS-EGFP)* line displayed EGFP expression in a wide variety of cell types throughout the embryo including those of the hindbrain, midbrain-hindbrain boundary, skeletal muscle and retina (Figure 1J-M). Unfortunately, the *Tg*(*ef1α:Gal4-ERT-VP16)* line becomes silenced prior to 48 hpf and is therefore only useful for early embryonic studies. In the absence of 4-OHT, no *UAS-EGFP* expression was detected with any of the Gal4-ERT lines; only the cardiac-specific *myl7:ECFP* which we employed as a transgenesis marker was observed (Figure 1B, 1E, and 1J). Additionally, we saw no indication of 4-OHT toxicity with any of the treatments. These results demonstrate that each of the Gal4-ERT lines provide the expected tissue specificity and strictly require 4-OHT for UAS-dependent transgene expression.

The Gal4-ERT system provides rapid induction of gene expression

We next sought to determine the temporal resolution of the Gal4-ERT system by measuring how rapidly it can drive expression of *UAS:EGFP* in the presence of estradiol analogs. We placed 24 hpf *Tg(krt5:Gal4-ERT-VP16; UAS:EGFP)* embryos into fish-

water containing 2 μM 4-OHT and monitored the emergence of EGFP expression. EGFP was first detected in the epidermis three hours post treatment. However, the expression was faint and non-homogenous (Figure 2C and 2C'). By four and a half hours post 4-OHT exposure, EGFP expression was markedly more robust and labeled nearly the entire epidermis (Figure 2D and 2D'). These results indicate that the Gal4-ERT system possesses activation kinetics suitable for time-sensitive studies of rapidly developing zebrafish embryos.

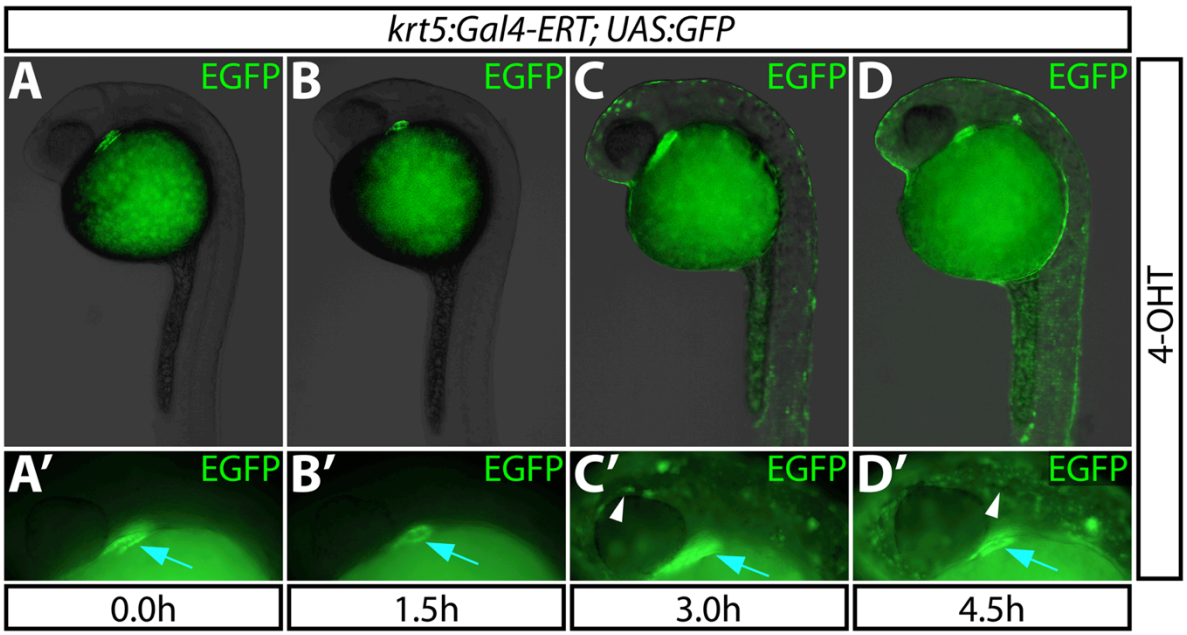

Figure 2. The Gal4-ERT system provides rapid induction of gene expression.
(A-D) Kinetics of EGFP expression in *Tg(krt5:Gal4-ERT-VP16; UAS:EGFP)* animals upon administration of 2 μM 4-OHT at 24 hpf for 0-4.5 hours. **(A'-D')** High magnification images demonstrating EGFP expression for each treatment. White arrowheads point to epidermal expression of EGFP; blue arrows indicate bleed-through from the heart muscle-specific ECFP transgenesis marker.

Transgene expression levels can be varied by tamoxifen dosage

In addition to spatiotemporal control over transgene expression, it is often desirable to control levels of transgene expression. Therefore, we determined if varying the dose of 4-OHT would affect the degree of transgene expression. We treated *Tg(krt5:Gal4-ERT-*

VP16; UAS:EGFP) embryos at sphere-stage with various concentrations of 4-OHT. At 24 hpf, embryos were harvested and fixed for imaging. We determined the fraction of EGFP-expressing epidermal cells and measured their normalized EGFP intensity. 4-OHT concentrations of 0.25 μM failed to produce detectable EGFP expression (data not shown). Embryos treated with 0.5 μM 4-OHT exhibited low-level EGFP in all presumptive epidermal cells (Figure 3A-B). Increasing the 4-OHT dose to 1 μM or 2 μM produced a relative gain in EGFP signal intensity with no indication of toxic effects (Figure 3C-E). Overall, increasing the dose from 0.5 μM to 2 μM yielded a 28% increase in EGFP levels ($p < 0.05$). At all effective concentrations, EGFP levels differed from cell-to-cell, which may reflect varying EGFP accumulation depending on cell cycle stage and the time lapse since a given epidermal cell was established and initiated *krt5* promoter activity. We repeated the experiment using *Tg(krt5:Gal4-ERT-VP16; UAS:Zebrabow)* fish, which expressed mCherry in the majority of epidermal cells when exposed to 0.5 μM 4-OHT (Figure S2D-E). Treating animals with 1 or 2 μM 4-OHT again produced notably higher mCherry expression levels and no sign of toxic effects (Figure S2F-G). Together, these results indicate that the Gal4-ERT system can be used to tune transgene expression to a desired level by titrating the concentration of 4-OHT.

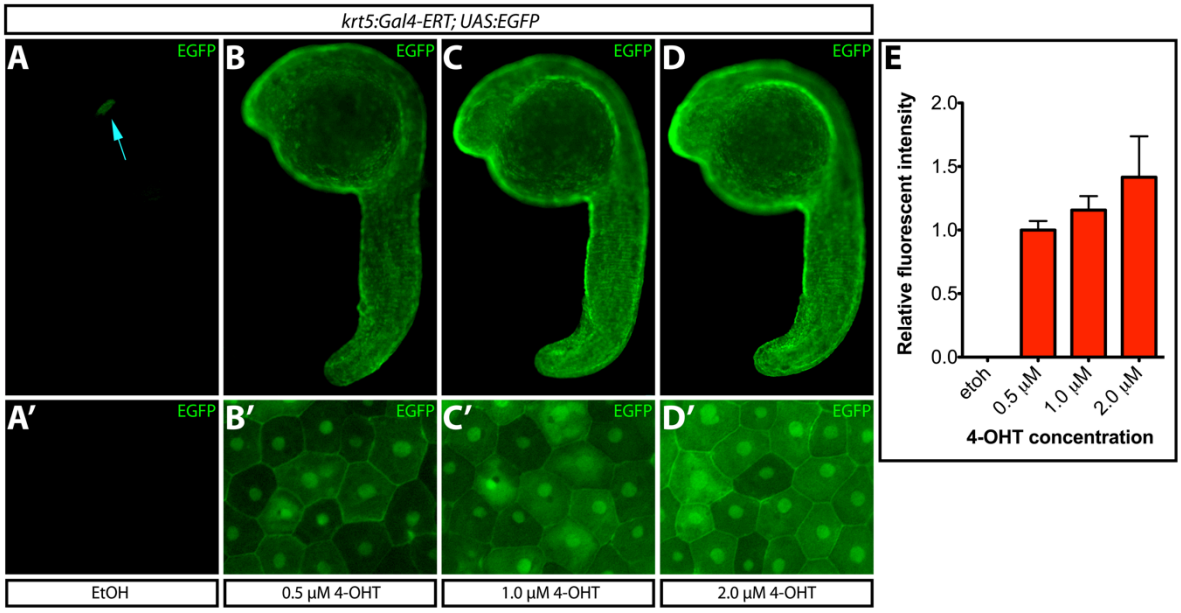

Figure 3. Transgene expression levels depend upon 4-OHT dosage.
(A-D) EGFP expression upon treatment of *Tg(krt5:Gal4-ERT-VP16; UAS:EGFP)* zebrafish with ethanol or the indicated dose of 4-OHT from 4-24 hpf. The blue arrow indicates *myl7:ECFP* expression. **(A'-D')** High-magnification images of ventral epidermis from fish in each treatment group. **(E)** Normalized EGFP intensity (to the 0.5 µM 4-OHT treated group) of fish treated with ethanol or 4-OHT. Error bars represent standard deviations.

Inducible transgene expression in adult zebrafish

While the zebrafish was developed as a model organism for developmental studies (Grunwald and Eisen, 2002), recent years have seen an increased use of zebrafish larvae and adults for behavioral, physiologic, and disease modeling (e.g. cancer) research. Further, given their remarkable ability to regenerate damaged organs, adult zebrafish have become a leading vertebrate model for regeneration studies (Gemberling et al., 2013). Therefore, we investigated the efficacy of the Gal4-ERT system in adult animals. We allowed *Tg(krt5:Gal4-ERT-VP16; UAS:EGFP)* fish to develop to adulthood and induced Gal4-ERT activity by the addition of 1 µM tamoxifen for one hour per day over three days and monitored the fish for EGFP expression. Although the pattern of *krt5* expression in adult zebrafish has not been characterized in detail, we were surprised to

observe that, in contrast to developing embryos/larvae, EGFP was not expressed in the epidermis. Rather, tamoxifen-exposed *Tg(krt5:Gal4-ERT-VP16; UAS:EGFP)* adult fish showed restricted EGFP expression in the eye that was drug dependent and increased in intensity following each treatment (Figure 4A-D). Treatment with 1 μM 4-OHT produced similar results (data not shown). A histological analysis of the eyes from tamoxifen-exposed *Tg(krt5:Gal4-ERT-VP16; UAS:EGFP)* fish revealed that EGFP was most notably induced in the photoreceptors, accumulating in the inner segment (Figure 4E-H). By in situ hybridization, *EGFP* transcripts remained present in the photoreceptors eight hours after treatment, which suggests that even transient tamoxifen exposure (only one hour) is sufficient to elicit robust transgene activation in adults with little or no background (Figure 4I). While we were unable to establish if endogenous *krt5* is similarly expressed, the *Tg(krt5:Gal4-ERT-VP16)* line provides a valuable tool for inducible transgene expression in adult zebrafish photoreceptors. More generally, our results validate use of the Gal4-ERT system for spatiotemporal control of transgene expression in adult zebrafish using small molecules.

Figure 4. Inducible transgene expression in adult zebrafish.
(A-D) Expression of EGFP in the eye of a single adult *Tg(krt5:Gal4-ERT-VP16; UAS:EGFP)* zebrafish prior to (A and B) and after (C and D) treatment with 1 μM tamoxifen for one hour per day for three consecutive days. Green arrows point to EGFP expression in the eye. The areas bounded by the dashed red box in A and C are shown at high magnification in B and D, respectively. **(E-H)** Immunostaining of paraffin sections with anti-EGFP antibodies (shown in green) in eyes from DMSO- (E and F) and tamoxifen-treated (G and H) *Tg(krt5:Gal4-ERT-VP16; UAS:EGFP)* fish. Panels F and H show overlays with anti-EGFP antibody staining in green, Hoechst-stained nuclei in blue, and auto-fluorescence in red. Fish were drug treated as in A-D. Green arrows indicate EGFP expression in photoreceptors and asterisks (*) denote auto-fluorescence in photoreceptor outer segments. (**I**) In situ hybridization for *EGFP* mRNA in a paraffin section from a 4-OHT treated animal. The blue arrow shows *EGFP* expression in photoreceptors.

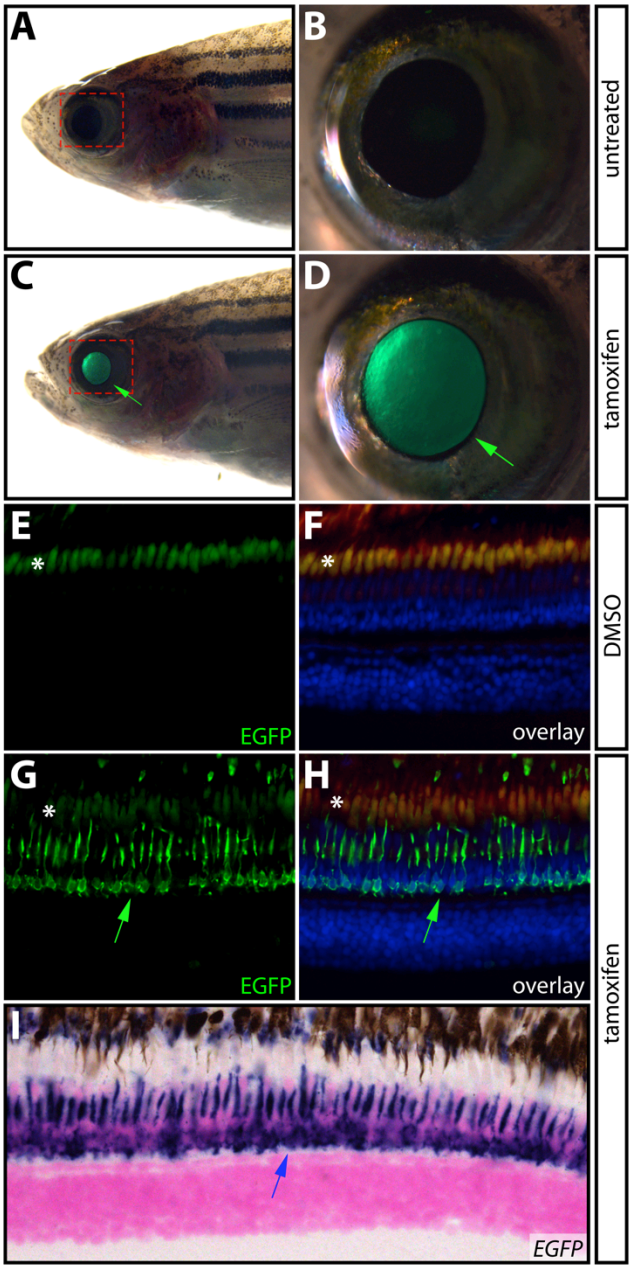

Using inducible expression to define temporal roles of Notch signaling

The high degree of spatiotemporal control over UAS-linked reporters prompted us to ascertain if the system is capable of generating inducible gain-of-function phenotypes. During zebrafish embryogenesis, the organizer forms the notochord, floor plate, and hypochord (Melby et al., 1996). Previous studies have established that the Notch signaling pathway within midline precursor cells favors development of the hypochord

and floor plate at the expense of the notochord (Latimer and Appel, 2006; Yamamoto et al., 2010). In support of this model, *Tg(hsp:Gal4; UAS:NICD)* fish ubiquitously overexpressing the Notch1a intracellular domain (NICD) following heat shock (Coffman et al., 1993; Lieber et al., 1993; Rebay et al., 1993; Scheer and Campos-Ortega, 1999; Struhl et al., 1993), display a dramatically reduced trunk notochord (Latimer and Appel, 2006). Given that *Tg(dusp6:Gal4-ERT-VP16; UAS:EGFP)* embryos exposed to 4-OHT from 0-12 hpf exhibited robust EGFP expression in the trunk midline (Figure 5A and 5B), mimicking endogenous *dusp6* (Tsang et al., 2004), we hypothesized expression of activated Notch1a within *dusp6*$^{+}$ cells would produce notochord developmental defects. We crossed *Tg*(*dusp6:Gal4-ERT-VP16)* to *Tg(UAS:NICD)* fish and treated resulting embryos with either vehicle or 4 μM 4-OHT beginning at 2 hpf. By 24 hpf, 4-OHT treated embryos were noticeably smaller than controls and had reduced and/or malformed notochords containing misshapen cells (Figure 5C-F), a phenotype reminiscent of that described upon global overexpression of NICD (Latimer and Appel, 2006; Yamamoto et al., 2010). Such notochord defects were observed in 27% (29/110) of 4-OHT treated embryos at 48 hpf (Figure S3). As 25% of the embryos would carry both transgenes, the phenotype was fully penetrant. Ethanol treated embryos from the same clutch had no notochord defects (0/100). *Tg*(*krt5:Gal4-ERT; UAS:NICD)* animals expressing NICD in the epidermis following the identical 4-OHT regimen also had normal notochords (Figure S3E-F). These studies show that NICD expression in midline cells is sufficient to disrupt notochord development and validate the Gal4-ERT approach for defining tissue-specific gene function.

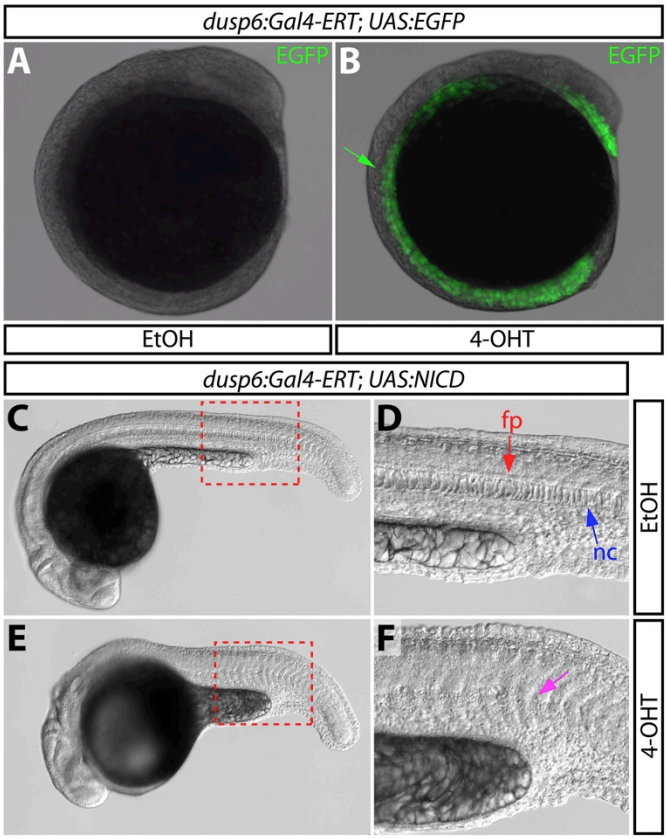

Figure 5. Overexpression of the Notch1 intracellular domain using the *dusp6:Gal4-ERT* driver disrupts notochord development.
(A and B) EGFP expression at the 10-somite stage in control (A) and 2 µM 4-OHT treated *Tg(dusp6:Gal4-ERT-VP16; UAS:EGFP)* fish. The green arrow points to EGFP expression at the midline. (**C-F)** DIC images of control (C and D) and 4-OHT treated (4 µM from 2-24 hpf, E and F) *Tg(dusp6:Gal4-ERT-VP16; UAS:NICD)* animals at 24 hpf. Regions bounded by the dashed red box in panels C and E are shown in high magnification in panels D and F, respectively. In panel D, the red arrow indicates the floor plate (fp) and the blue arrow indicates the notochord (nc); in panel E, the magenta arrow highlights the reduced notochord and disorganized floor plate.

Lastly, we tested whether the inducible Gal4-ERT system could be used to map the developmental window in which notochord development is sensitive to elevated Notch signaling. We treated embryos with vehicle or 4-OHT at 4 hpf, 6 hpf, 8 hpf, or 10 hpf and scored fish for a notochord reduction phenotype at 24 hpf. The frequency of notochord defects remained constant when embryos were treated with 4-OHT at or before 6 hpf (occurring in approximately 25% of embryos, the expected frequency of double heterozygous animals). In contrast, the number of affected animals decreased when the

treatment began at 8 hpf and approached zero when fish were first exposed at 10 hpf (Figure 6A-E, relative penetrance plotted in F). By immunostaining for the myc tag on the NICD transgene, we confirmed that these latter embryos expressed NICD (Figure 6A-E), demonstrating that the lack of a phenotype when 4-OHT was added at 10 hpf was not due to a failure to induce NICD. In situ hybridization for the floor plate and notochord marker *sonic hedgehog* (*shha*) (Echelard et al., 1993; Krauss et al., 1993) further confirmed that the phenotype was fully suppressed when exposed to drug at 10 hpf in contrast to earlier treatments (Figure 6G-I). These results suggest that Notch activation within midline cells can inhibit notochord formation during gastrulation (between 5 and 10 hpf). After this period, the cells are refractory to elevated levels of Notch signaling. These results are consistent with published data proposing that Notch mediates cell fate decision in the organizer between a notochord and hypochord fate (Appel et al., 1999; Latimer and Appel, 2006; Yamamoto et al., 2010). The tamoxifen-inducible NICD approach we describe could be a useful tool to help determine how Notch mediates this and other cell fate decisions. Generally, this study illustrates how an inducible Gal4-ERT system provides sufficient spatiotemporal control over transgene expression to map narrow windows of cell-type specific gene function.

Figure 6. Using inducible expression to define temporal roles of Notch1 signaling in notochord development.

(A-E) Expression of myc-tagged NICD by immunostaining with myc antibodies on 24 hpf *Tg(dusp6:Gal4-ERT-VP16; UAS:NICD)* embryos treated with ethanol (A) or 4 μM 4-OHT at the indicated times (B-E). Blue arrows indicate myocardial ECFP expression to mark transgenic animals and magenta arrows show expression of myc-tagged NICD. Panel insets display high magnification images of boxed regions where red arrows indicates the notochord (A and E) and the missing notochord (B-D). **(F)** Penetrance of the 4-OHT induced notochord defects in *Tg(dusp6:Gal4-ERT-VP16; UAS:NICD)* animals, treated with 4-OHT at various stages of development, is shown relative to the 4-24 hpf treatment (1.0 indicates complete penetrance). The double asterisk indicates a significant difference between 4-24 h and 10-24 h 4-OHT treated fish ($P < 0.005$). Individual points represent independent experiments with separate clutches. **(G-I)** Expression of *shha* in the floor plate of animals treated with ethanol (G) or with 4-OHT for the indicated times (H-I). Boxed regions are shown at higher magnification in the panel insets. Red arrows indicate *shha* expressing floor plate cells.

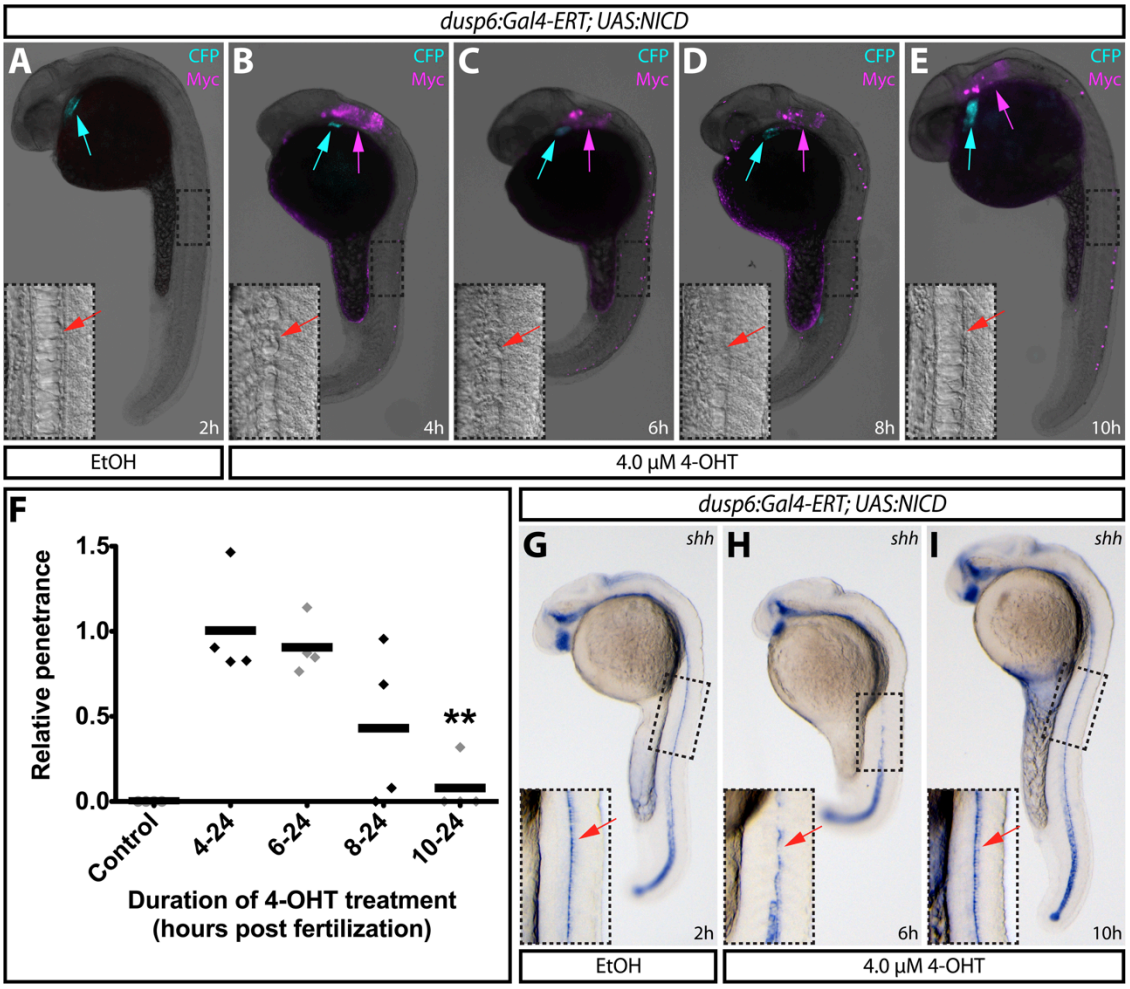

CONCLUSIONS

Our results validate the use of the Gal4-ERT system in zebrafish by demonstrating how it can direct transgene expression in a cell-type specific and tamoxifen/4-OHT-dependent manner. The approach has substantial advantages over other methods to induce transgene expression in zebrafish, most notably heat shock sensitive promoters. First, the tamoxifen system is dose dependent and therefore transgene expression can be tuned to a desired level by titrating the concentration of tamoxifen/4-OHT added directly to the fish water. Second, at doses that activate Gal4-ERT, tamoxifen/4-OHT causes no adverse affects to zebrafish. In contrast, by definition, heat shock treatment is of substantial stress to

zebrafish and may be detrimental to animal health and lead to mixed or obscured results. Finally, heat shock promoters are broadly expressed upon heat shock whereas tissue-specificity is desired or required for many experiments. Tetracycline-inducible transgene expression represents a parallel methodology with similar advantages for zebrafish studies (Knopf et al., 2010), albeit with a more limited number of available Tet-responsive transgenes. Importantly, Gal4-ERT and Tet-On systems are orthogonal and could be used to independently induce expression of two transgenes either simultaneously or sequentially.

Gerety et. al. (Gerety et al., 2013) have also demonstrated the feasibility of a Gal4-based tamoxifen inducible transgene system in zebrafish. There are similarities and differences between this report and our study. First, Gerety et al. (2013) use a ERT-Gal4 fused to two copies of a truncated VP16 transactivation domain (Asakawa et al., 2008) whereas we use Gal4-ERT fused to a single copy of a VP16 (Louvion et al., 1993). Despite these differences, both inducible Gal4-fusion proteins require similar concentrations of 4-OHT for transgene expression and the kinetics of induction are comparable (Gerety et al., 2013). Gerety et al. (2013) additionally observe the reversal of gene expression following tamoxifen removal. The reversal kinetics may be slow, as we did not see a notable decrease in EGFP expression 24 hours after removing tamoxifen from embryos (data not shown), although the long half-life of EGFP protein complicates this analysis. Using a line (*cldnb:ERT2-Gal4*) directing Gal4-ERT expression primarily in the skin and lateral line, Gerety et al. (2013) show the approach can be used to drive tissue-specific expression. We present two additional Gal4-ERT lines (*dusp6:Gal4-ERT* and *krt5:Gal4-*

ERT) that provide spatially restricted and tamoxifen-controlled transgene activation. We further validate using the Gal4-ERT system in adult zebrafish. Both reports demonstrate use of the Gal4-ERT system to generate gain-of-function phenotypes. We extend this approach to determine tissue-specific and temporal windows of gene function during development. Collectively, the two reports provide a robust validation of the capability and versatility of the Gal4-ERT system in zebrafish and provide an initial collection of transgenic tools for immediate use.

Potential applications for Gal4-ERT inducible expression transcend the reporter and inducible gain-of-function experiments demonstrated to date. For example, the approach could be used for cell-specific loss-of-function studies by the inducible expression of dominant negative proteins, pathway inhibitors, or shRNAs for RNA interference. Additionally, the inducible expression of a *UAS:Cre* line in concert with floxed reporter lines could improve cell lineage analyses. Lastly, the utility of the system in adults opens up previously intractable experiments in neuroscience, cancer modeling, and organ regeneration research.

CHAPTER IV

DENOUEMENT

In Chapter II, I utilized contemporary genetic tools to 1) provide an in-depth comparison of loss-of-function methods to show that antisense morpholinos are prone to off-target effects in zebrafish and 2) describe novel findings regarding the *in vivo* roles of Kdm6b-demethylases during cardiovascular development and morphogenesis. I utilized CRISPR/Cas9 to generate loss-of-function models of both *kdm6ba* and its ohnolog *kdm6bb* and demonstrated that these genes function redundantly during late stage proliferation during heart ventricle maturation.

These results represent the first *in vivo* descriptions of Kdm6b demethylase function during cardiovascular development and support the hypothesis that the primary function of H3K27 demethylases is to contribute to late stage organ maturation rather than early lineage commitment and differentiation. These conclusions favor a model in which Kdm6b demethylases are dispensable for the events that shape the early embryo including proliferation, migration, and the regulation of cell fate decisions. Instead, my data suggests that Kdm6b demethylases promote a wave of proliferation and maturation that takes place only after the formation of the rudimentary heart. Furthermore, I show that H3K27me3 levels are retained in *kdm6b*-deficient trabeculating cardiomyocytes. Despite this clear correlation of proliferation and levels of H3K27me3, it will be interesting for future studies to determine if Kdm6b operates via H3K27me3

demethylation within this context, or if its mechanism of action is demethylase independent.

In Chapter III, I demonstrate a novel transgenic tool based on a modified GAL4/UAS system that allows for the spatiotemporal control of transgene expression. My expression system uses new tissue-specific transgenic zebrafish lines that express the Gal4 transcription factor fused to the estrogen-binding domain of the human estrogen receptor. I show these Gal4-ERT driver lines confer rapid, tissue-specific induction of UAS-controlled transgenes following tamoxifen exposure in both embryos and adult fish. I demonstrate how this technology can be used to define developmental windows of gene function by spatiotemporal-controlled expression of constitutively active Notch1 in embryos. Given the array of existing UAS lines, the modular nature of this system will enable many previously intractable zebrafish experiments.

APPENDIX

SUPPLEMENTAL MATERIAL (CHAPTER II)

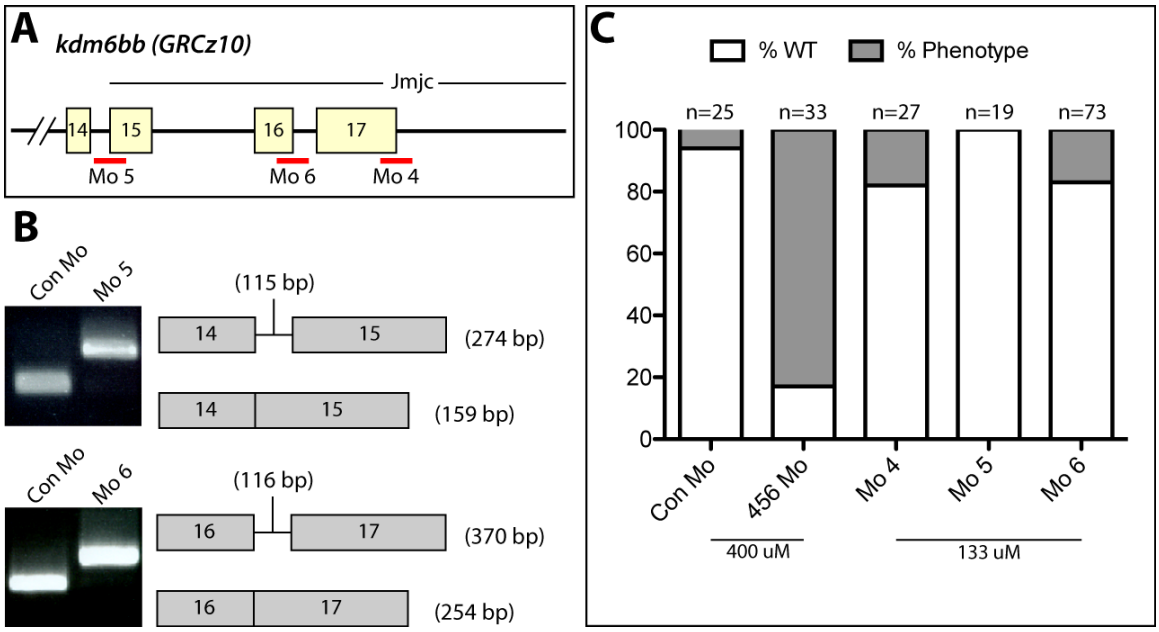

Figure S1. Morpholinos Mo 5 and Mo 6 prevent proper splicing of *kdm6bb* transcript
(A) Schematic of Jmjc coding region of *kdm6bb*. (B) PCR on cDNA extracted from single morpholino-injected embryos. (C) Relative % phenotype in control and morphant embryos at varying morpholino concentrations.

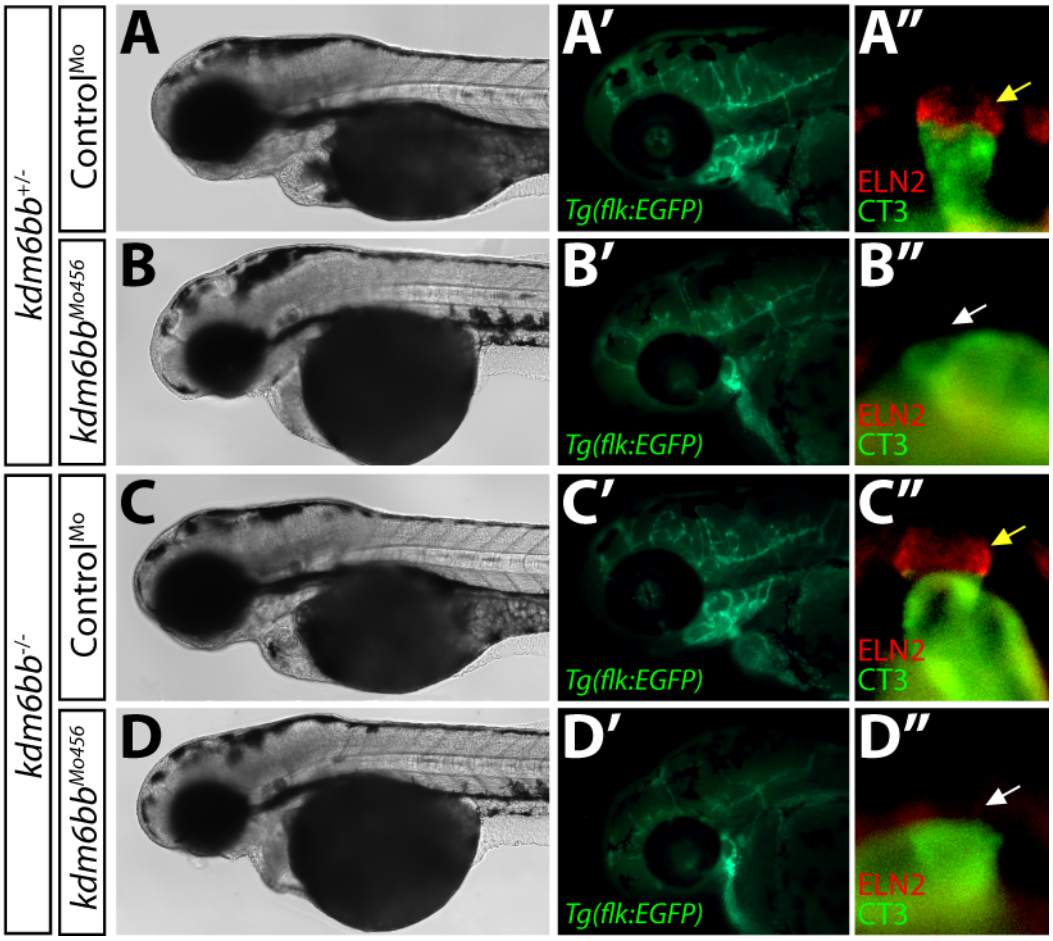

Figure S2. Morphant phenotypes persist in *kdm6bb* mutant embryos
Morpholino injections into both *kdm6bb*$^{-/-}$ and *kdm6bb*$^{+/-}$ clutch mates shown by whole mount DIC (A-D), *Tg(flk:EGFP)* reporter (A'-D') and OFT immunostaining (A"-D"). Yellow arrows denote normal OFT and white arrows highlight an absent OFT.

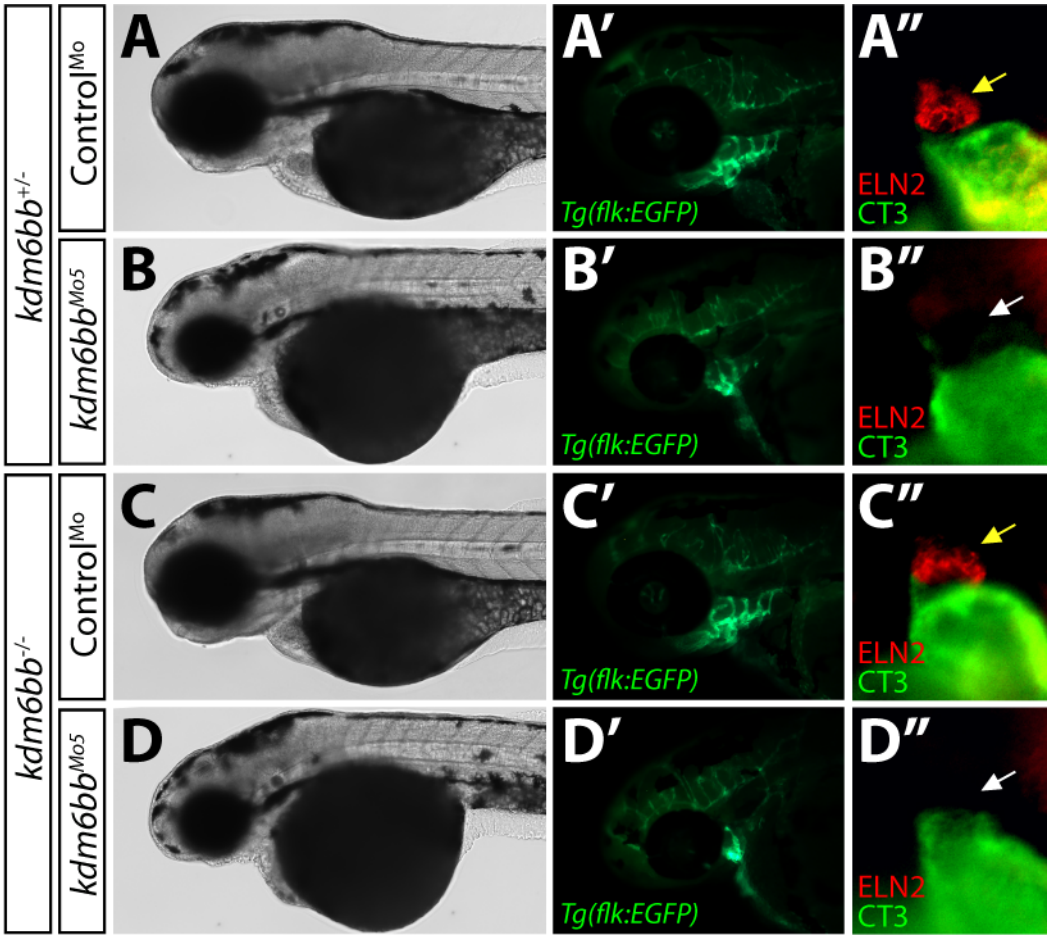

Figure S3. Morphant phenotypes persist in *kdm6bb* mutant embryos injected with morpholino #5
Morpholino injections into both *kdm6bb*$^{-/-}$ and *kdm6bb*$^{+/-}$ clutch mates shown by whole mount DIC (A-D), *Tg(flk:EGFP)* reporter (A'-D') and OFT immunostaining (A"-D"). Yellow arrows denote normal OFT and white arrows highlight an absent OFT.

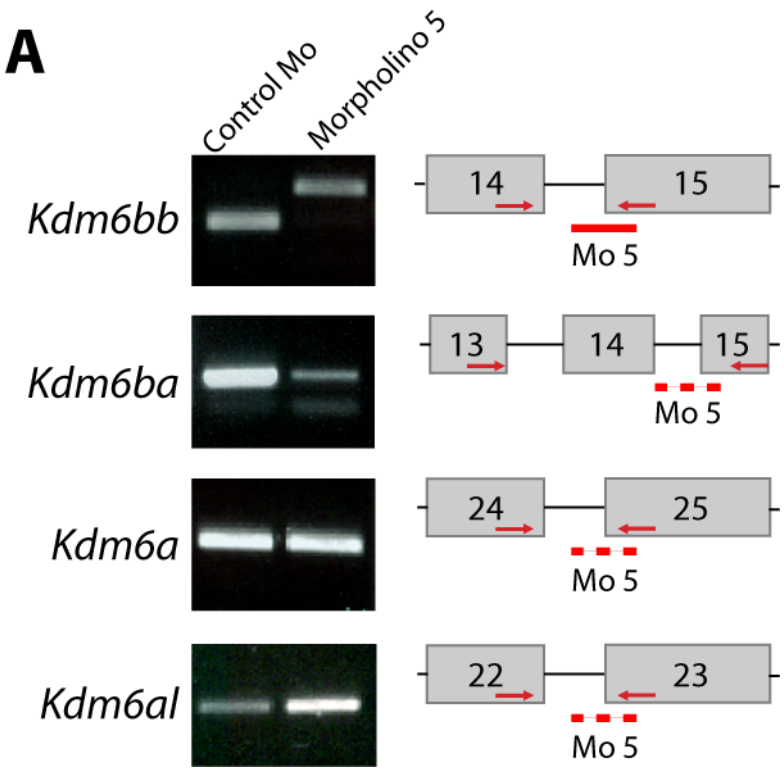

Figure S4. Morpholino #5 does not appear to affect splicing of other kdm6b-family members
PCR of cDNA along with schematic of the region amplified.

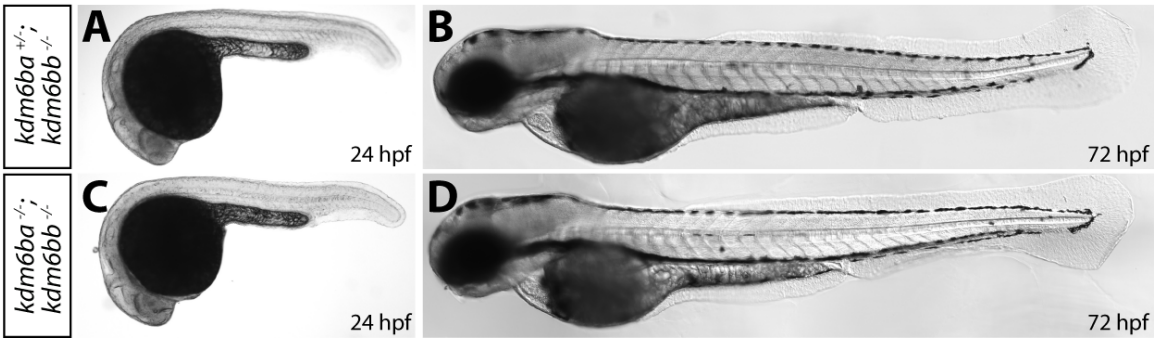

Figure S5. Early development of *kdm6b*-deficient embryos is unaffected
(A-B) DIC images of 24 hpf (A) and 72 hpf (B) control embryos. (C-D) DIC images of *kdm6b*-deficient embryos at 24 hpf (C) and 72 hpf (D) animals.

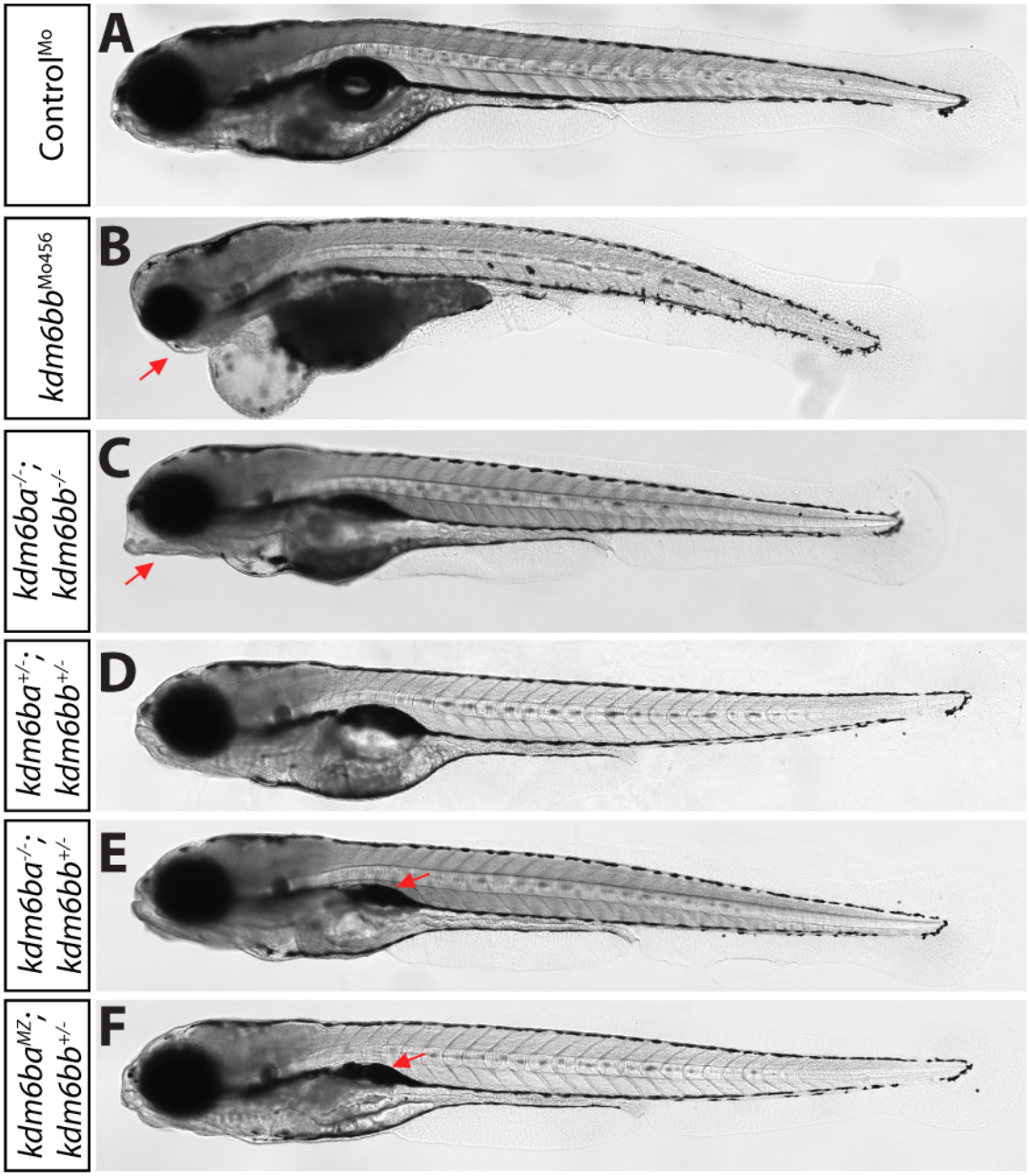

Figure S6. 5 dpf morphants and kdm6bb mutants show different craniofacial phenotypes that are not recapitulated in *kdm6ba*^{MZ} *kdm6bb*$^{+/-}$ embryos

(A-C) 5 dpf DIC images of morphants and *kdm6ba*$^{-/-}$;*kdm6bb*$^{-/-}$ double mutants. (D-F) 5dpf DIC images of the progeny from a cross between a *kdm6ba*$^{-/-}$;*kdm6bb*$^{+/+}$ female and a *kdm6ba*$^{+/-}$;*kdm6bb*$^{-/-}$ male.

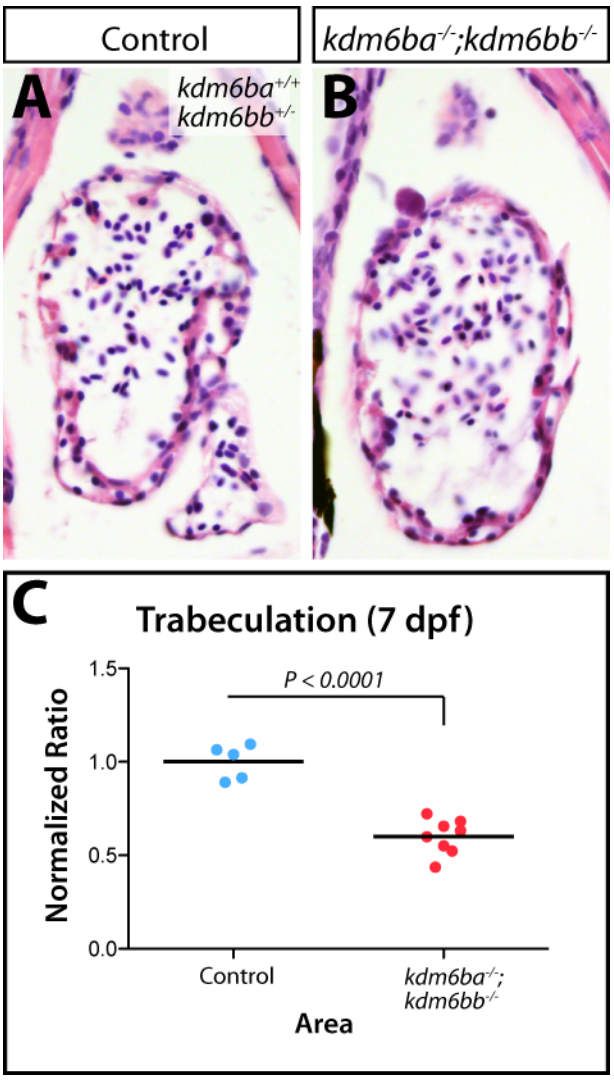

Figure S7. Decreased ventricular area in coronal sections of 7 dpf *kdm6b*-deficient embryos. (A-B) H&E of coronal sections of the ventricle at 7 dpf. (C) Quantified area of 7 dpf ventricular coronal sections. P-value determined via students two-tailed *t-test*.

APPENDIX

SUPPLEMENTAL MATERIAL (CHAPTER III)

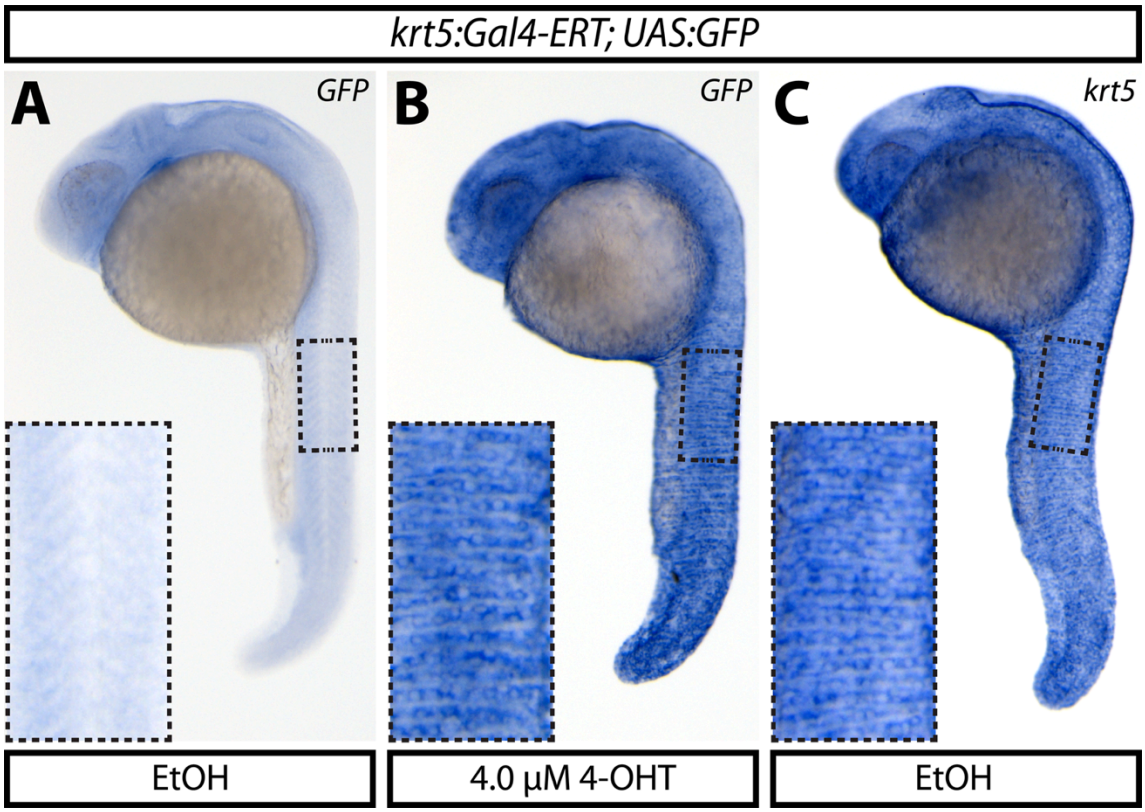

Figure S1: *krt5:Gal4-ERT* expression matches that of endogenous *krt5*.
(**A-C**) Whole mount in situ hybridization of *GFP* expression in ethanol (A) or 4-OHT-exposed (B) 24 hpf Tg(*krt5:Gal4-ERT-VP16; UAS:EGFP)* embryos compared to endogenous *krt5* expression (C). Boxed regions are shown at higher magnification in the panel insets.

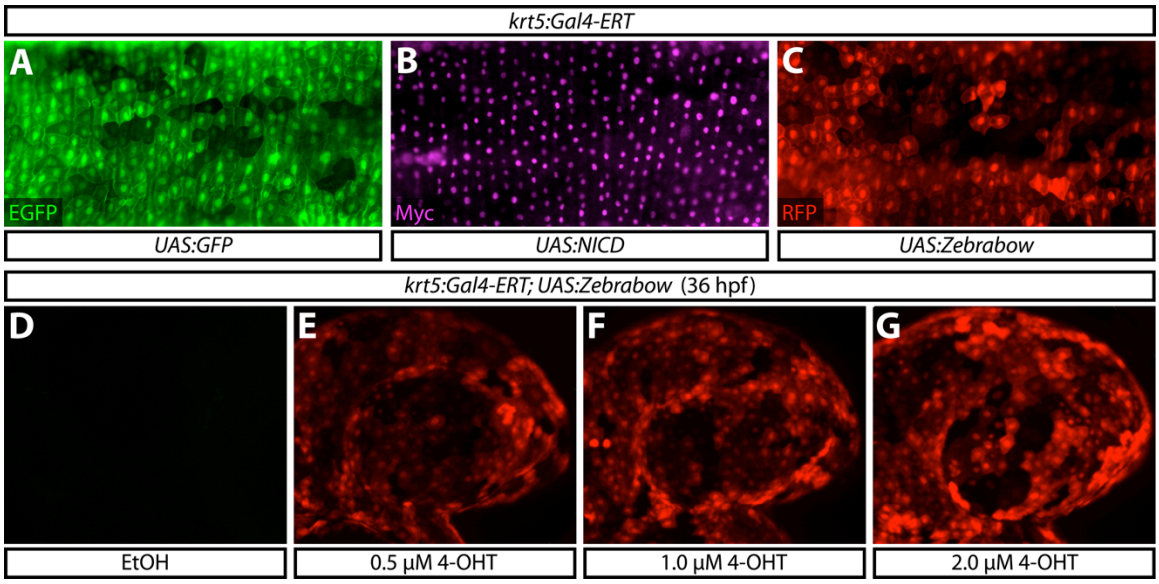

Figure S2: Multiple UAS reporter lines produce robust and dose dependent responses to activated Gal4-ERT.
(A-C) The *krt5:Gal4-ERT* line is compatible with *UAS:EGFP* (A), *UAS:NICD* shown via anti-Myc immunostaining (B), and *UAS:Zebrabow* (C) reporter lines at 36 hpf. (**D-G**) mCherry expression upon treatment of *Tg(krt5:Gal4-ERT-VP16; UAS:Zebrabow)* animals with ethanol or the indicated dose of 4-OHT from 4-36 hpf.

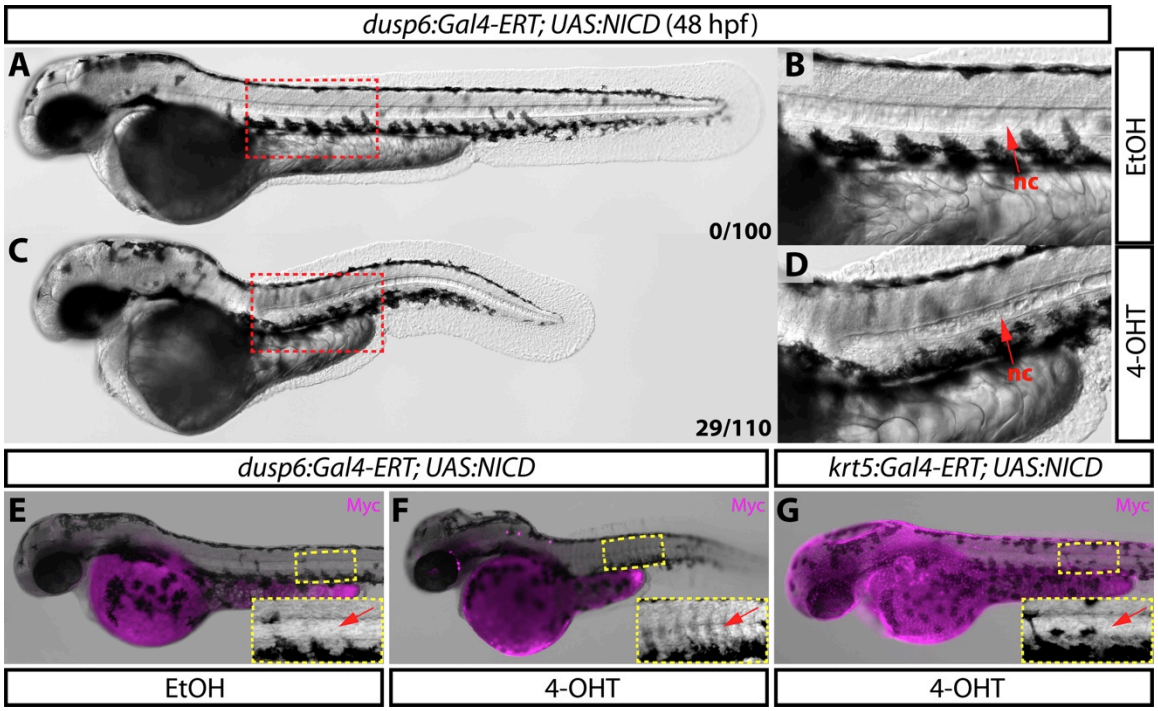

Figure S3: Tissue-specific notochord defects upon *dusp6:Gal4-ERT* driven *NICD* overexpression persist in 48 hpf zebrafish.
(A-D) DIC images of *Tg(dusp6:Gal4-ERT-VP16; UAS:NICD)* animals treated with either ethanol (A-B) or 4 μM 4-OHT from 2-48 hpf (C-D). Boxed regions in A and C are shown in higher magnification in B and D respectively. Red arrows indicate notochord. Numbers in A and C reflect the quantity of animals displaying a notochord defect in each treated population (25% double transgenic animals). **(E-G)** Bright-field images overlaid with anti-myc immunostaining (magenta) of *Tg(dusp6:Gal4-ERT-VP16; UAS:NICD)* (E-F) and *Tg(krt5:Gal4-ERT-VP16; UAS:NICD)* (G) fish demonstrates that notochord defects are only observed when *UAS:NICD* is driven by the *dusp6:Gal4-ERT* cassette (F). Boxed regions are shown in higher magnification in panel inset and red arrows indicate the notochord (nc).

REFERENCES CITED

Akerberg, A. A., Stewart, S. and Stankunas, K. (2014). Spatial and temporal control of transgene expression in zebrafish. *PLoS ONE* **9**, e92217.

Akerberg, B. N., Sarangam, M. L. and Stankunas, K. (2015). Endocardial Brg1 disruption illustrates the developmental origins of semilunar valve disease. *Dev. Biol.* **407**, 158–172.

Alder, O., Lavial, F., Helness, A., Brookes, E., Pinho, S., Chandrashekran, A., Arnaud, P., Pombo, A., O'Neill, L. and Azuara, V. (2010). Ring1B and Suv39h1 delineate distinct chromatin states at bivalent genes during early mouse lineage commitment. *Development* **137**, 2483–2492.

Appel, B., Fritz, A., Westerfield, M., Grunwald, D. J., Eisen, J. S. and Riley, B. B. (1999). Delta-mediated specification of midline cell fates in zebrafish embryos. *Curr. Biol.* **9**, 247–256.

Asakawa, K., Suster, M. L., Mizusawa, K., Nagayoshi, S., Kotani, T., Urasaki, A., Kishimoto, Y., Hibi, M. and Kawakami, K. (2008). Genetic dissection of neural circuits by Tol2 transposon-mediated Gal4 gene and enhancer trapping in zebrafish. *Proc. Natl. Acad. Sci. U.S.A.* **105**, 1255–1260.

Azuara, V., Perry, P., Sauer, S., Spivakov, M., Jørgensen, H. F., John, R. M., Gouti, M., Casanova, M., Warnes, G., Merkenschlager, M., et al. (2006). Chromatin signatures of pluripotent cell lines. *Nat. Cell Biol.* **8**, 532–538.

Bailey, G. S., Poulter, R. T. and Stockwell, P. A. (1978). Gene duplication in tetraploid fish: model for gene silencing at unlinked duplicated loci. *Proc. Natl. Acad. Sci. U.S.A.* **75**, 5575–5579.

Bassett, A. R., Tibbit, C., Ponting, C. P. and Liu, J.-L. (2013). Highly efficient targeted mutagenesis of Drosophila with the CRISPR/Cas9 system. *CellReports* **4**, 220–228.

Bergmann, O., Bhardwaj, R. D., Bernard, S., Zdunek, S., Barnabé-Heider, F., Walsh, S., Zupicich, J., Alkass, K., Buchholz, B. A., Druid, H., et al. (2009). Evidence for cardiomyocyte renewal in humans. *Science* **324**, 98–102.

Bernstein, B. E., Mikkelsen, T. S., Xie, X., Kamal, M., Huebert, D. J., Cuff, J., Fry, B., Meissner, A., Wernig, M., Plath, K., et al. (2006). A bivalent chromatin structure marks key developmental genes in embryonic stem cells. *Cell* **125**, 315–326.

Blum, M., De Robertis, E. M., Wallingford, J. B. and Niehrs, C. (2015). Morpholinos: Antisense and Sensibility. *Dev. Cell* **35**, 145–149.

Brand, A. H. and Perrimon, N. (1993). Targeted gene expression as a means of altering cell fates and generating dominant phenotypes. *Development* **118**, 401–415.

Brunet, F. G., Roest Crollius, H., Paris, M., Aury, J.-M., Gibert, P., Jaillon, O., Laudet, V. and Robinson-Rechavi, M. (2006). Gene loss and evolutionary rates following whole-genome duplication in teleost fishes. *Mol. Biol. Evol.* **23**, 1808–1816.

Burgold, T., Spreafico, F., De Santa, F., Totaro, M. G., Prosperini, E., Natoli, G. and Testa, G. (2008). The histone H3 lysine 27-specific demethylase Jmjd3 is required for neural commitment. *PLoS ONE* **3**, e3034.

Burgold, T., Voituron, N., Caganova, M., Tripathi, P. P., Menuet, C., Tusi, B. K., Spreafico, F., Bévengut, M., Gestreau, C., Buontempo, S., et al. (2012). The H3K27 demethylase JMJD3 is required for maintenance of the embryonic respiratory neuronal network, neonatal breathing, and survival. *CellReports* **2**, 1244–1258.

Cao, R., Wang, L., Wang, H., Xia, L., Erdjument-Bromage, H., Tempst, P., Jones, R. S. and Zhang, Y. (2002). Role of Histone H3 Lysine 27 Methylation in Polycomb-Group Silencing. *Science* **298**, 1039–1043.

Cardiac compensation for lack of trabeculae in ErbB2-deficient zebrafish (648.3) (2014). Cardiac compensation for lack of trabeculae in ErbB2-deficient zebrafish (648.3). *FASEB J*.

Chang, J., Wang, M., Gui, W., Zhao, Y., Yu, L. and Zhu, G. (2012). Changes in thyroid hormone levels during zebrafish development. *Zoolog Sci* **29**, 181–184.

Chattergoon, N. N., Giraud, G. D., Louey, S., Stork, P., Fowden, A. L. and Thornburg, K. L. (2012). Thyroid hormone drives fetal cardiomyocyte maturation. *FASEB J* **26**, 397–408.

Chi, N. C., Shaw, R. M., Jungblut, B., Huisken, J., Ferrer, T., Arnaout, R., Scott, I., Beis, D., Xiao, T., Baier, H., et al. (2008). Genetic and physiologic dissection of the vertebrate cardiac conduction system. *PLoS Biol.* **6**, e109.

Cloos, P. A. C., Christensen, J., Agger, K. and Helin, K. (2008). Erasing the methyl mark: histone demethylases at the center of cellular differentiation and disease. *Genes Dev.* **22**, 1115–1140.

Coffman, C. R., Skoglund, P., Harris, W. A. and Kintner, C. R. (1993). Expression of an extracellular deletion of Xotch diverts cell fate in Xenopus embryos. *Cell* **73**, 659–671.

Coffman, J. A., Dickey-Sims, C., Haug, J. S., McCarthy, J. J. and Robertson, A. J. (2004). Evaluation of developmental phenotypes produced by morpholino antisense targeting of a sea urchin Runx gene. *BMC Biol.* **2**, 6.

Dahl, J. A., Reiner, A. H., Klungland, A., Wakayama, T. and Collas, P. (2010). Histone H3 lysine 27 methylation asymmetry on developmentally-regulated promoters distinguish the first two lineages in mouse preimplantation embryos. *PLoS ONE* **5**, e9150.

Danielian, P. S., White, R., Hoare, S. A., Fawell, S. E. and Parker, M. G. (1993). Identification of residues in the estrogen receptor that confer differential sensitivity to estrogen and hydroxytamoxifen. *Molecular Endocrinology* **7**, 232–240.

De Santa, F., Totaro, M. G., Prosperini, E., Notarbartolo, S., Testa, G. and Natoli, G. (2007). The histone H3 lysine-27 demethylase Jmjd3 links inflammation to inhibition of polycomb-mediated gene silencing. *Cell* **130**, 1083–1094.

Delgado-Olguín, P., Huang, Y., Li, X., Christodoulou, D., Seidman, C. E., Seidman, J. G., Tarakhovsky, A. and Bruneau, B. G. (2012). Epigenetic repression of cardiac progenitor gene expression by Ezh2 is required for postnatal cardiac homeostasis. *Nat Genet* **44**, 343–347.

Echelard, Y., Epstein, D. J., St-Jacques, B., Shen, L., Mohler, J., McMahon, J. A. and McMahon, A. P. (1993). Sonic hedgehog, a member of a family of putative signaling molecules, is implicated in the regulation of CNS polarity. *Cell* **75**, 1417–1430.

Eisen, J. S. and Smith, J. C. (2008). Controlling morpholino experiments: don't stop making antisense. *Development* **135**, 1735–1743.

Ekker, S. C. and Larson, J. D. (2001). Morphant technology in model developmental systems. *Genesis* **30**, 89–93.

Feil, R., Wagner, J., Metzger, D. and Chambon, P. (1997). Regulation of Cre recombinase activity by mutated estrogen receptor ligand-binding domains. *Biochem. Biophys. Res. Commun.* **237**, 752–757.

Fischer, J. A., Giniger, E., Maniatis, T. and Ptashne, M. (1988). GAL4 activates transcription in Drosophila. *Nature* **332**, 853–856.

Foley, J. E., Maeder, M. L., Pearlberg, J., Joung, J. K., Peterson, R. T. and Yeh, J.-R. J. (2009). Targeted mutagenesis in zebrafish using customized zinc-finger nucleases. *Nat Protoc* **4**, 1855–1867.

Force, A., Lynch, M., Pickett, F. B., Amores, A., Yan, Y. L. and Postlethwait, J. (1999). Preservation of duplicate genes by complementary, degenerative mutations. *Genetics* **151**, 1531–1545.

Gemberling, M., Bailey, T. J., Hyde, D. R. and Poss, K. D. (2013). The zebrafish as a model for complex tissue regeneration. *Trends in Genetics* **29**, 611–620.

Gerety, S. S., Breau, M. A., Sasai, N., Xu, Q., Briscoe, J. and Wilkinson, D. G.

(2013). An inducible transgene expression system for zebrafish and chick. *Development* **140**, 2235–2243.

Giniger, E., Varnum, S. M. and Ptashne, M. (1985). Specific DNA binding of GAL4, a positive regulatory protein of yeast. *Cell* **40**, 767–774.

Grunwald, D. J. and Eisen, J. S. (2002). Headwaters of the zebrafish — emergence of a new model vertebrate. *Nat. Rev. Genet.* **3**, 717–724.

Guner-Ataman, B., Paffett-Lugassy, N., Adams, M. S., Nevis, K. R., Jahangiri, L., Obregon, P., Kikuchi, K., Poss, K. D., Burns, C. E. and Burns, C. G. (2013). Zebrafish second heart field development relies on progenitor specification in anterior lateral plate mesoderm and nkx2.5 function. *Development* **140**, 1353–1363.

Gupta, V. and Poss, K. D. (2012). Clonally dominant cardiomyocytes direct heart morphogenesis. *Nature* **484**, 479–484.

Halloran, M. C., Sato-Maeda, M., Warren, J. T., Su, F., Lele, Z., Krone, P. H., Kuwada, J. Y. and Shoji, W. (2000). Laser-induced gene expression in specific cells of transgenic zebrafish. *Development* **127**, 1953–1960.

Halpern, M. E., Rhee, J., Goll, M. G., Akitake, C. M., Parsons, M. and Leach, S. D. (2008). Gal4/UAS Transgenic Tools and Their Application to Zebrafish. *http://dx.doi.org/10.1089/zeb.2008.0530*.

Hami, D., Grimes, A. C., Tsai, H.-J. and Kirby, M. L. (2011). Zebrafish cardiac development requires a conserved secondary heart field. *Development* **138**, 2389–2398.

Han, P., Bloomekatz, J., Ren, J., Zhang, R., Grinstein, J. D., Zhao, L., Burns, C. G., Burns, C. E., Anderson, R. M. and Chi, N. C. (2016). Coordinating cardiomyocyte interactions to direct ventricular chamber morphogenesis. *Nature* **534**, 700–704.

Haubner, B. J., Schneider, J. and Schweigmann, U. (2016). Functional recovery of a human neonatal heart after severe myocardial infarction. *Circulation*.

He, A., Ma, Q., Cao, J., Gise, von, A., Zhou, P., Xie, H., Zhang, B., Hsing, M., Christodoulou, D. C., Cahan, P., et al. (2012). Polycomb repressive complex 2 regulates normal development of the mouse heart. *Circ. Res.* **110**, 406–415.

Hong, S., Cho, Y.-W., Yu, L.-R., Yu, H., Veenstra, T. D. and Ge, K. (2007). Identification of JmjC domain-containing UTX and JMJD3 as histone H3 lysine 27 demethylases. *Proc. Natl. Acad. Sci. U.S.A.* **104**, 18439–18444.

Hoshijima, K., Jurynec, M. J. and Grunwald, D. J. (2016). Precise Editing of the Zebrafish Genome Made Simple and Efficient. *Dev. Cell* **36**, 654–667.

Hruscha, A., Krawitz, P., Rechenberg, A., Heinrich, V., Hecht, J., Haass, C. and

Schmid, B. (2013). Efficient CRISPR/Cas9 genome editing with low off-target effects in zebrafish. *Development* **140**, 4982–4987.

Hwang, W. Y., Fu, Y., Reyon, D., Maeder, M. L., Tsai, S. Q., Sander, J. D., Peterson, R. T., Yeh, J.-R. J. and Joung, J. K. (2013). Efficient genome editing in zebrafish using a CRISPR-Cas system. *Nat Biotechnol* **31**, 227–229.

Issaeva, I., Zonis, Y., Rozovskaia, T., Orlovsky, K., Croce, C. M., Nakamura, T., Mazo, A., Eisenbach, L. and Canaani, E. (2007). Knockdown of ALR (MLL2) reveals ALR target genes and leads to alterations in cell adhesion and growth. *Mol. Cell. Biol.* **27**, 1889–1903.

Jahangiri, L., Sharpe, M., Novikov, N., Gonzalez-Rosa, J. M., Borikova, A., Nevis, K., Paffett-Lugassy, N., Zhao, L., Adams, M., Guner-Ataman, B., et al. (2016). The AP-1 transcription factor component Fosl2 potentiates the rate of myocardial differentiation from the zebrafish second heart field. *Development* **143**, 113–122.

Jaillon, O., Aury, J.-M., Brunet, F., Petit, J.-L., Stange-Thomann, N., Mauceli, E., Bouneau, L., Fischer, C., Ozouf-Costaz, C., Bernot, A., et al. (2004). Genome duplication in the teleost fish Tetraodon nigroviridis reveals the early vertebrate proto-karyotype. *Nature* **431**, 946–957.

Jao, L.-E., Wente, S. R. and Chen, W. (2013). Efficient multiplex biallelic zebrafish genome editing using a CRISPR nuclease system. *Proc. Natl. Acad. Sci. U.S.A.* **110**, 13904–13909.

Jiang, W., Wang, J. and Zhang, Y. (2013). Histone H3K27me3 demethylases KDM6A and KDM6B modulate definitive endoderm differentiation from human ESCs by regulating WNT signaling pathway. *Cell Res* **23**, 122–130.

Jin, S.-W., Beis, D., Mitchell, T., Chen, J.-N. and Stainier, D. Y. R. (2005). Cellular and molecular analyses of vascular tube and lumen formation in zebrafish. *Development* **132**, 5199–5209.

Jopling, C., Sleep, E., Raya, M., Martí, M., Raya, A. and Izpisua Belmonte, J. C. (2010). Zebrafish heart regeneration occurs by cardiomyocyte dedifferentiation and proliferation. *Nature* **464**, 606–609.

Kakidani, H. and Ptashne, M. (1988). GAL4 activates gene expression in mammalian cells. *Cell* **52**, 161–167.

Kartikasari, A. E. R., Zhou, J. X., Kanji, M. S., Chan, D. N., Sinha, A., Grapin-Botton, A., Magnuson, M. A., Lowry, W. E. and Bhushan, A. (2013). The histone demethylase Jmjd3 sequentially associates with the transcription factors Tbx3 and Eomes to drive endoderm differentiation. *EMBO J.* **32**, 1393–1408.

Kenessey, A. and Ojamaa, K. (2006). Thyroid hormone stimulates protein synthesis in the cardiomyocyte by activating the Akt-mTOR and p70S6K pathways. *Journal of*

Biological Chemistry **281**, 20666–20672.

Kim, S. W., Yoon, S.-J., Chuong, E., Oyolu, C., Wills, A. E., Gupta, R. and Baker, J. (2011). Chromatin and transcriptional signatures for Nodal signaling during endoderm formation in hESCs. *Dev. Biol.* **357**, 492–504.

Klose, R. J. and Zhang, Y. (2007). Regulation of histone methylation by demethylimination and demethylation. *Nat. Rev. Mol. Cell Biol.* **8**, 307–318.

Knopf, F., Schnabel, K., Haase, C., Pfeifer, K., Anastassiadis, K. and Weidinger, G. (2010). Dually inducible TetON systems for tissue-specific conditional gene expression in zebrafish. *Proc. Natl. Acad. Sci. U.S.A.* **107**, 19933–19938.

Kok, F. O., Shin, M., Ni, C.-W., Gupta, A., Grosse, A. S., van Impel, A., Kirchmaier, B. C., Peterson-Maduro, J., Kourkoulis, G., Male, I., et al. (2014). Reverse Genetic Screening RevealsPoor Correlation between Morpholino-Induced and Mutant Phenotypes in Zebrafish. *Dev. Cell* 1–12.

Krauss, S., Concordet, J. P. and Ingham, P. W. (1993). A functionally conserved homolog of the Drosophila segment polarity gene hh is expressed in tissues with polarizing activity in zebrafish embryos. *Cell* **75**, 1431–1444.

Kwan, K. M., Fujimoto, E., Grabher, C., Mangum, B. D., Hardy, M. E., Campbell, D. S., Parant, J. M., Yost, H. J., Kanki, J. P. and Chien, C.-B. (2007). The Tol2kit: a multisite gateway-based construction kit for Tol2 transposon transgenesis constructs. *Dev. Dyn.* **236**, 3088–3099.

Lan, F., Bayliss, P. E., Rinn, J. L., Whetstine, J. R., Wang, J. K., Chen, S., Iwase, S., Alpatov, R., Issaeva, I., Canaani, E., et al. (2007). A histone H3 lysine 27 demethylase regulates animal posterior development. *Nature* **449**, 689–694.

Latimer, A. J. and Appel, B. (2006). Notch signaling regulates midline cell specification and proliferation in zebrafish. *Dev. Biol.* **298**, 392–402.

Laughon, A. and Gesteland, R. F. (1984). Primary structure of the Saccharomyces cerevisiae GAL4 gene. *Mol. Cell. Biol.* **4**, 260–267.

Law, S. H. W. and Sargent, T. D. (2014). The serine-threonine protein kinase PAK4 is dispensable in zebrafish: identification of a morpholino-generated pseudophenotype. *PLoS ONE* **9**, e100268.

Lawson, N. D. (2016). Reverse Genetics in Zebrafish: Mutants, Morphants, and Moving Forward. *Trends in Cell Biology* **26**, 77–79.

Lee, S., Lee, J. W. and Lee, S.-K. (2012). UTX, a histone H3-lysine 27 demethylase, acts as a critical switch to activate the cardiac developmental program. *Dev. Cell* **22**, 25–37.

Li, M., Iismaa, S. E., Naqvi, N., Nicks, A., Husain, A. and Graham, R. M. (2014a). Thyroid hormone action in postnatal heart development. *Stem Cell Res* **13**, 582–591.

Li, Q., Wang, H. Y., Chepelev, I., Zhu, Q., Wei, G., Zhao, K. and Wang, R.-F. (2014b). Stage-Dependent and Locus-Specific Role of Histone Demethylase Jumonji D3 (JMJD3) in the Embryonic Stages of Lung Development. *PLoS Genet* **10**, e1004524.

Li, W. H. (1980). Rate of gene silencing at duplicate loci: a theoretical study and interpretation of data from tetraploid fishes. *Genetics* **95**, 237–258.

Lieber, T., Kidd, S., Alcamo, E., Corbin, V. and Young, M. W. (1993). Antineurogenic phenotypes induced by truncated Notch proteins indicate a role in signal transduction and may point to a novel function for Notch in nuclei. *Genes Dev.* **7**, 1949–1965.

Lin, Y. S., Carey, M. F., Ptashne, M. and Green, M. R. (1988). GAL4 derivatives function alone and synergistically with mammalian activators in vitro. *Cell* **54**, 659–664.

Liu, J., Bressan, M., Hassel, D., Huisken, J., Staudt, D., Kikuchi, K., Poss, K. D., Mikawa, T. and Stainier, D. Y. R. (2010). A dual role for ErbB2 signaling in cardiac trabeculation. *Development* **137**, 3867–3875.

Louvion, J. F., Havaux-Copf, B. and Picard, D. (1993). Fusion of GAL4-VP16 to a steroid-binding domain provides a tool for gratuitous induction of galactose-responsive genes in yeast. *Gene* **131**, 129–134.

Lynch, M. and Force, A. (2000). The probability of duplicate gene preservation by subfunctionalization. *Genetics* **154**, 459–473.

Ma, J. and Ptashne, M. (1987). Deletion analysis of GAL4 defines two transcriptional activating segments. *Cell* **48**, 847–853.

Ma, J., Przibilla, E., Hu, J., Bogorad, L. and Ptashne, M. (1988). Yeast activators stimulate plant gene expression. *Nature* **334**, 631–633.

Manna, S., Kim, J. K., Baugé, C., Cam, M., Zhao, Y., Shetty, J., Vacchio, M. S., Castro, E., Tran, B., Tessarollo, L., et al. (2015). Histone H3 Lysine 27 demethylases Jmjd3 and Utx are required for T-cell differentiation. *Nat Commun* **6**, 8152.

Margueron, R. and Reinberg, D. (2011). The Polycomb complex PRC2 and its mark in life. *Nature* **469**, 343–349.

Melby, A. E., Warga, R. M. and Kimmel, C. B. (1996). Specification of cell fates at the dorsal margin of the zebrafish gastrula. *Development* **122**, 2225–2237.

Miao, M., Bruce, A. E. E., Bhanji, T., Davis, E. C. and Keeley, F. W. (2007). Differential expression of two tropoelastin genes in zebrafish. *Matrix Biol.* **26**, 115–124.

Mikkelsen, T. S., Ku, M., Jaffe, D. B., Issac, B., Lieberman, E., Giannoukos, G., Alvarez, P., Brockman, W., Kim, T.-K., Koche, R. P., et al. (2007). Genome-wide maps of chromatin state in pluripotent and lineage-committed cells. *Nature* **448**, 553–560.

Miller, S. A., Mohn, S. E. and Weinmann, A. S. (2010). Jmjd3 and UTX Play a Demethylase-Independent Role in Chromatin Remodeling to Regulate T-Box Family Member-Dependent Gene Expression. *Molecular Cell* **40**, 594–605.

Molina, G. A., Watkins, S. C. and Tsang, M. (2007). Generation of FGF reporter transgenic zebrafish and their utility in chemical screens. *BMC Dev. Biol.* **7**, 62.

Morales Torres, C., Laugesen, A. and Helin, K. (2013). Utx is required for proper induction of ectoderm and mesoderm during differentiation of embryonic stem cells. *PLoS ONE* **8**, e60020.

Mosammaparast, N. and Shi, Y. (2010). Reversal of histone methylation: biochemical and molecular mechanisms of histone demethylases. *Annu. Rev. Biochem.* **79**, 155–179.

Mullins, M. C., Hammerschmidt, M., Haffter, P. and Nüsslein-Volhard, C. (1994). Large-scale mutagenesis in the zebrafish: in search of genes controlling development in a vertebrate. *Curr. Biol.* **4**, 189–202.

Müller, J., Hart, C. M., Francis, N. J., Vargas, M. L., Sengupta, A., Wild, B., Miller, E. L., O'Connor, M. B., Kingston, R. E. and Simon, J. A. (2002). Histone methyltransferase activity of a Drosophila Polycomb group repressor complex. *Cell* **111**, 197–208.

Nasevicius, A. and Ekker, S. C. (2000). Effective targeted gene "knockdown" in zebrafish. *Nat Genet* **26**, 216–220.

Ohtani, K., Vlachojannis, G. J., Koyanagi, M., Boeckel, J. N., Urbich, C., Farcas, R., Bonig, H., Marquez, V. E., Zeiher, A. M. and Dimmeler, S. (2011). Epigenetic Regulation of Endothelial Lineage Committed Genes in Pro-Angiogenic Hematopoietic and Endothelial Progenitor Cells. *Circ. Res.* **109**, 1219–1229.

Ohtani, K., Zhao, C., Dobreva, G., Manavski, Y., Kluge, B., Braun, T., Rieger, M. A., Zeiher, A. M. and Dimmeler, S. (2013). Jmjd3 controls mesodermal and cardiovascular differentiation of embryonic stem cells. *Circ. Res.* **113**, 856–862.

Paige, S. L., Thomas, S., Stoick-Cooper, C. L., Wang, H., Maves, L., Sandstrom, R., Pabon, L., Reinecke, H., Pratt, G., Keller, G., et al. (2012). A Temporal Chromatin Signature in Human Embryonic Stem Cells Identifies Regulators of

Cardiac Development. *Cell* **151**, 221–232.

Pan, Y. A., Freundlich, T., Weissman, T. A., Schoppik, D., Wang, X. C., Zimmerman, S., Ciruna, B., Sanes, J. R., Lichtman, J. W. and Schier, A. F. (2013). Zebrabow: multispectral cell labeling for cell tracing and lineage analysis in zebrafish. *Development* **140**, 2835–2846.

Perry, S. F., Wilson, R. J., Straus, C., Harris, M. B. and Remmers, J. E. (2001). Which came first, the lung or the breath? *Comp. Biochem. Physiol., Part A Mol. Integr. Physiol.* **129**, 37–47.

Peshkovsky, C., Totong, R. and Yelon, D. (2011). Dependence of cardiac trabeculation on neuregulin signaling and blood flow in zebrafish. *Dev. Dyn.* **240**, 446–456.

Porrello, E. R., Mahmoud, A. I., Simpson, E., Hill, J. A., Richardson, J. A., Olson, E. N. and Sadek, H. A. (2011). Transient Regenerative Potential of the Neonatal Mouse Heart. *Science* **331**, 1078–1080.

Poss, K. D., Wilson, L. G. and Keating, M. T. (2002). Heart regeneration in zebrafish. *Science*.

Ramadoss, S., Chen, X. and Wang, C.-Y. (2012). Histone demethylase KDM6B promotes epithelial-mesenchymal transition. *Journal of Biological Chemistry* **287**, 44508–44517.

Rebay, I., Fehon, R. G. and Artavanis-Tsakonas, S. (1993). Specific truncations of Drosophila Notch define dominant activated and dominant negative forms of the receptor. *Cell* **74**, 319–329.

Robu, M. E., Larson, J. D., Nasevicius, A., Beiraghi, S., Brenner, C., Farber, S. A. and Ekker, S. C. (2007). p53 Activation by Knockdown Technologies. *PLoS Genet* **3**, e78.

Rossi, A., Kontarakis, Z., Gerri, C., Nolte, H., Hölper, S., Krüger, M. and Stainier, D. Y. R. (2015). Genetic compensation induced by deleterious mutations but not gene knockdowns. *Nature* **524**, 230–233.

Rugg-Gunn, P. J., Cox, B. J., Ralston, A. and Rossant, J. (2010). Distinct histone modifications in stem cell lines and tissue lineages from the early mouse embryo. *Proc. Natl. Acad. Sci. U.S.A.* **107**, 10783–10790.

Sadowski, I., Ma, J., Triezenberg, S. and Ptashne, M. (1988). GAL4-VP16 is an unusually potent transcriptional activator. *Nature* **335**, 563–564.

Samsa, L. A., Yang, B. and Liu, J. (2013). Embryonic cardiac chamber maturation: Trabeculation, conduction, and cardiomyocyte proliferation. *Am J Med Genet C Semin Med Genet* **163C**, 157–168.

Satoh, T., Takeuchi, O., Vandenbon, A., Yasuda, K., Tanaka, Y., Kumagai, Y., Miyake, T., Matsushita, K., Okazaki, T., Saitoh, T., et al. (2010). The Jmjd3-Irf4 axis regulates M2 macrophage polarization and host responses against helminth infection. *Nat. Immunol.* **11**, 936–944.

Scheer, N. and Campos-Ortega, J. A. (1999). Use of the Gal4-UAS technique for targeted gene expression in the zebrafish. *Mech. Dev.* **80**, 153–158.

Scott, E. K. (2009). The Gal4/UAS toolbox in zebrafish: new approaches for defining behavioral circuits. *J. Neurochem.* **110**, 441–456.

Shin, J., Chen, J. and Solnica-Krezel, L. (2014). Efficient homologous recombination-mediated genome engineering in zebrafish using TALE nucleases. *Development* **141**, 3807–3818.

Shpargel, K. B., Sengoku, T., Yokoyama, S. and Magnuson, T. (2012). UTX and UTY Demonstrate Histone Demethylase-Independent Function in Mouse Embryonic Development. *PLoS Genet* **8**, e1002964.

Shpargel, K. B., Starmer, J., Yee, D., Pohlers, M. and Magnuson, T. (2014). KDM6 Demethylase Independent Loss of Histone H3 Lysine 27 Trimethylation during Early Embryonic Development. *PLoS Genet* **10**, e1004507.

Stankunas, K., Hang, C. T., Tsun, Z.-Y., Chen, H., Lee, N. V., Wu, J. I., Shang, C., Bayle, J. H., Shou, W., Iruela-Arispe, M. L., et al. (2008). Endocardial Brg1 represses ADAMTS1 to maintain the microenvironment for myocardial morphogenesis. *Dev. Cell* **14**, 298–311.

Stewart, S. and Stankunas, K. (2012). Limited dedifferentiation provides replacement tissue during zebrafish fin regeneration. *Dev. Biol.*

Stewart, S., Tsun, Z.-Y. and Izpisua Belmonte, J. C. (2009). A histone demethylase is necessary for regeneration in zebrafish. *Proc. Natl. Acad. Sci. U.S.A.* **106**, 19889–19894.

Struhl, G., Fitzgerald, K. and Greenwald, I. (1993). Intrinsic activity of the Lin-12 and Notch intracellular domains in vivo. *Cell* **74**, 331–345.

Takahata, N. and Maruyama, T. (1979). Polymorphism and loss of duplicate gene expression: a theoretical study with application of tetraploid fish. *Proc. Natl. Acad. Sci. U.S.A.* **76**, 4521–4525.

Takeuchi, J. K., Lou, X., Alexander, J. M., Sugizaki, H., Delgado-Olguín, P., Holloway, A. K., Mori, A. D., Wylie, J. N., Munson, C., Zhu, Y., et al. (2011). Chromatin remodelling complex dosage modulates transcription factor function in heart development. *Nat Commun* **2**, 187.

Thisse, C. and Thisse, B. (2008a). High-resolution in situ hybridization to whole-mount

zebrafish embryos. *Nat Protoc* **3**, 59–69.

Thisse, C. and Thisse, B. (2008b). High-resolution in situ hybridization to whole-mount zebrafish embryos. *Nat Protoc* **3**, 59–69.

Tsang, M., Maegawa, S., Kiang, A., Habas, R., Weinberg, E. and Dawid, I. B. (2004). A role for MKP3 in axial patterning of the zebrafish embryo. *Development* **131**, 2769–2779.

Urasaki, A., Morvan, G. and Kawakami, K. (2006). Functional dissection of the Tol2 transposable element identified the minimal cis-sequence and a highly repetitive sequence in the subterminal region essential for transposition. *Genetics* **174**, 639–649.

Van Laarhoven, P. M., Neitzel, L. R., Quintana, A. M., Geiger, E. A., Zackai, E. H., Clouthier, D. E., Artinger, K. B., Ming, J. E. and Shaikh, T. H. (2015). Kabuki syndrome genes KMT2D and KDM6A: functional analyses demonstrate critical roles in craniofacial, heart and brain development. *Hum. Mol. Genet.* **24**, 4443–4453.

Walker, M. B. and Kimmel, C. B. (2007). A two-color acid-free cartilage and bone stain for zebrafish larvae. *Biotech Histochem* **82**, 23–28.

Wamstad, J. A., Alexander, J. M., Truty, R. M., Shrikumar, A., Li, F., Eilertson, K. E., Ding, H., Wylie, J. N., Pico, A. R., Capra, J. A., et al. (2012). Dynamic and Coordinated Epigenetic Regulation of Developmental Transitions in the Cardiac Lineage. *Cell* **151**, 206–220.

Wang, C., Lee, J.-E., Cho, Y.-W., Xiao, Y., Jin, Q., Liu, C. and Ge, K. (2012). UTX regulates mesoderm differentiation of embryonic stem cells independent of H3K27 demethylase activity. *Proc. Natl. Acad. Sci. U.S.A.* **109**, 15324–15329.

Wang, Y., O'Malley, B. W., Tsai, S. Y. and O'Malley, B. W. (1994). A regulatory system for use in gene transfer. *Proc. Natl. Acad. Sci. U.S.A.* **91**, 8180–8184.

Wang, Y.-H., Chen, Y.-H., Lin, Y.-J. and Tsai, H.-J. (2006a). Spatiotemporal expression of zebrafish keratin 18 during early embryogenesis and the establishment of a keratin 18:RFP transgenic line. *Gene Expr. Patterns* **6**, 335–339.

Wang, Y.-H., Chen, Y.-H., Lu, J.-H., Lin, Y.-J., Chang, M.-Y. and Tsai, H.-J. (2006b). Epidermis-restricted expression of zebrafish cytokeratin II is controlled by a −141/+85 minimal promoter, and cassette −141/−111 is essential for driving the tissue specificity. *Differentiation* **74**, 186–194.

Watterson, G. A. (1983). On the time for gene silencing at duplicate Loci. *Genetics* **105**, 745–766.

Webster, N. J., Green, S., Jin, J. R. and Chambon, P. (1988). The hormone-binding domains of the estrogen and glucocorticoid receptors contain an inducible

transcription activation function. *Cell* **54**, 199–207.

Welstead, G. G., Creyghton, M. P., Bilodeau, S., Cheng, A. W., Markoulaki, S., Young, R. A. and Jaenisch, R. (2012). X-linked H3K27me3 demethylase Utx is required for embryonic development in a sex-specific manner. *Proc. Natl. Acad. Sci. U.S.A.* **109**, 13004–13009.

Williams, K., Christensen, J., Rappsilber, J., Nielsen, A. L., Johansen, J. V. and Helin, K. (2014). The histone lysine demethylase JMJD3/KDM6B is recruited to p53 bound promoters and enhancer elements in a p53 dependent manner. *PLoS ONE* **9**, e96545.

Winata, C. L., Korzh, S., Kondrychyn, I., Zheng, W., Korzh, V. and Gong, Z. (2009). Development of zebrafish swimbladder: The requirement of Hedgehog signaling in specification and organization of the three tissue layers. *Dev. Biol.* **331**, 222–236.

Woods, I. G., Wilson, C., Friedlander, B., Chang, P., Reyes, D. K., Nix, R., Kelly, P. D., Chu, F., Postlethwait, J. H. and Talbot, W. S. (2005). The zebrafish gene map defines ancestral vertebrate chromosomes. *Genome Res.* **15**, 1307–1314.

Xiang, Y., Zhu, Z., Han, G., Lin, H., Xu, L. and Chen, C. D. (2007). JMJD3 is a histone H3K27 demethylase. *Cell Res* **17**, 850–857.

Yamamoto, M., Morita, R., Mizoguchi, T., Matsuo, H., Isoda, M., Ishitani, T., Chitnis, A. B., Matsumoto, K., Crump, J. G., Hozumi, K., et al. (2010). Mib-Jag1-Notch signalling regulates patterning and structural roles of the notochord by controlling cell-fate decisions. *Development* **137**, 2527–2537.

Ye, L., Qiu, L., Zhang, H., Chen, H., Jiang, C., Hong, H. and Liu, J. (2016). Cardiomyocytes in Young Infants With Congenital Heart Disease: a Three-Month Window of Proliferation. *Sci Rep* **6**, 23188–23188.

Zhang, F., Xu, L., Xu, L., Xu, Q., Li, D., Yang, Y., Karsenty, G. and Chen, C. D. (2015). JMJD3 promotes chondrocyte proliferation and hypertrophy during endochondral bone formation in mice. *Journal of Molecular Cell Biology* **7**, 23–34.

Zhou, Y., Cashman, T. J., Nevis, K. R., Obregon, P., Carney, S. A., Liu, Y., Gu, A., Mosimann, C., Sondalle, S., Peterson, R. E., et al. (2011). Latent TGF-β binding protein 3 identifies a second heart field in zebrafish. *Nature* **474**, 645–648.